Reviews in Mineralogy & Geochemistry
Vol. 86 pp. 35–95, 2021

Discoveries of Mass Independent Isotope Effects in the Solar System: Past, Present and Future

Mark H. Thiemens

Department of Chemistry and Biochemistry
University of California San Diego
La Jolla, California 92093
USA

mthiemens@ucsd.edu

Mang Lin

State Key Laboratory of Isotope Geochemistry
Guangzhou Institute of Geochemistry,
Chinese Academy of Sciences
Guangzhou, Guangdong 510640
China

University of Chinese Academy of Sciences
Beijing 100049
China

linm@gig.ac.cn

THE BEGINNING OF ISOTOPES

Discovery and chemical physics

The history of the discovery of stable isotopes and later, their influence of chemical and physical phenomena originates in the 19th century with discovery of radioactivity by Becquerel in 1896 (Becquerel 1896a–g). The discovery catalyzed a range of studies in physics to develop an understanding of the nucleus and the properties influencing its stability and instability that give rise to various decay modes and associated energies. Rutherford and Soddy (1903) later suggested that radioactive change from different types of decay are linked to chemical change. Soddy later found that this is a general phenomenon and radioactive decay of different energies and types are linked to the same element. Soddy (1913) in his paper on intra-atomic charge pinpointed the observations as requiring the observations of the simultaneous character of chemical change from the same position in the periodic chart with radiative emissions required it to be of the same element (same proton number) but differing atomic weight. This is only energetically accommodated by a change in neutrons and it was this paper that the name "*isotope*" emerges. The discovery of the positive ray spectrograph, later termed mass spectrometer by Aston (1919) was a major breakthrough in understanding not only nuclear decay and stability but also led to the first calculations of different physical chemical properties by isotopic substitution. Lindemann (1919) tackled the problem as to how isotopic substitution might alter a chemical property, in this specific case the differential vapor pressures of lead of masses 206 and 207. It was not known that vibrational properties of the isotopically substituted species were different, and the calculation required an independent approach. At this time quantum mechanics was developed to the extent that harmonic oscillations could be utilized

1529-6466/21/0086-0002$10.00 (print)
1943-2666/21/0086-0002$10.00 (online)
http://dx.doi.org/10.2138/rmg.2021.86.02

in energy calculations. In the Planck Einstein hypothesis atomic heat may be quantified with a harmonic oscillation at frequency ν and with quantized absorption and emission of energy modified to permit the oscillation absorption to be via continua. In his statistical mechanical approach, it was determined that there may exist a difference from a second order effect, that would be small and arising from the mass differences in vibrational energies. This second order effect is due to a difference in "*Nullpunktsenergie*" or zero-point energy (ZPE). This is one of the earliest applications of stable isotopes in physics and is the groundwork for the later developments in isotope chemistry by Urey and colleagues. In the same year, Lindemann and Aston (1919) demonstrated the effect of isotope substitution in a paper "The Possibility of Chemical Separation of Isotopes" revealing that the effects are general and encompass thermodynamics, diffusion, chemical separation from equilibrium differences, and gravity resulting in a range of applications in physics, chemistry and biology.

The work cited above launched investigations into stable isotope effects and applications that continue up to the writing of this Chapter. In a recent review paper by Thiemens and Lin (2019) some of the early applications of stable isotopes are discussed. The Lindemann work on isotope effects, particularly in the prediction of the isotopic differences in zero-point energy was of fundamental importance in quantum chemistry at the time and is also the very basis of many applications in isotope geochemistry. As discussed by Thiemens and Lin (2019), the use of quantum effects to discover the oxygen isotopes in the Department of Chemistry of the University of California Berkeley (Giauque and Johnston 1929a,b) was considered a very early proof of the validity of the quantum theory. The atmospheric absorption bands of oxygen were recognized as possessing a structure that was inconsistent with classical interpretations. It was noted that the absorption bands arising from the 1.6-eV excitation levels of O_2 to low lying rotational bands. Most of these originate from the one expected for a non-polar diatomic, two rotating nuclei system with only alternate rotational bands populated. The lines are P and R types are doublets. However, besides the A band, there is an A′ ghost (or *Planet B*), the same as A band but energetically different. This ghost arises due to the asymmetry of the rotational bands and appearance of all lines from the ^{18}O–^{16}O as compared to symmetric ^{16}O–^{16}O. The symmetry observation is a quantum mechanical effect and an important observation for quantum theory and the discovery of ^{18}O. It was quickly discovered as a result of the isotopic asymmetry that there is an oxygen isotope of mass 17. The spectroscopy required state of the art (in 1929) measurements and were done at the Mt. Wilson Observatory.

The line position of oxygen isotopic absorption lines at different frequencies in the Schumann Runge bands (175 nm < λ < 205 nm) were used by Cicerone and Mccrumb (1980) some 50 years later to calculate the transmission functions of ultraviolet (UV) light through the earth's atmosphere. It was shown that with increasing optical length there is "isotopic self-shielding" in the atmosphere, the first suggestion of self-shielding. They abandoned the effect as subsequent isotopic exchange obliterates the self-shielding effect. Of special relevance to this Chapter is that in the first demonstration of a mass independent oxygen isotope effect by Thiemens and Heidenreich (1983) there was a suggestion that the symmetry effect and self-shielding in the early solar system could be an important process for production of the oxygen isotopic anomalies, though based upon new measurements and mechanistic understanding of the chemical physics of the quantum chemical isotope effects render shielding improbable. Further experiments and investigation of the effect lead to greater insight into the quantum chemistry (Heidenreich and Thiemens 1986) and deeper understanding of chemical reaction isotopic selection mechanisms. It suggests that symmetry isotope effects may be general effects in nature, which will be thoroughly reviewed and discussed later in this chapter.

The field of isotope chemistry and applications in nature initiates in the 1930s, in a series of papers by Urey. Following the discovery of oxygen isotope by Giauque and colleagues at Berkeley, Urey initiated a search for isotopes of hydrogen. A full historical account of this

discovery is given by Brickwedde (1982). It should be recognized that at the time of the discovery of oxygen isotopes and Urey's interest in hydrogen isotopes the neutron discovery by Chadwick had not been published. The effect of isotopic species on the Balmer α-lines of atomic hydrogen and deuterium were calculated from the Balmer series formula and searched for by atomic discharge. By measurement of these lines as a function of temperature above and at the liquification temperature of H_2 (14 K) the distinct α-line of deuterium was recognized, and deuterium was discovered (Urey et al. 1932a,b). The near simultaneous discovery of the isotopes of oxygen and hydrogen catalyzed numerous studies of chemically manifested isotope effects.

A limit to the first measurements of natural samples was the ability to measure the variation of isotope variations at high precision. Most studies involving the physical chemistry of processes were done for processes producing large isotopic variation, such as evaporation, condensation, diffusion or equilibria. The role of isotopes in defining biological chemical mechanisms was recognized immediately and experiments were done using isotope spiking techniques. In the first measurement of any isotope in meteorites, Manian et al. (1934) reported the ratio of O^{16}:O^{18} [isotope notation at that time, prior to introduction of the δ notation by Craig (1953)] in stone meteorites. The motivation was to use oxygen isotope ratio measurements to understand the source region of stony meteorites which at the time was thought to be interstellar space as deduced from the high heliospheric velocity (Manian et al. 1934). In this early work extraction of oxygen from the silicates was achieved using carbon tetrachloride at high temperature and chemical conversion to water that was ultimately electrolytically decomposed and the mass spectrometric measurements were made on O_2. The oxygen isotopic composition of the meteorites Mocs (Transylvanian L6), Knyinya (L5) and Homestead (L5) were found to be the same as a terrestrial granite from Stoningtom, Maine. Early measurements of hydrogen isotopes immediately after their discovery by Bradley and Urey (1932) found the composition in obsidian from a Crater of Mt. Kilauea, Devonian water, and hydrogen from helium bearing gas to be identical. The general consensus at this time was that *there is no variation in elemental isotopic variations in terrestrial or meteoric matter*.

The dawn of stable isotope geochemistry

Following the paper of Manian et al. (1934) there were isotopic measurements of the isotopes of natural materials that showed no variation. It was largely accepted that these materials are homogenized at a level such that any isotope effect was minimal. Spectroscopic measurements of vibrational frequency differences and calculations of equilibrium constants revealed that ΔG for these exchange reactions produce equilibrium partition functions that were too small to be measured.

The inability to measure isotope ratios at high precision disallowed any isotope study of natural samples. To specifically address this, Nier (1947) developed a new mass spectrometer that was specifically designed to measure isotope ratios in light elements at much high precision not achievable by other spectrometric means. The new mass spectrometer differed in that it was all metal, with better vacuum characteristics achieved. Rather than measuring ion beams of individual masses separately to report as a ratio of current, the beams' currents are collected simultaneously in two faraday collectors and passed through a decadal resistance circuit to precisely null out the currents. In addition, this allowed different gains on each collector to allow gain in the minor isotope signal. A final aspect of the new approach was that the measurement of an unknown sample isotope ratio was measured and switchover to a standard of know composition was done to allow even greater precision, much like the dual beam spectrophotometer invented by Beckman some 7 years previously. The Nier paper provided the first opportunity to measure isotope ratios commensurate with the expected variation in nature.

In the same year as the publication of Nier (1947), Urey (1947) and Bigeleisen and Mayer (1947) reported methodologies for a more precise calculation of equilibrium constants for exchange reactions. As described by Urey (1947) the technique takes advantage of the

ability to use gas phase molecules where high precision spectroscopic data was available. With the determination of the isotopically substituted species vibrational frequencies the exchange between two species may be determined. The approach ideally requires knowing the energy between the product dissociated state and the lowest energy of the ground state (*Nullpunktsenergie*). Since the ZPE energy could not be known a methodology for determination of it was developed.

The basis for many isotope effects relies on application of determination of the energy partitioning of the isotopic species this ZPE approach is general in its application as will be discussed. In the approach of Urey (1947), using the vibrational frequency, partition function (Q) for an individual molecule may be determined. In particular, the vibrational partition function Q_{vib} is treated as $e^{-u/2}/(1-e^{-u})$, where u equals $hc\omega/kT$ by considering a simple harmonic oscillator behavior. The ZPE and the energy difference between the potential energy well and ground vibrational state, is therefore included in this consideration. For example, the isotopic partition function ratio of water is expressed as:

$$\frac{H_2{}^{18}O}{H_2{}^{16}O} = 1.0667 = \frac{Q_2}{Q_1}\left(\text{at } 298\text{K}\right) \tag{1}$$

The physical interpretation of this the isotope partitioning between the separated atom and its ground state with a 66.7 parts per thousand (or per mil, ‰) preference for the $^{18}O/^{16}O$ ratio to be in the bound water molecule. Similarly, Q_2/Q_1 for CO_2 is:

$$\left(\frac{C^{18}O_2}{C^{16}O_2}\right)^{\frac{1}{2}} = 1.1172 = \frac{Q_2}{Q_1}\left(\text{at } 298\text{K}\right) \tag{2}$$

Note the factor in the exponent has a factor of 1/2 in the exponent which accounts for the 2 exchangeable oxygen atoms in CO_2. The equilibrium constant of oxygen isotopic exchange between CO_2 and H_2O then is simply the ratio of Equations (2) to (1), i.e., 1.1172/1.0667 = 1.047. In current notation this is a $\delta^{18}O$ for CO_2 as 47‰ greater than the water it exchanges with, not far for the present-day atmospheric CO_2 isotopic composition and reasonable given that spectroscopic measurements were significantly less precise in 1947 than today. Since the partition function ratio is a function of temperature, the isotopic exchanges between different molecules depend on temperature. As Craig recalled (https://www.balzan.org/en/prizewinners/harmon-craig/rome-23-11-1998-craig), Urey suddenly realized that there was a geological thermometer on his hands.

AN OVERVIEW OF STABLE ISOTOPE GEOCHEMISTRY

Mass dependent effects and applications

The previous section has discussed the origins of isotopes and isotope effects. Though it was nearly a half century later, the calculation of the differential vapor pressure of isotopes (Lindemann 1919; Lindemann and Aston 1919) in 1919 and their separation factors from chemical equilibria lead to an extensive array of applications once the isotope ratio mass spectrometer design of Nier (1947) was available. For example, the temperature dependent isotope separation of isotopically substituted water (oxygen or hydrogen) in evaporation and condensation provides the only mechanism by which we can determine the global earth temperatures over many relevant time periods such as glacial-interglacial times. Figure 1 is an example showing the ice core isotopic composition retrieved from Dome Fuji at Antarctica and corresponding isotopically determined temperatures over glacial–interglacial cycles in the past 0.36 million years (Uemura et al. 2012).

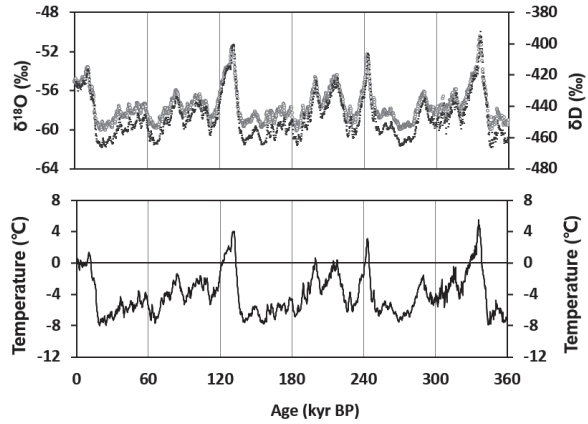

Figure 1. Dome Fuji ice core isotopic composition and temperatures. Data from Uemura et al. (2012). The oxygen and hydrogen isotopes in the top figure are used to calculate the temperatures in bottom figure. Without stable isotopes the temperature change on this time period could not be quantitatively determined.

If not for this application, the ability to understand the earth's climate system and its change would be severely restricted if not impossible. The development of the technique by which the temperatures of the oceans over long time periods for oxygen isotopic measurements of foraminiferal carbonate tests in the Urey's laboratory at Chicago has also led to a deeper understanding of e.g., climate change and heat transfer of the ocean's circulation conveyor belt. Although it is now widely acknowledged that kinetic isotopic fractionation occurs during many biomineralization processes (the so-called "vital effects"), the oxygen isotopic variation in foraminiferal remains a powerful tool to reconstruct the fluctuation of Earth's climate system on astronomical timescales as noted by Emiliani in his pioneering works (Emiliani 1955). Figure 2 is an example showing the covariation of benthic foraminifera $\delta^{18}O$ values and alkenone-derived sea surface temperature in the Pliocene (Caballero-Gill et al. 2019), a period exhibiting glacial–interglacial cycles linked to variations in Earth's obliquity.

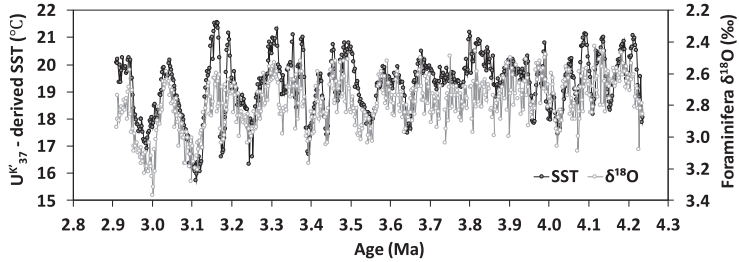

Figure 2. Southwest Pacific benthic foraminifera $\delta^{18}O$ values and alkenone-derived sea surface temperature records. Data from Caballero-Gill et al. (2019).

Another simple isotope effect derives from the differential mass dependent isotope effect on isotopes by gravity. It is of course well known that Newtonian physics dictates that due to gravity, there is a force between the mass of two bodies. For isotopes and earth this mass effect manifests itself at the top of the atmosphere due to the escape of atoms at the top of the atmosphere, a process governed by kinetic velocities, the planet's required escape velocity, and mean free path. In equilibrium, the velocity distribution of molecules follows

the Maxwell–Boltzmann distribution and the most probable velocity v_0 equals to $(2kT/m)^{1/2}$, where k is the Boltzmann constant, T is the local temperature, and m is the mass of the escaping molecules. The escape velocity of the planet v_e equals to $(2GM/r)^{1/2}$, where G is the gravitational constant, M is the mass of the planet, and r is the distance from the center of planet. The ratio of v_e^2 to v_0^2 is defined as a dimensionless parameter (λ) that is governed by the gravitational potential energy and molecule thermal kinetic energy:

$$\lambda = \frac{GMm}{rkT} \tag{3}$$

The escape flux of molecules from a planet (Φ) is derived from the kinetic theory of gases:

$$\Phi = \frac{n_c v_0}{2\sqrt{\pi}}(1+\lambda)\exp(-\lambda) \tag{4}$$

where n_c is the number density of escaping molecules at the exobase. The Equation (4) is known as the Jeans escape formula, named after James Jeans, the pioneer who calculated this process (Jeans 1904). There are other important atmospheric escape mechanisms such as hydrodynamic escape, sputtering, charge exchange, photochemical escape and ion-drag effects, but the Jeans escape is a fundamental one that depicts a general picture for the evolution of planetary atmospheres as a function of atmospheric composition, planet size, and exobase temperature. The Jeans escape formula clearly shows that lighter isotopes escape to space faster than those with heavier isotopes, and a mass dependent isotope effect therefore occurs during the Jeans escape. If the planetary atmosphere has been escaping over a long time (billions of years), light isotopes will be preferentially removed, and the atmosphere will become enriched in heavy isotopes. The relatively large ratio of $^{15}N/^{14}N$ in the Martian atmosphere was firstly detected by the Viking Lander, providing evidence for long-term erosion of the Martian atmosphere (Mcelroy et al. 1976). The isotopic composition of volatiles is a crucial tracer for tracking the evolution of Martian atmosphere, climate, and habitability. Such works are still under way by Martian meteorite isotopic measurements and *in situ* observations such as the Curiosity and MAVEN missions.

In geochemistry it is by now well established that due to the development of the calculation of the equilibrium constant in an exchange reaction (Bigeleisen and Mayer 1947; Urey 1947), one may very precisely determine the temperature of formation of a rock containing two different minerals that have equilibrated with each other. The temperature dependence of the equilibrium constant is determined by laboratory measurements allowing the measurement of the oxygen isotopic composition of the two minerals to determine the temperature (e.g., review by Thiemens 2006).

In the identification of mass independent isotope effects, the basis for mass dependent effects should be resolved. Classically, the energy is determined by summing over all available energy states Q_i. These typically are translational, rotational, vibrational, and electronic. Figure 3 shows the different energy partitions and their ultimate reliance upon nuclidic mass differences for a given element's isotopes.

The energy partitioning by translation is that of motion, velocity and energy collisions resulting in a Boltzmann distribution of velocities or energies. The rotational energies are basically expressed in terms of the angular moment of inertia I. These two energy forms are conventionally described in classical forms as they are very accurate above room temperature. The vibration of a molecule depends upon the spring constant, which reflects the nature of the chemical bond and is usually described in quantum mechanical equations. The nuclear term is a small energy term that arises only in the case where the nucleus is odd Z and possesses a nuclear spin and hyperfine magnetic moment. The overlap integral of the hyperfine moment with the magnetic moment of the electrons, providing a hyperfine coupling (*nuc*).

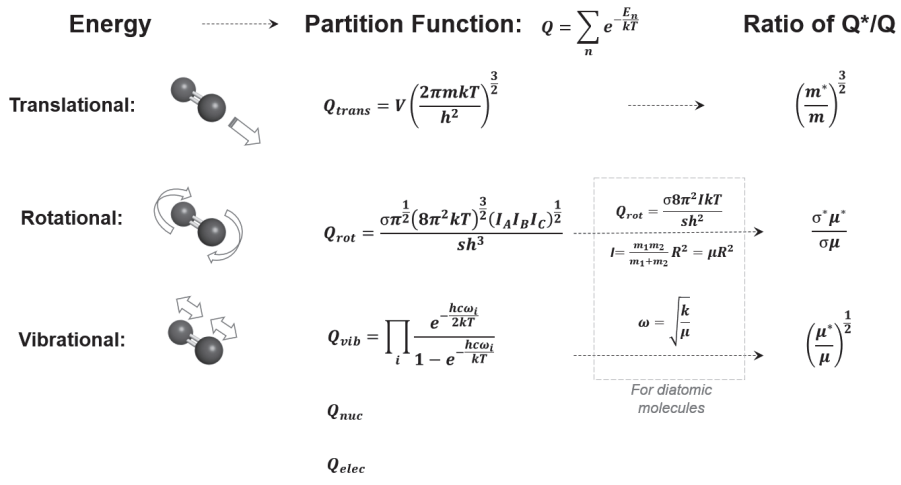

Figure 3. The partitioning of energy between different contributions: translation, rotation, vibration, nuclear hyperfine and electronic.

The isotopic contributions of this effect are reviewed by Buchachenko (2001, 2013, 2018) and Thiemens (2006). The electronic component is generally not considered as a consequence of the Born–Oppenheimer approximation. This derives from the relative sizes of the electrons and nucleons and the fact that changes in chemistry from electronic changes occur on a time scale that nuclear positional change is too small to result in an isotope effect.

An important observation is that when you look at the ratio of two isotopes, of masses m and m^*, given that they both are embedded in the same equation, there is a cancellation of all terms except mass (or reduced mass μ). Thus in the translational ratio, the magnitude of the fractionation is governed by a power of 3/2 dependency, rotational by 1, and vibrational, 1/2. The same mass relation would hold for gravity. It is noted that symmetry numbers σ are considered in rotational partition function calculations, but this term is cancelled out in many cases and in their magnitude in energy are much less than vibrational energy. The role of symmetry in isotope effects will be discussed later, especially in its role of reaction selectivity. The result is that all of the variations are mass dependent. Geochemical reactions are governed in large part by exchange, and thus a vibrational energy effect. The commonly used expression of this from a geochemical perspective is a three-isotope plot to express a mass fractionation line. In Figure 4 the mass fractionation line is shown for terrestrial and lunar samples and the slope ca. 1/2 reflects the mass effect, with mass difference of 1 for $\delta^{17}O$ and 2 for $\delta^{18}O$.

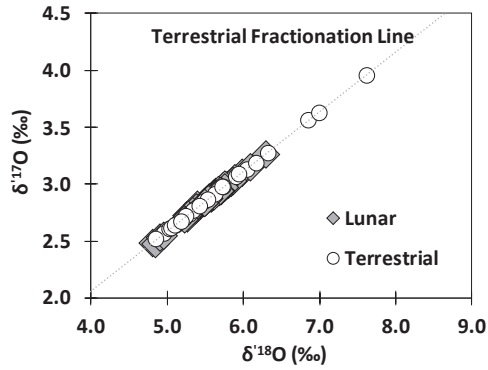

Figure 4. Triple oxygen isotope compositions of basalt and glass from the Earth and Moon. Data from Cano et al. (2020).

As will be discussed in many Chapters of this volume, at the precision of present days' measurements, the actual slope of a mass dependent fractionation line varies due to the small variations in fractionation factors of many kinetic processes and the different masses of the oxygen bearing species, ranging from the bare nuclides for ^{16}O, ^{17}O, ^{18}O to large organic species that may range into hundreds of amu (atomic mass unit). The advance in analytical technique allows a better understanding of our Earth using mass dependent isotope effects with ^{17}O, which was not normally done some 20 years ago, but a first example of the use of high precision triple oxygen isotopic analysis was measurements of atmospheric molecular oxygen, which possesses a miniscule mass independent isotope component deriving from the O_3–O_2–CO_2 coupling with photosynthesis and primary productivity (Luz et al. 1999). Model calculations further quantify that ~1/3 of the ^{17}O deficit in O_2 relative to the reference water fractionation line are associated with mass independent reactions (Young et al. 2014). The high precision definition of the slope in a multi-isotope system has also found one of its most significant applications in sulfur that has been used to track the origin and evolution of life. The ability to precisely recognize a UV driven mass independent process in the early earth from the background biogeochemical signal was critical (Farquhar et al. 2000). Much of the theoretical and experimental basis for the assignment of the source of anomalies derived from work done for oxygen. Studies from both systems are now commonly used between them to amplify understanding of the fundamental contributory processes. We will focus on mass independent oxygen isotope effects in the rest of this chapter.

Mass independent isotope effects and applications

Traditionally only one isotope ratio had been used in isotope ratio measurements, e.g., $\delta^{18}O$ for natural samples, with $\delta^{17}O$ not considered. One of the first recognitions that mass independence could be used to identify other processes, specifically nuclear is from sulfur isotope studies. Hulston and Thode (1965b) pointed out that physical and chemical processes are all mass dependent as shown in Figure 3. Deviation from that relationship then must result from a nuclear process and might be observed in meteoritic material. Sulfur has four stable isotopes (^{32}S, ^{33}S, ^{34}S, ^{36}S) and with a mass range of 4 amu it has the potential to be a uniquely precise and sensitive nuclear and chemical diagnostic tool. In the case of sulfur, its chemical change will reflect the mass dependent processes relations. Such phenomena, the relation $\delta^{33}S/\delta^{34}S = 0.5$, was shown for the first time by Hulston and Thode (1965b). The relation $\delta^{36}S/\delta^{34}S = 1.9$ also defines mass fractionation lines. It was shown in the same year that measurements of iron meteorites of long exposure age (>billion years) have excess ^{33}S and ^{36}S produced by spallation reactions of high energy galactic cosmic rays with iron (Hulston and Thode 1965a). The deviation from the mass dependent fractionation line then is a direct measure of cosmic ray exposure, which was subsequently used in other iron (Gao and Thiemens 1989), stony (Gao and Thiemens 1993b) and carbonaceous chondritic (Gao and Thiemens 1993a) meteorites to better define the spallation yields of the nuclides, and the grouping of the individual meteoritic groups.

The first observation of a mass independent isotope effect of oxygen was in the first condensates in the early solar system, the calcium aluminum rich inclusions (CAI) in the Allende meteorite (Clayton et al. 1973). In Figure 5 it may be seen that rather than the mass dependent fractionation line of $\delta^{17}O = 0.52\delta^{18}O$ (Fig. 4) expected from the application of the different physical and chemical process of Figure 3 applied to a common terrestrial environment, a relation of $\delta^{17}O = \delta^{18}O$ is observed. As discussed by Clayton et al. (1973), this unexpected deviation could only be explained in two ways: either as an equal simultaneous alteration of ^{17}O and ^{18}O or the addition of pure ^{16}O. Following (Hulston and Thode 1965a), it was assumed that since chemistry is ruled out this must be nuclear, and consistent with nucleosynthetic processes, particular supernovae injecting pure ^{16}O.

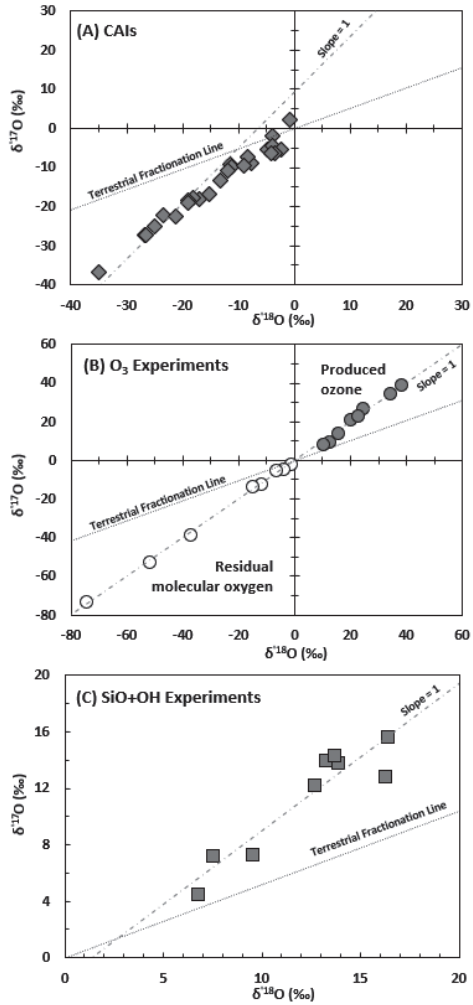

Figure 5. Triple oxygen isotope compositions of **(a)** CAIs (normalized to a carbonaceous chondrite reference standard; Clayton et al. 1973), **(b)** O_3 and residual O_2 in O_3 experiments (normalized with respect to starting oxygen; Thiemens and Heidenreich 1983), **(c)** SiO_2 in SiO + OH experiments [with respect to mass dependent SiO_2 (starting SiO and calculated O bulk)] (Chakraborty et al. 2013).

A decade later Thiemens and Heidenreich (1983) demonstrated that the simple process of ozone formation from O_2 dissociation produces the same slope observed by Clayton et al. (1973) and was the first demonstration of a chemically produced mass independent isotope effect in any element. In Figure 5b, it is observed that in the reaction, isotopic mass balance is maintained and thus a seemingly simple chemistry is involved. Given that this was the first mass independent fractionation, there was no theoretical basis for the effect. After careful consideration of the experiments, supernova injection was eliminated. The conclusion of Thiemens and Heidenreich (1983) was that there are two possibilities. First, it may be a consequence of isotopic symmetry with equal $^{16}O^{17}O$, $^{16}O^{18}O$ reaction rates versus $^{16}O^{16}O$. This recognizes that as discussed in the section on the discovery of oxygen isotopes (Giauque and Johnston 1929a,b) there is a doubling of the asymmetric species in the rotational states

compared to symmetric and consequently that may be a relevant factor. Secondly, there could be an effect of self-shielding in O_2, as had been suggested for CO in interstellar molecular cloud. As discussed, Cicerone and Mccrumb (1980) had already suggested that self-shielding may occur in the earth's atmosphere from self-shielding of O_2 leading to ozone formation. Stratospheric ozone isotopic measurements with ~400‰ ^{18}O enrichments by Mauersberger (1981) seemed consistent with this premise. Later reassessment of the data however led to retraction of this stratospheric data (Mauersberger et al. 2001). The atmospheric ozone hypothesis from self-shielding was later abandoned as it was found that the fate of the anomalous oxygen atom is to undergo isotopic exchange between the product oxygen atom and molecular oxygen removing any shielding anomaly.

For the nebular, self-shielding in CO to occur the $\delta^{17}O = \delta^{18}O$ effect arises as a consequence of the natural abundance of oxygen isotopes. Optical absorption occurs with a radial dependency as a factor of $e^{-\sigma cl}$ where σ is the absorption cross section, c the molecular number density and l the path length. The product cl is the column density and is typically the unit used in atmospheric and astrophysical sciences. In the most simplified and ideal case cross sections for all isotopologues are the same but well separated at a given wavelength region and state (with a constant incident radiation intensity for all species), photolysis rates of isotopologues only depend on abundances of isotopologues. Since the abundance of ^{16}O is orders of magnitude higher than ^{17}O and ^{18}O, a $\delta^{17}O = \delta^{18}O$ effect is obtained. In a more realistic case, the optical depth becomes important (Lyons et al. 2014, 2020). It becomes opaque to light transmission in a region of the column where ^{17}O and ^{18}O are not (Fig. 6). The results are that there is a limited optical region where the $\delta^{17}O = \delta^{18}O$ occurs because photons that can be absorbed by ^{16}O are all shielded and there is therefore no interaction between ^{16}O and photons. The relation terminates when ^{18}O becomes opaque and there will be a region where pure ^{17}O photolyzes followed by no absorption at all. It should be noted that there is only a restricted optical region through the column of gas where the slope 1 effect occurs. The radial dependency in self-shielding produces a region where the $\delta^{17}O = \delta^{18}O$ occurs, but it is an interior zone in a photochemical column. If the CAI data (Fig. 5a) was explained by CO self-shielding, it is only this layer where the required isotopic composition exists and must somehow be purely extracted from the surrounding layers. This restriction is particularly important in evaluating the plausibility of some self-shielding scenarios (e.g., molecular cloud chemistry and photochemistry). In the isotopic cross section are not equal to each other the slope 1 will not occur anywhere.

In a later paper, Navon and Wasserburg (1985) modeled shielding of O_2 in a nebular environment and concluded that isotopic exchange may effectively remove the shielding effect. They also discussed the potential role of CO in trapping the isotopic anomalies and suggested experimental and theoretical studies of both carbon and oxygen isotopes in CO self-shielding. The theory of isotopic self-shielding in CO was exhumed by Clayton (2002) though with no new measurements or models. The processes associated with understanding the mechanisms for the ultimate disproof/proof of this theory rest upon basic chemical and quantum chemical physics. In the original theory it was assumed that there was no chemical process that could produce a mass independent isotopic composition, and ultimately experiment and theory provided new insight into mass independent isotope effects via symmetry dependent reactions. In the case of self-shielding there is a basic assumption that is no isotope effect in the dissociation process itself. Experiments have shown that the assumption is incorrect and simultaneously shown that there is much to be learned about the actual process of not only CO, but any gas phase molecule. We will come back to the detailed experimental results and underlying chemical physics in the next section.

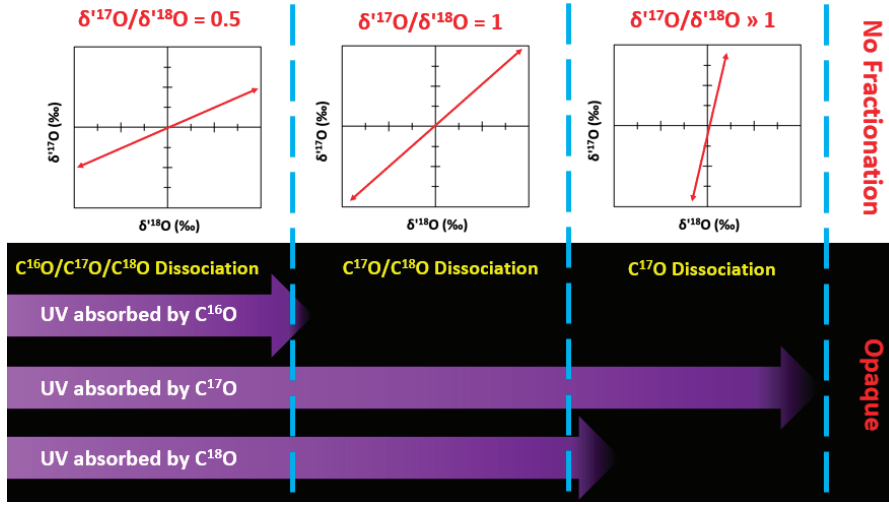

Figure 6. Schematic illustration showing the CO isotopic self-shielding process and variation of triple oxygen isotope composition over path length. In the CO self-shielding model, it is assumed that absorption lines of $C^{16}O$, $C^{17}O$ and $C^{18}O$ are well separated and therefore the energies of photons these isotopologues absorbed differ. The reaction rates of $C^{16}O$, $C^{17}O$ and $C^{18}O$ are controlled by the availability of UV photons absorbed by these isotopologues, which ultimately depends on the abundance of these isotopologues in the column due to shielding. It is assumed that there is no isotope effect in the photodissociation process. UV photons absorbed by $C^{16}O$ can only pass through a short distance due to the high number density of $C^{16}O$ in the column. After that, only $C^{17}O$ and $C^{18}O$ can access required UV photons for photodissociation and therefore the $\delta^{17}O/\delta^{18}O = 1$ slope occurs. At some distance further, $C^{18}O$ dissociation is restricted by $C^{18}O$ shielding, leading to a region where pure $C^{17}O$ dissociation occurs. At the end there is an opaque region of no dissociation at all. The distance shown in the schematic illustration is not to scale. The $\delta^{17}O/\delta^{18}O = 1$ slope zone is larger but still restricted to a specific optical region.

As the self-shielding theory cannot explain the O_3 experiment results (Thiemens and Heidenreich 1983), the other proposed mechanism in the original paper, symmetry-driven isotopic fractionation becomes central. The reaction mechanism for the sequestering of the isotope effect is of immediate importance for very many isotope geochemistry and cosmochemistry applications, especially for synthesis of the meteoritic oxygen isotope anomalies. For the source of the $\delta^{17}O = \delta^{18}O$ isotopic anomaly in ozone formation and reactions in general, a mechanism based upon chemical reaction dynamic theory was proposed by Heidenreich and Thiemens (1986). There are a number of competing theoretical approaches, but all ultimately are reliant upon the role of isotopic symmetry.

In a gas phase chemical reaction, there are three separate steps. First, reaction of an atom with a molecule to ABC^*:

$$A + BC \leftrightarrow ABC^* \rightarrow ABC \qquad \text{(R1)}$$

The species ABC^* is a short live species (10^{-13} sec) that must remove its excess energy or re-dissociate back into $A + BC$ or $AB + C$. This is accomplished by collision within a restricted number of vibrations and most ABC^* species re-dissociate. The result is that given the short lifetime and number of collisions, within a short period of time there is a steady state is established and the lifetime is driven by the number of pathways to stabilization. As discussed by Heidenreich and Thiemens (1986), the number of states are the vibrational and rotational levels. Taking oxygen isotopes as an example, the species could be $^{16}OX^{16}O$, $^{16}OX^{17}O$ and $^{16}OX^{18}O$, where X denotes that this may be any element. At the isotope level, the numbers of vibrational

states are the same, but wavelength shifted. Meanwhile, there are doubling of the rotational states for $^{16}OX^{17}O$ and $^{16}OX^{18}O$. Heidenreich and Thiemens (1986) discusses the case of ozone. The doubling of states and its origin has been detailed in a previous section on the discovery of oxygen isotopes. The increased state enhances lifetime and in turn stabilization probability. The result is an enhanced probability for isotopically asymmetric ozone to stabilize and the product formation rate is based upon symmetry rather than mass, which produces a $\delta^{17}O = \delta^{18}O$ effect.

There are three points of significance. First this is a general effect as oxygen predominantly coordinates species. Second, the effect is based upon symmetry and lifetime of the excited state and occurs for all gas phase reactions and not a specially ozone reaction feature. Finally, a most important feature is that in a gas phase reaction such as (R1), during stabilization, even though the oxygen atom may have a unique isotopic composition such as from shielding, the selectivity and rapidity of the exchange reaction will reset the original composition. This chemical feature will be developed and discussed further in ensuing sections.

In atmospheric chemistry it is well known that ozone is a major driving species controlling the oxidation state of the atmosphere. Ozone chemical and photochemical reactions in the stratosphere are drivers of a preponderance of oxidation reactions and its dissociation in the stratosphere not only provides a UV screen for the troposphere the heat generation creates the stability of the stratosphere and hence, a role in climate. Tropospheric ozone via its dissociation and subsequent reaction of the product atomic oxygen with water provides the hydroxyl radical that though low in its concentration (a million molecules per cm^3) its high reactivity mechanistically renders it a dominant oxidant species of reduced species. Ozone, with its large mass isotopic anomaly is consequently identifiable in all atmospheric oxygen bearing molecules and captures reaction source and process information that would not be otherwise identifiable. Figure 7 is an updated triple oxygen isotope plot showing atmospheric species acquiring signatures of mass independent fractionation effects. It is noted that there is a miniscule mass independent isotope component in O_2 as well as tropospheric CO_2 resulted

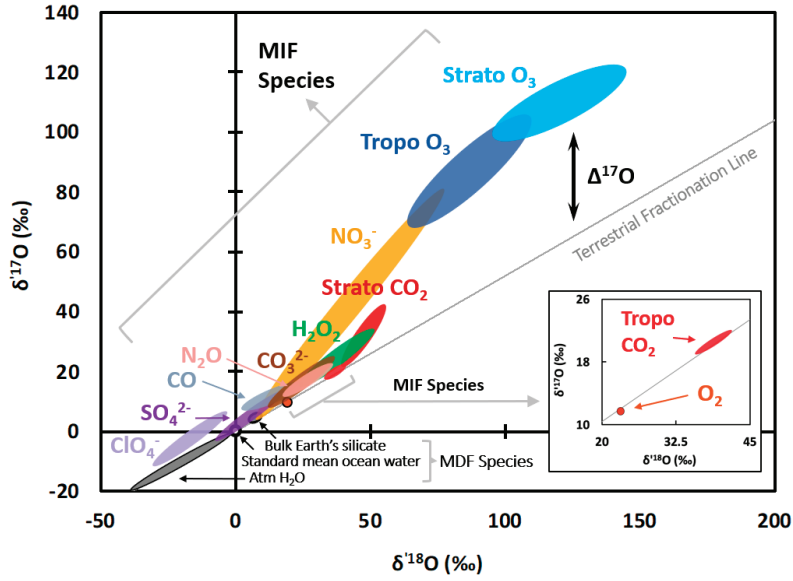

Figure 7. Oxygen isotopic compositions of atmospheric MIF (Mass Independent Fractionation) molecular species that have been measured to date. Note that ozone in the atmosphere has $\delta^{18}O$ values that are twice that of CAI and a $\Delta^{17}O$ of approximately 48‰, also double CAI.

from stratospheric O_3–O_2–CO_2 cycling and its magnitudes is mainly controlled by the fluxes of stratosphere-to-troposphere transport, photosynthesis and primary productivity. The stability of most of the ultimate oxidation products especially sulfate is generally high and consequently of utility in probing many of the Earth's major cycles (C, N, O, S), both present and past as well as Mars and meteorites. The major discoveries in a wide range of geoscience research fields using mass independent isotope effects and their applications have been reviewed earlier (Thiemens 1999, 2006, 2012; Bao 2015; Crockford et al. 2019; Thiemens and Lin 2019). Here we focus on existing advances and unsolved problems in fundamental chemical physics of mass independent isotope effects and triple oxygen isotope systematics of the solar system.

In the next section we discuss the physical chemistry of mass independent oxygen reactions in two broad categories and where they occur in the nature. This includes chemical reactions that produce new products and photodissociation that break bonds. Both processes are prevalent in the Earth's and Martian atmospheres as well as the solar nebula. Each chapter of this book draws upon these basic phenomena and, our ability to understand these effects at the basic level will elevate our ability to interpret isotopic measurements. This is particularly so for photodissociation where wavelength dependencies are known but cannot be modeled at an appropriate level.

FUNDAMENTAL CHEMICAL PHYSICS OF MASS INDEPENDENT ISOTOPE EFFECTS: WHAT IS KNOWN AND WHAT NEEDS TO BE KNOWN

Bond formation processes

The process of gas phase bond formation is one of extraordinary complexity. For a simple reaction such as (R1), there is an array of parameters that must be included in predicting the products at the isotopic level. These include the energy partitioning between translation, vibration, rotation and electronic. Furthermore, angular distribution of collisions as a function of their energy and angular approach cross section are important. The three-dimensional geometry of the reaction and products hyper spherical potential energy surfaces must be known and the dynamics are important. Many of the important processes occur on femtosecond (10^{-15} seconds) time scales. The limit in computation is largely in the many body problem, beyond H_2, the number of interactions becomes computationally formidable, and approximations are typically required. When the system of interest is at the isotopic level, the difficulties become greater due to the requirement of higher resolution of all relevant processes.

For mass independent processes in chemical reaction theory, a chemical minireview of mass independent chemistry by Thiemens and Lin (2019) has detailed the details of the development of the chemical physics of mass independent chemistry. For the geochemical application of mass independent oxygen chemistry to natural systems there are key points that are significant, which will be thoroughly discussed in the ensuing sections.

The role of symmetry

The role of symmetry as compared to mass as a reaction control has led to a field of new applications. As noted, the role of oxygen is important as it typically coordinates other species, both in the gas phase and solid. Its role in the early solar system during condensation has been predicted based upon this feature and Chakraborty et al. (2013) experimentally demonstrated the reactions:

$$O + SiO \rightarrow SiO_2 \quad \text{(R2)}$$

$$OH + SiO \rightarrow SiO_2 + H \quad \text{(R3)}$$

Reactions (R2) and (R3) are isotopically symmetry dependent, an effect that appears in the product OSiO and subject to the same selection process with $\delta^{17}O/\delta^{18}O = 1$ as in ozone formation (Figs. 5c and 8). The role of symmetry also extends beyond oxygen and includes sulfur (Fig. 8). Recognizing that another test of symmetry may be available in sulfur, Bainssahota and Thiemens (1989) performed experiments to test this. It was shown for the symmetry dependent reaction:

$$SF_5 + SF_5 \rightarrow S_2F_{10} \quad \text{(R4)}$$

a purely symmetric molecule is created and a mass independent isotopic anomaly was observed. The effect of energy and mechanism of creation of the reactive S_2F_{10} was studied and it was shown that the $S_2F_{10}^*$ state was responsible for the anomaly. Consequently, the symmetry effect is not restricted to oxygen. Babikov (2017) has provided mechanistic details for atmospheric generation of sulfur anomalies for a host of symmetry dependent reactions. These reactions were not seriously considered in most of previous Archean sulfur studies, which were mainly focused on photodissociation (Thiemens and Lin 2019). Recent models (Babikov et al. 2017; Harman et al. 2018; Liu et al. 2019) have demonstrated that these symmetry dependent reactions may be important in the Archean atmosphere. Most recently, Lin et al. (2018) employed a 5 sulfur isotope approach (4 stable sulfur and radioactive ^{35}S isotopes) in sulfate aerosols and revealed that the structure of the mass independent sulfur isotopes may require two distinct mass independent processes, apart from mass dependent processes, to define both the Archean and present day sulfur record. This includes both photochemical and potentially symmetry driven sulfur reactions, echoing with theoretical predictions by Babikov (2017). A pilot experimental test of symmetry-dependent isotope effects in elemental sulfur recombination reactions was carried out by Lin and Thiemens (2020). A first hint that alternative reactions for mass independent sulfur are needed was observed and discussed by Shaheen et al. (2014) who observed that the largest mass independent sulfur anomaly in aerosol sulfate was in 1998–99 during a year of no volcanoes and new mechanisms of production and sulfur sources are required. Additionally, it is observed that there are very few years devoid of anomalous sulfur in the Earth's atmosphere and more understanding is needed to interpret the modern and Archean records.

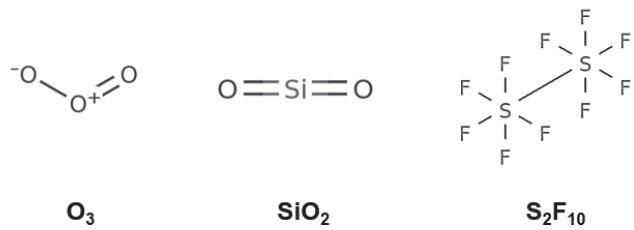

Figure 8. Symmetry molecules that acquire MIF signatures during their formation and are experimentally observed. Titanium is shown in Figure 10.

As discussed, the role of symmetry as a significant factor was included in the original work (Thiemens and Heidenreich 1983) and specifically associated with the transition state a few years later (Heidenreich and Thiemens 1986). To experimentally resolve the role of symmetry, Yang and Epstein (1987a,b) performed an extensive set of experiments using isotopically enriched (^{17}O, ^{18}O) of varying enrichment factors and reaction extent to define the role of symmetry when the terminal enrichment is higher and also for enrichments with double enrichments of normally minor species of molecular oxygen ($^{17}O^{18}O$, $^{18}O^{18}O$). The experiments were consistent with the conclusions of Heidenreich and Thiemens (1986)

that defined the transition state O_3* as the source of the mass independent selection process. In a series of follow up work of Yang and Epstein's experiments, again using isotopic spikes of the nuclidic species of ^{16}O,^{17}O, and ^{18}O, nearly all of the isotopic variants were investigated (Morton et al. 1989; Mauersberger et al. 1993, 1999; Wolf et al. 2000; Janssen et al. 2001). In these works, the role of symmetry was underscored (Fig. 9). The fully symmetric $^{16}O^{16}O^{16}O$ (666) and $^{18}O^{18}O^{18}O$ (888) possess similar rate constants as compared to the asymmetric variants. Extremely low reaction rates (10^{-2} of $^{16}O^{16}O^{16}O$) were found in symmetric $^{16}O^{18}O^{16}O$ (686) and $^{18}O^{16}O^{18}O$ (868). In general, the asymmetric isotope species are all enriched compared to symmetric as reviewed by Thiemens and Lin (2019). The effect is clearly seen when the rate constants for the individual isotopic species are measured.

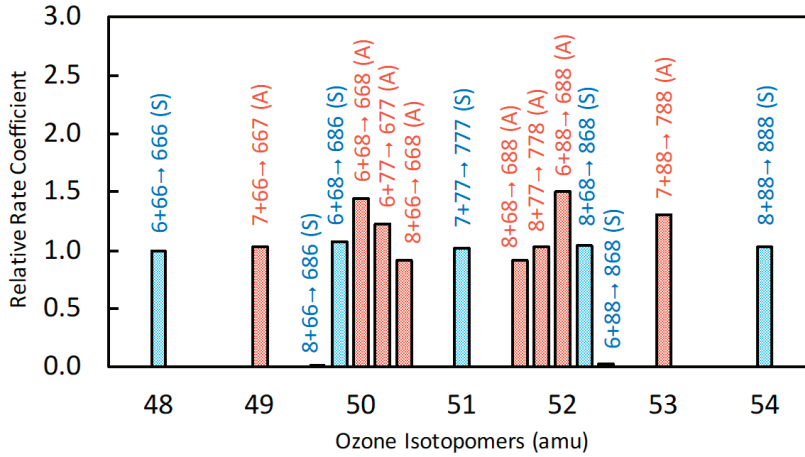

Figure 9. The variation of ozone formation rates with respect to isotopic enrichment. 666 represents $^{16}O^{16}O^{16}O$. Data from Janssen et al. (2001). Note the preference for asymmetric (**A; red**) vs symmetric (**S; blue**) species.

As will be discussed the data displayed above has been most important in developing a basic physical chemical model for the symmetry dependent ozone effect. The experimental effect of pressure (Morton et al. 1990; Thiemens and Jackson 1990) and temperature (Morton et al. 1990) on the isotopic enrichment are key parameters in not only developing a fully quantum mechanical understanding of the ozone symmetry effect, but most relevant for this paper is their application in nature. The inverse isotope effect observed by Thiemens and Jackson (1990) is particularly important. For example, in the case of the SiO+OH work an asymmetric product is observed with equal $^{17,18}O$ enrichment (Fig. 5c) (Chakraborty et al. 2013). The mass independent deviation from the mass dependent fractionation line (conventionally expressed as $\Delta^{17}O = \delta^{17}O - 0.52\,\delta^{18}O$, with $\Delta^{17}O = 0‰$ for mass dependence) (Fig. 7) is measured to be 10‰ at near room temperature. An inverse isotope effect produces a *larger* isotope effect at higher temperature rather than e.g., in isotope exchange reactions are smaller. With increasing temperature, they converge on an equilibrium exchange factor of 1. For the SiO reaction, under nebular condensation temperatures (1700 K or higher) the $\Delta^{17}O$ would be significantly higher and extend across the meteorites range. The temperature effects on symmetry dependent isotope effects may also play an important role in sulfur recombination reactions, which are strictly thermochemical gaseous reactions relevant to many high temperature planetary processes such as impacts and volcano activities as discussed by Lin and colleagues (Lin et al. 2018; Lin and Thiemens 2020).

Since the first discovery of the mass independent effect in ozone formation (Heidenreich and Thiemens 1983), though deceivingly simple in appearance, the data shown in Figure 5b has escaped a fully accountable theory. The paper of Heidenreich and Thiemens (1986) first introduced the source of the effect as symmetry based, the short-lived transition state, state density and number of states. Measurements of the rates of isotopically substituted species and their pressure and temperature dependencies provide a quantitative basis for modeling efforts along with the isotopic partitioning observed in Figure 5b. Work by Hathorn and Marcus (1999, 2000) provided the first models for these parameters that used the transition state stabilization process and the number of states that exit, or couple to the stable ozone product. The limit, which still exists, is that though the parameters above impressively account for most the isotopomeric species, the model must include an empirical fit (an η value) to the magnitude of the isotope effect. The theory is consistent with RRKM (Rice–Ramsperger–Kassel–Marcus) theory that quantifies energy sharing in the transition state between rotational/vibrational states of the isotopic species with a preference included due to state density (Gao and Marcus 2001).

The extraordinary difficulty of providing a full quantum mechanical treatment of the ozone isotope effect is another fundamental problem to be solved. Babikov and his colleagues have attempted at a near fully quantum mechanical treatment of the effect rather than an RRKM statistical mechanical approach. In the first papers in this series, the difference in approach is that Babikov et al. (2003a,b) employed the full three-dimensional surface treatment in the model along with the difference in zero-point energy and also later work by Gao and Marcus (2001). The results of the calculation show that there is resonance in the asymmetric metastable states that are sparse in the symmetric. The use of the potential energy surfaces allows for decay of the densely packed metastable states through three exit channels for $O_2 + O$. With the advancement in computational power, better three-dimensional potential energy surfaces may be determined, and this was incorporated into a more sophisticated quantum mechanical approach to isotopic ozone formation. In this treatment, the new parameters to be included are ZPE, scattering resonances, and tunneling (Teplukhin and Babikov 2018a,b; Teplukhin et al. 2018). These most recent new works take advantage of the new computational ability to calculate three-dimension potential energy surfaces at much higher resolution and to define the resonances of the metastable state. Shaped resonances below the centrifugal barrier and populated by tunneling have been introduced as a new consideration in the generation of the isotope effect and mechanisms to evaluate these properties described. What is clear is that the isotope community has facilitated in the development of quantum mechanical processes that could not otherwise be detected, much as in the case of the discovery of hydrogen and oxygen isotope. From a geochemical application perspective, the new theories underscore that the isotope effect in ozone formation is general and applies to other isotopic systems, including non-ozone species.

Besides oxygen and sulfur, a recent work by Robert et al. (2020) has extended the observed species capable of a symmetry driven isotope effect to include titanium. The experiments were done in a plasma (2450 MHz) of $TiCl_4/C_5H_{12}$ in a flow system. The solid products of organic titanium rich grains were collected from the quartz walls and measure with a NanoSIMS (Nanoscale Secondary Ion Mass Spectrometer). The remarkable experiments show that there is a massive isotope effect in ^{50}Ti, with a mass independent component observed in the grains that extends from −200 to 1200‰ (Fig.10). It is concluded that the results are interpretable on a symmetry basis, either via the symmetry based reaction recombination reaction, or, as a consequence of the scattering reactions with a higher degree of scattering for the encounter between two indistinguishable isotopes ($i=j$) and distinguishable ($i\neq j$) where i and j are a given nuclide (Reinhardt and Robert 2018). This is a significant advancement not only in theory but also in deeper understanding of the formation processes of the solar system and planets.

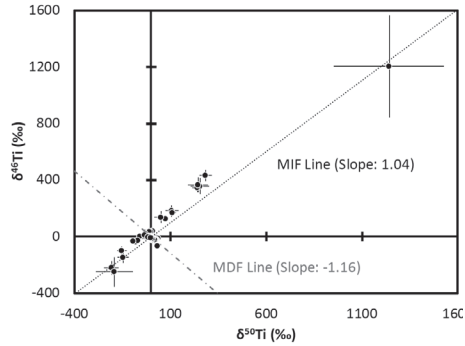

Figure 10. Mass independent fractionation of titanium isotopes in $TiCl_4/C_5H_{12}$ plasma experiments. Data from Robert et al. (2020). Note the slope one line.

Whether the oxygen isotopic composition of the Earth and Moon is the same is one of key questions to be answered for constraining the impact energy of the giant impact model. In a recent work, a mass independent character in lunar samples has been suggested by Cano et al. (2020). By investigating the slight difference in $\Delta^{17}O$ values among various mineral phases, they were able to show that an anomalously depleted $\Delta^{17}O$ reservoir may exist and contrary to commonly held theory the oxygen isotopic composition of the moon and earth may not be the same (Fig. 11). Specifically, secondary effects derived from the condensation of silicate cloud generated by the impact of Theia produce the anomalous reservoir at the surface of lunar magma ocean. The mass independent effects in SiO+OH reactions (Fig. 5c) (Chakraborty et al. 2013) are involved. In the future, a more extensive set of lunar samples and enhanced statistics, plus further pushing the precision of $\Delta^{17}O$ measurements are vital in the pursuit of deeper details of lunar origin.

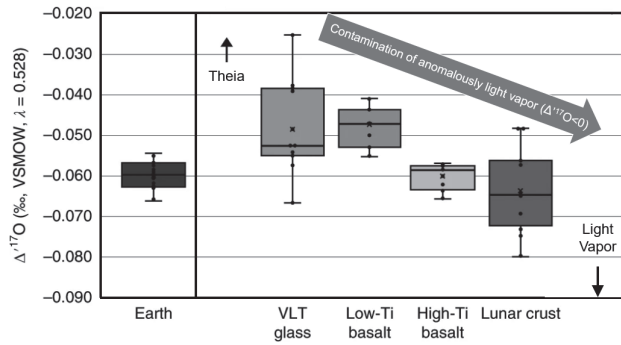

Figure 11. $\Delta^{17}O$ values of different lunar rocks and the bulk silicate Earth. The predicted $\Delta^{17}O$ values of Theia and isotopically anomalously light silicate vapor is schematically shown. Modified from Cano et al. (2020).

For isotope effects associated with bond formation, as a consequence of symmetry, mass independent oxygen isotope effects are observed in all atmospheric species and most of them are derived ultimately from ozone. In the solar nebula, the condensation of the first solids are likely recorders of the first process of nucleation and gas to particle formation as a consequence of the coordination of oxygen. In this process due to the transition state fragility and selection rules, the process is the record of the earliest events leading to the solids of the solar system and in the moon forming event (Cano et al. 2020). The role of symmetry is a general phenomenon in gas phase reactions and may be observed in other elements, including Titanium (Robert et al. 2020)

and sulfur effects (Bainssahota and Thiemens 1989) produced in the Archean (Babikov 2017; Harman et al. 2018; Lin et al. 2018; Liu et al. 2019; Lin and Thiemens 2020). Though state-of-the-art understanding of the chemical mechanism of mass independent isotope effects has advanced considerably, the complexity of the calculations at state-of-the-art computation has limits. For the future, models that can predict a priori what the effects would be would be a major advancement and a plus up for guiding experiments that are difficult, especially for gas to solid reactions of relevance in the solar nebula (Chakraborty et al. 2013) and applications in the Archean and present day atmosphere (Lin et al. 2018; Lin and Thiemens 2020).

Bond breaking isotope effects

The Chapman cycle is a series of reactions accounting for the O_3 production and destruction in the stratosphere (R5–R8):

$$O_2 + h\nu \rightarrow 2O \quad \text{(R5)}$$

$$O + O_2 + M \rightarrow O_3 + M \quad \text{(R6)}$$

$$O + O_3 \rightarrow 2O_2 \quad \text{(R7)}$$

$$O_3 + h\nu \rightarrow O_2 + O(^1D) \quad \text{(R8)}$$

where hν represents a single photon of light and $O(^1D)$ represents an electronically excited state energetically above the ground state atomic oxygen $O(^3P)$. It was not until the paper of Cicerone and Mccrumb (1980) that the issue of stable isotope effects that occur during photodissociation was quantitatively considered. The model was for self-shielding in the earth's atmosphere by O_2. A recalculation of the $^{18}O^{16}O$ shielding effect was done line by line through the relevant absorption region of the O_2 absorption spectrum and shown that this level of detail is needed to determine the precise photochemical dissociation coefficient J_i for the $^{32}O_2$ and $^{34}O_2$ molecules (Blake et al. 1984; Omidvar and Frederick 1987). The coefficients vary by approximately two orders of magnitude through the mesosphere and most of the stratosphere (Fig. 12). The results between the two line by line calculations differ considerably and exemplify the difficult in the modeling. It was shown however that in spite of the massive isotope effect, the rapidity of the isotope exchange process removes the anomaly (Kaye and Strobel 1983).

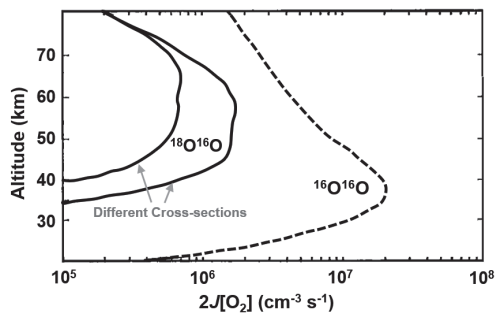

Figure 12. Calculated profiles of odd-oxygen production rates from $^{16}O^{16}O$ (**dashed line**) and $^{18}O^{16}O$ (**solid lines**; note that two different cross sections were employed) in the first consideration of isotopologues photodissociation in the terrestrial atmosphere. Modified from Cicerone and Mccrumb (1980).

Though isotopic self-shielding of O_2 does not allow the sequestration of an isotopic anomaly in a stable species, the potential for a mass independent tracer in the stratosphere from the photolysis of ozone does afford a possibility since it is known that the formation of ozone through the oxygen recombination Reaction (R6) produces a large mass independent

isotopic composition. Though the early balloon-borne mass spectrometer measurement of a massive ^{18}O enrichment was an artifact, subsequent return sample measurements have shown that stratospheric ozone is mass independent and consistent with experiments (e.g., Mauersberger et al 2001). Photodissociation of ozone enriched in the heavy isotopes ($^{17}O^{16}O^{16}O$, $^{18}O^{16}O^{16}O$ vs. $^{16}O^{16}O^{16}O$) from Reaction (R8) has the effect of producing a reservoir of isotopically enriched, highly reactive $^{17}O(^1D)$ and $^{18}O(^1D)$ atoms. It was recognized by Yung et al. (1991) that as a consequence of the high energy of the $O(^1D)$ atoms, the barrier to exchange with CO_2 via the following reaction is lowered:

$$^{17,18}O(^1D) + C^{16}O_2 \leftrightarrow {}^{16}O(^1D) + C^{17,18}O_2 \qquad \text{(R9)}$$

The isotopic exchange reaction (R9) is rapid and the ozone isotopic anomaly is passed on to CO_2, which was observed by Thiemens et al. (1991) that stratospheric balloon collected CO_2 is mass independent in composition with a deviation from mass dependent components by greater than 10‰ above 30 km. This was the first observation of a mass independent oxygen isotopic composition in any non-meteorite sample. Most importantly, it was shown in later stratospheric and mesospheric sampling using a cryogenically whole air sampler (CWAS) that the isotopic composition of CO_2 varies across the entire upper atmosphere (Thiemens et al. 1995). The work also measured the concentration of N_2O and CH_4 in the same samples and an inverse relation is observed with the $\delta^{18}O$ of the CO_2 (Thiemens et al. 1995). This relationship is a direct proof of the involvement of the atomic oxygen atom as the isotope effect in (R6) results from the reaction of the anomalous ozone derived atom and a branch of reactions between $O(^1D)$ and N_2O and CH_4:

$$O(^1D) + CH_4 \leftrightarrow OH + CH_3 \qquad \text{(R10)}$$

$$O(^1D) + N_2O \leftrightarrow O_2 + N_2 \qquad \text{(R11)}$$

Reactions (R10) and (R11) are both sink reactions for removal of these significant greenhouse gases.

A significant point for not only atmospheric chemistry is that one creates a range of mass independent reservoirs in the same place and time that vary in the $\Delta^{17}O$. The anomaly is transferred between different molecules in the stratosphere (Lyons 2001). A consequence is that in e.g., the solar nebula, the isotopic composition between the various meteorite classes in $\Delta^{17}O$ in one model or another is thought to be a spatial difference which has always placed major constraints on evolutionary models. In the case of shielding for example, the requirement is that in the self-shielding depth character, there is only a restricted layer that produces the required $\delta^{17}O = \delta^{18}O$ effect (Fig. 6) and, stored immediately as a stable ice product to avoid the back isotopic exchange that would remove the isotopic anomaly by the process modeled by Navon and Wasserburg (1985). Somehow, in spite of its large UV absorption coefficient for photo destruction, it must be transported across solar nebular without loss of its signature. If, however there is a formation process that creates a steady state reservoir, mixing is not necessary. Figure 7 shows that in a given cubic centimeter of air there are at least three oxygen mass independent isotopic reservoirs simultaneously present (CO_2, O_2, and O_3). It should be noted that due to the scale, a counter negative $\Delta^{17}O$ reservoir in O_2 is not apparent as others. The $\Delta^{17}O$ value is smaller compared to others but in a reservoir that constitutes 20.95% of the entire atmosphere. The nebular processes will be discussed later.

When the mass independent effect was first observed by Thiemens and Heidenreich there was no laboratory-based experiments that quantified isotope effects at high precision. Bhattacharya and Thiemens (1988) provided the first experimental observations of the ozone photodissociation process, which was a small mass independent isotope effect with a slight deviation from mass dependence. Chakraborty and Bhattacharya (2003) were able to

demonstrate that the effect varies with wavelength and is mass dependent in the visible and mass independent in the UV actinic regions. In the experiments, there are also competing processes that are simultaneous processes that need to be separated. First there is the primary interest of ozone photolysis reaction (R8), but it is confounded by the effects of the reaction with atomic oxygen (R7). To calculate the isotope effects from modeling of spectral data is highly complex and a semi analytical approach was developed by Liang et al. (2004) for simple molecules and was later applied specifically to ozone photolysis and stratospheric chemistry (Miller et al. 2005; Liang et al. 2006). The difficulty of both the experiments and theories was discussed by Cole and Boering (2006). The next level down in isotopic resolution was to model the dissociation pathways during ozone photolysis of the isotopomers and their electronic branching for asymmetric *vs* symmetry effects (Ndengue et al. 2012, 2014). For applications in the Antarctic and for resolution of the physical chemical processes, the ozone isotope effects for ozone trapped in ice were measured (Bahou et al. 1997). The work was of significant for applications in nature as it resolved the isotopic perturbations of absorption properties in ice (such as polar work) and the rates at which a species trapped in ice can photodissociate. The advantage of solid matrix photochemical experiments such as this described by Bahou et al. (1997) is that following the photolysis the products are trapped consequently avoiding the problem discussed above of complications arising from secondary reactions. McCabe et al. (2005) reported isotopic measurements of nitrate in ice photodecomposition to correct values reported in South Pole nitrate (McCabe et al. 2007). Besides interpretation of the decades long nitrate oxygen isotopes South Pole snow pit samples, the natural and laboratory ice photodissociation experiments are relevant today in the troposphere and polar regions as well as ice as a reservoir in the early solar system. In the self-shielding models, it is assumed that there is no photolysis of ice or interference from other molecules trapped in the ice or coated on surfaces.

The photodissociation process of ozone is clearly complex and an up to date analysis of the isotopic fractionation processes is provided by Huang et al. (2019). The complexity of detailing a fully comprehensive detail of the bond breakage remains a forefront of physical chemistry problem that increases in resolution with time. In the case of ozone, Wen and Thiemens (1990, 1991) adopted an approach that was thermal as compared to photochemical to compare the results of the differential mechanism of an $O–O_2$ bond breakage. In a thermal dissociation process the mechanism of energy acquisition leading to the bond scission differ. In the thermal case there is an energy rise form the thermal Boltzmann driven molecular ensemble which raises the energy levels up to dissociation. The energy jumps are quantized as they are rotational states and obey quantum mechanical properties for their population and transfer. The mechanism of energy transfers and notably the transition from quantized energy states to dissociate involves selection rules. In these works, the simple thermal dissociation of the ozone molecule was studied by thermally dissociation at 90 and 110 °C following the reaction yield and isotope results as a function of time (Fig. 13)

The results are not that expected for a thermal dissociation process. The decomposition process produces a slope one compared to 1/2 expected for a thermal bond breakage, and the product O_2 is enriched in ^{17}O, ^{18}O, the reverse of the value expected from conventional kinetic isotope effects. In analysis of the data, unimolecular compositional theory of Troe (1977) was applied and incorporated isotopic kinetic modeling developed by Kaye (1986). The unimolecular theory was that for low pressure steady state energy transfer. The vibrational energy transfer is included in molecules of variable densities of state. Such considerations also include a variable height of the centrifugal barrier in determination of the transition probabilities. Also considered are the low-pressure limit of energy transfer and the non-equilibrium population of excited states and weak energy transfers. In the unimolecular decomposition theory, one predicts a mass dependent process with an expected 1/2 slope. Given that thermal energy transfer processes are common in natural systems and bond breakage, for example mineral formation and equilibration, one does not see this reversal in isotope effect. What is needed is

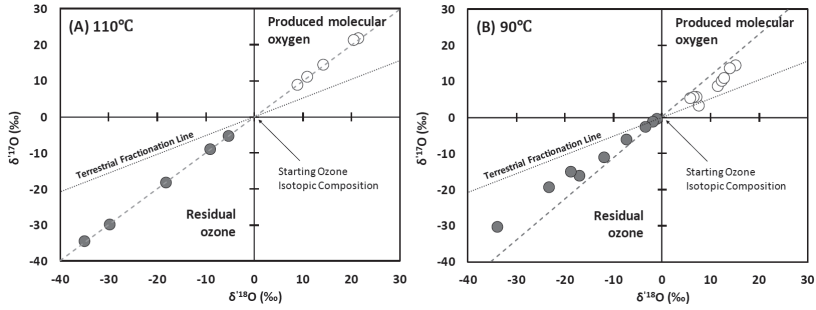

Figure 13. Triple oxygen isotope compositions of O_2 and residual O_3 in the thermal dissociation experiments (Wen and Thiemens 1991). The $\delta^{17}O = \delta^{18}O$ effect is observed but completely reversed from that of ozone formation as shown in Figure 5b.

a model such as that of Babikov and colleagues designed to study the isotopic partitioning at the quantum level and the concomitant fractionation processes and determine the microscopic reversibility. This is another example where isotopic measurements exceed what is quantum mechanically computationally possible, but potentially tractable with suitable approximations. Research into the subject of isotope effects during a gas phase thermal decomposition are of potential application for atmospheres, e.g., the atmosphere of Venus at a surface temperature of 467 °C with the presence of gas phase species such as sulfur oxide and likely oxygen radical intermediates is of relevance. Further investigations into the underlying chemical physics would add insight into the isotopic selectivity, energy dependence, and quantum dynamics of reactions that occur into and out of the hyper spherical surfaces of ozone and by extension other molecules. These are facets that are not adequately known and needed at present.

Physical chemical details of photodissociation general process

The intricacies of photodissociation are complex and there exist many mechanisms by which it occurs. There are many varieties of photochemistry and photoionization and not all need be discussed here. A review of a subset was presented by Thiemens et al. (2012). Many of the photodissociation effects applied in planetary and astrophysical environments are of a specific type of pre-dissociation. For example, relevant molecules for multi-isotope systems where mass independent isotope effects may occur in pre-dissociation include O_2, O_3, CO_2, CO, SO_2, and OCS. For these reactions, the process in general is outlined below.

In Figure 14, a general schematic of photodissociation is shown. The *y*-axis is the potential energy and *x*-axis is the internuclear distance between atoms. The ground state of the molecule (the lowest state in vibration and rotation) is shown and its energy is labeled as ZPE. The vibrational levels differ for the different energies of the molecules for the isotopic species as discussed in detail. The higher mass is a lower frequency and stronger energy and thus for a given vibrational line on a given state, the heavy isotope will be lower in potential energy. At the top of the ground state potential energy curve, the asymptote of the curve is the dissociation energy (De) of the molecule of interest. It is important to note that the distance from the ZPE to De is the energy of bond breakage, but it is not photochemically achieved by climbing states to De. In Figure 14a, the process in a simple system occurs by absorption at that energy to an excited state molecule, which reflects a less stable, different electronic configuration of the ground state molecule. They have spectroscopic notation that define this by the electronic configuration and e.g., if they are single, doublet of triplet. The ground states upon absorption at a given wavelength transits to the excited state, which also possesses vibrational and rotational levels with isotopic lines. The energy associated with this is generally driven by the transition dipole moment and it occurs at a given inter atomic separation. The excitation, as the vertical upward arrow in the figure must cross the potential energy surface

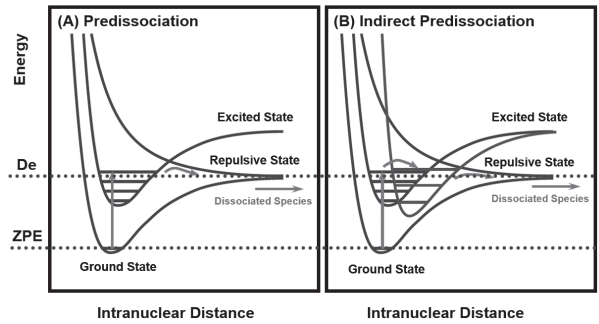

Figure 14. Schematic potential energy curves of ground, excited, and repulsive states and pathways of predissociation. **(a)** Simple predissociation with only one excited state and repulsive curve; **(b)** Indirect predissociation with ground state exciting to an excited state, crossing to a second state then repulsive state. Modified from Heays et al. (2017).

of the excited state. The probability of intersection is determining by Frank Condon factors. If the ground and excite states lie one above another exactly at the *R* distance of the well of the curves, this is the greatest Frank Condon Factor region. Figure 14b shows that potential energy surfaces of different excited electronic states may cross each other. There is a high probability that a non-radiative transition between these states occurs if their vibrational levels overlap. This is a non-adiabatic process. An isotopically substituted molecule possesses slightly different vibrational energy levels compared to the original molecule because of the change of mass. The shift of vibrational levels caused by isotopes may significantly change the probability of resonance between two different electronic states as the intersystem crossing is highly sensitive to positions of vibrational energy levels. If the energy state transits to a repulsive potential energy surface (as shown by curved arrows in Fig. 14), the molecule normally dissociates and an isotope effect can be observed in photodissociation products because of different transition probabilities, i.e., photodissociation rates. A small change of mass in isotopically substituted molecules may lead to a large isotope effect, which is difficult to precisely predict due to uncertainties in calculating the vibrational energy levels at isotopic levels.

Specific examples of isotope effects in dissociation: carbon dioxide

Carbon dioxide is the most abundant molecule in the Martian atmosphere and given the thin optical opacity, most of the atmosphere is exposed to dissociative UV energies. The dissociation of N_2 into atomic nitrogen in part facilitates its escape from the gravitational energy well and fractionates the residual nitrogen in the atmosphere, resulting in a high $^{15}N/^{14}N$ ratio. In the Earth's atmosphere, N_2 photolysis does not occur until an altitude of approximately 120 km and peaks at 175 km, providing a source of atomic nitrogen to the thermosphere (Thiemens et al. 2012). In the Martian atmosphere, CO_2 photolysis is significant and consequently of interest in interpreting the Martian atmospheric record, present and past. Reconstructing atmospheric CO_2 concentration in the early Mars and the escape rate of carbon and especially the UV-driven photochemical product O atom to space (Tian et al. 2009) via isotopic measurements in the Martian atmosphere and regolith is a necessary component in understanding the climate, habitability, and potential existence of life in Noachian Mars. Carbonates and sulfates from Martian meteorites are known to possess mass independent oxygen isotopic compositions that reflect the ozone, water CO_2 cycles and reflect the evolution of those interactions over time (Farquhar et al. 1998; Farquhar and Thiemens 2000; Shaheen et al. 2015). Terrestrial atmospheric carbonates are also known to possess a mass independent isotopic composition that includes the heterogeneous chemistry of ozone, CO_2 and water in the 10 nm surface film of the aerosols (Shaheen et al. 2010).

In the Martian atmosphere, CO_2 is exposed to UV light and subject to photodissociation. The necessary O_3–O_2 photochemical isotopic parameters for modeling the Martian atmosphere are reasonably well known as discussed in this paper and other reviews (Thiemens 2006; Thiemens and Lin 2019). The fractionation factor associated with CO_2 at a relevant UV wavelength was reported by Bhattacharya et al. (2000). In this work, line dissociations at 185 and 254 nm and continuum at 120–160 nm were measured for the isotopic fractionation factor. The different wavelengths allow for exploration of different electronic states to be identified. Ideally one would measure nm by nm across the absorption spectrum, but laboratory experiments are restricted to a small group of light sources, none of which are tunable across wavelength. Synchrotron radiation is the only tunable UV source which requires that the entire separation and collection apparatus must be constructed at a beam line and disassembled following allotted time sources. At shorter wavelengths, such as for CO dissociation, there are no windows that are transparent and windowless experiments must be done involving differential pumping while allowing sample collection. Consequently, most isotope chemistry research is done at select lines from laboratory emission or continuum sources. Figure 15a shows the relevant electronic states that are accessed in the experiments (Bhattacharya et al. 2000). The ground state of the molecule is linear and a singlet ($^1\Sigma_g^+$) with three vibrational modes. A given wavelength utilized in the experiments is shown by the upward arrow in the figure. This shows what energy of the excited state molecules is accessed and most probable. For example, at 184.9 nm, the Franck Condon region of excitation intersects favorable with the $^1B_2$ state but minimally with the $^3B_2$ state. The CO_2 molecule has different vibrational modes and Figure 15a represents a cut through the three-dimensional surface.

The experimental results of Bhattacharya et al. (2000) (Fig. 15b) are striking for several reasons. First, there is a clear wavelength dependency. For the Kr-continuum source lamp (120–160 nm) the effect is mass dependent with a depletion in $\delta^{17}O$ and $\delta^{18}O$ with respect to the makeup CO_2 gas by 50‰ on average for the product O_2 and CO. Secondly, at 184.9 nm,

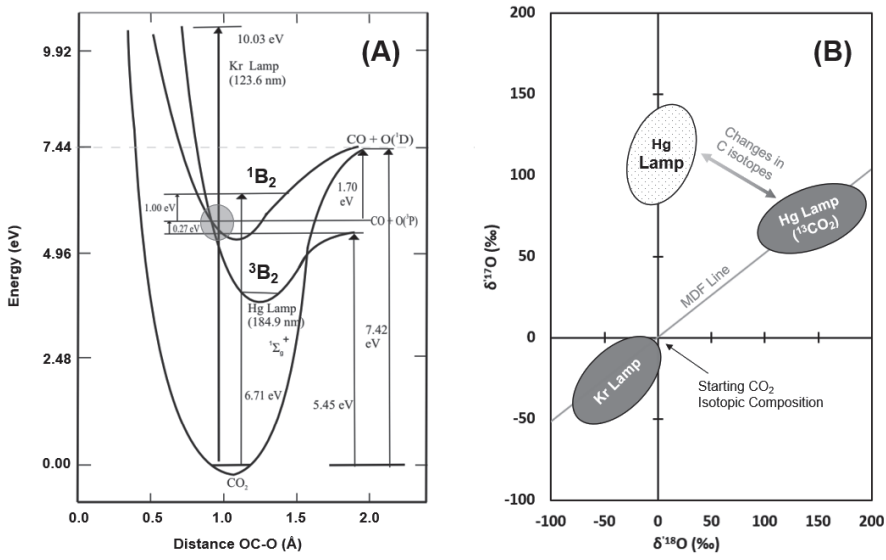

Figure 15. **(A)** Schematic potential energy surfaces of ground and selected excited states of CO_2 that are relevant to CO_2 photolysis experiments by Bhattacharya et al. (2000). Modified from Mahata and Bhattacharya (2009a). **(B)** Triple oxygen isotope compositions of photolysis products in the experiment. Modified from Bhattacharya et al. (2000). In Panel B, the remarkable observation is the change from the open balloon Hg lamp to solid mercury lamp in oxygen isotopes by only variation of the ^{13}C abundance.

there is essentially a pure ^{17}O effect, with a $\delta^{17}O$ enrichment of between 90 and 140‰ and none in $\delta^{18}O$. At 184.9 nm, as shown in Figure 15a, the excitation is to a lower vibrational energy level of the $^1B_2$ state. This energy level crosses to the $^3B_2$ state (see the shaded circle in Fig. 15a) and is above the dissociation energy level of the triplet state, consequently photodissociation occurs, though it is a forbidden crossing. In such crossing the probability of transition may be calculated, though it is not achievable at the isotopic level for a tri-atomic molecule due to the requirement of knowing the three-dimensional potential energy surfaces at high resolution. In general, and as shown by the Babikov models for ozone formation, there are resonance between excited states, and they derive by the overlap in energy. In each state ($^1B_2$, $^3B_2$) these states are primarily the vibrational-rotational levels. If the overlap they cross and in this case dissociate, the wavelength difference must be very small (less than 1 cm^{-1}). The first calculation for this effect was done for N_2 by Muskatel et al. (2011) and this sensitivity was shown in detail for the state crossings. The larger dependence of wavelength is shown in Figure 15b as the 123.6 nm region experiments show mass dependence instead of the ^{17}O enrichment at 184.9 nm.

If the crossing is the source of the isotopic effect, there should be a highly resolved wavelength dependence. Rather than altering the light source in which the absorption features are different, the same 184.9 nm experiments were duplicated with the only difference being that ^{13}C-enriched CO_2 (99%) was used. The only difference in the experiments was the shift in vibrational frequency from predominantly $^{12}CO_2$ to $^{13}CO_2$. In Figure 15b it is observed that the isotope effect is enormous; from a pure ^{17}O effect of 100‰ ($\Delta^{17}O$) to a mass dependent change of ca. 150‰ ($\delta^{18}O$) at $\Delta^{17}O = 0$. This clearly shows that the crossing is the source of the effect and a very sensitive effect of vibrational states. It may not be argued that there is a secondary effect of ozone formation as this large difference was achieved only by the change in carbon isotopic abundance. Such isotopically sensitive inter-system crossing revealed by experiments using isotopically enriched molecules is also observed in quadruple sulfur isotope systematics such as CS_2 polymerization reactions (Zmolek et al. 1999) and SO_2 photolysis reactions (Franz et al. 2013) and recently discussed by Thiemens and Lin (2019).

As shown in Figure 3, nuclear spin energies are small and conventionally negligible in contributing to chemical energy. For isotopes possessing a nuclear spin, magnetic, or hyperfine, coupling between unpaired electrons and magnetic nuclei in paramagnetic species such as radicals may spin-flip the radicals and allow the reaction between spin-allowed and spin-forbidden channels and produce a magnetically modulated isotope effect (Buchachenko 2001, 2013, 2018). Bhattacharya et al. (2000) also suggested that given that the enrichment is in ^{17}O which possess a nuclear spin the effect may be a nuclear spin, or hyperfine enrichment process. Mahata and Bhattacharya (2009a) developed a set of experiments over a wider range of experimental parameters and suggest that the effect is likely hyperfine induced. In the experiments the carbon and oxygen isotopic compositions of the products were measured and the enrichment ratio of $^{17}O/^{13}C$ is 2.2 ± 0.2, which is attributed to the ratio of the nuclear spins of oxygen/carbon and their g-factors (dimensionless magnetic moments). In a follow up experiment (Mahata and Bhattacharya 2009b) the temperature relation for the process was studied and a non-mass dependent isotopic distribution with increase in temperature is observed and attributed to a change associated with the transition dipole moment and change in Boltzmann distribution, with an underlying hyperfine effect.

In a full first principles approach by Schmidt et al. (2013) the isotopic structure and dissociative processes in the 150–210 nm were modeled. The success of the model is observed in the close agreement with independent measurements of the cross sections. The structure of the molecule is noted from the involvement in the geometry change of the bending motion of the molecule and linkage from spin-orbit coupling to the deep wells at bent geometries in the $2^1A''$and $1^1A''$ potential energy surfaces connections to the dissociative state. The model compares to the isotopic measurements and potentially a detailed model to explain the data.

As discussed by Bhattacharya et al. (2000) the CO_2 photodissociation experiments and massive isotope effect observed at 184.9 nm may be operative in the Martian atmosphere. Later measurements of carbonates and sulfates from Martian SNC meteorites demonstrated that the interactions of the atmosphere and surface of Mars sequester a record of these interactions. After Thiemens and Heidenreich (1983)'s suggestion that the ozone $\delta^{17}O = \delta^{18}O$ effect is responsible for the CAI isotopic compositions this is the first suggestions of mechanistically how an atmospheric (or nebular) chemically produced mass independent signal may be transferred to solids. As in the case of the discovery of isotopes and isotope effects in nature, the ultimate success of these applications resides in the development of deeper understanding of the basic physical chemistry.

PHOTODISSOCIATION IN THE EARLY SOLAR SYSTEM AND SELF-SHIELDING MODELS

Triple oxygen isotope composition in CAI is a window for understanding the formation and evolution of the early solar system and planets. Thiemens and Heidenreich (1983) discussed the mechanisms by which a chemically produced mass independent isotope effect may arise. One was based upon symmetry influences, which has ultimately proven to be a commonly accepted basis. Secondly, they suggested that it could also arise from self-shielding in the solar nebula as an oxygen isotope *abundance* produces a $\delta^{17}O = \delta^{18}O$ composition due to the large difference in abundance of ^{16}O and $^{17,18}O$ (Fig. 6). A basis was suggested that self-shielding had reputably been observed in CO in interstellar molecular clouds and that during a T-Tauri phase of the sun, UV radiation may be enhanced by a factor of 10^4. It was also suggested that self-shielding in N_2 and H_2 could produce the high ^{15}N, ^{2}H enrichments observed in chondritic meteorites. Models for the early solar system by Navon and Wasserburg (1985) modeled the fate of the oxygen atom post self-shielding. As a rapidity of the radical exchange, the isotope effect produced in the oxygen product was removed, which is consistent in the case of ozone and the effect arising from the gas phase symmetry driven chemical reaction. This is an important fatal point for self-shielding, irrespective of self-shielding is that the fate of the product, be it isotope exchange or the subsequent chemical reaction forming a solid, or destruction of that product must be fully considered at an isotopic level. As discussed in the previous section CO_2 is an example of how the dissociation process itself gives rise to a major isotope effect. Each of these limits is discussed in the ensuing discussion.

Self-shielding models

Nearly 20 years after the suggestion of self-shielding in the nebula, Clayton (2002) resurrected the self-shielding model and in a commentary suggested self-shielding as the source of the CAI oxygen isotopic anomalies. The basis for CO self-shielding was the observation of self-shielding in interstellar molecular clouds and an active T-Tauri phase sun as discussed in Thiemens and Heidenreich (1983). The paper however did not address the issue of how the signal was not erased by isotopic exchange as the fate of the product oxygen was not considered. It was suggested that as known in the astrophysics community, for self-shielding to occur one needs to occur, the ^{12}CO and ^{13}CO abortion lines are separated by 45 cm^{-1} allowing differential absorption due to the large difference in the isotopic abundances of approximately 100:1. For CO this is known to occur at 105 nm, but not at other wavelengths as they either do not have differential absorption or the relevant UV region is opaque due to H_2 absorption. This also assumes that all absorbed light leads to dissociation and there is no leakage back to the ground state (or a quantum yield of 1).

To circumvent the issue of *isotope* exchange, shielding was suggested as taking place on the edges of the solar nebular and past 10 AU where temperatures are sufficiently low that the product ^{18}O,^{17}O atoms are frozen as water ice and the fate of isotopic exchange presumably avoided (Yurimoto and Kuramoto 2004; Lyons and Young 2005; Sakamoto et al. 2007;

Young 2007a,b). In these models, CO self-shielding could have occurred at the inner annulus or surface of the solar protoplanetary disk, or the molecular cloud prior to collapsing to form the solar protoplanetary disk. The UV source may also have originated from outside the nebula and clustered massive star formation in nearby regions or the sun itself. The ice created in the outer edges of the solar system is then transported intact where it is transported intact to the inner solar system where the water is chemically converted to meteorites of varying isotopic composition, from ^{16}O-delepted new-PCP (poorly characterized phase) in Acfer-094 to ^{16}O-enriched CAI and Acfer-214 a006 inclusion (Fig. 16). As discussed by Lyons et al. (2009) the mechanism by which the anomaly is safely transferred and preserved in a silicate is not known or if it is possible. The occurrence of aqueous alteration in carbonaceous chondrites is well known (e.g., Clayton and Mayeda 1984; Young 2001; Benedix et al. 2003; Airieau et al. 2005; Tyra et al. 2007) but there remain uncertainties in the detailed mechanisms and concomitant isotope effects. The unaddressed problems with self-shielding are partitioned into three areas, all based on the basic physical chemistry of the isotope effects. These include: (1) the CO photodissociation process itself; (2) unfractionated storage in water ice and its isotopic stability; (3) conversion of water ice after transport through a turbulent nebula to mineral phases.

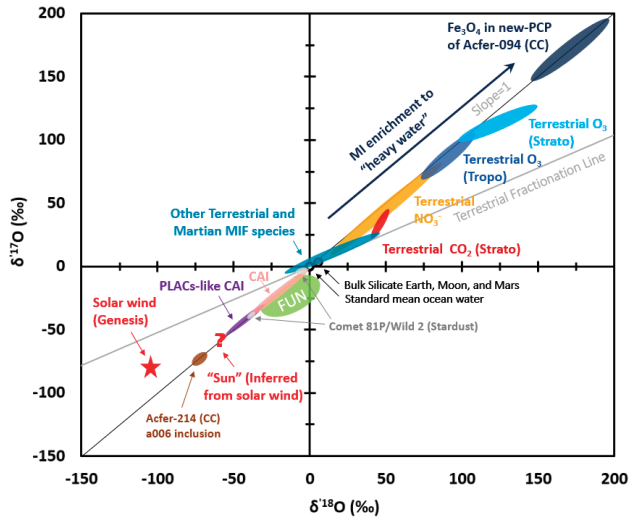

Figure 16. Oxygen isotopic compositions of MIF species in the solar system that have been measured to date.

Mass independent isotope effects in CO photodissociation

The isotope effects in CO photodissociation when the models were proposed were unknown. There is a basic assumption in self-shielding models that there is no additional isotope effect in photodissociation and the isotopic fractionation in self-shielding is only linked to the abundance of isotopes. To specifically examine this issue, Chakraborty and colleagues (Chakraborty et al. 2008, 2012, 2018) experimentally tested the model directly. These are the only experiments that directly test self-shielding. In self-shielding models (Clayton 2002; Yurimoto and Kuramoto 2004; Lyons and Young 2005; Sakamoto et al. 2007; Young 2007a,b) and radio astronomical measurements of CO in interstellar molecular clouds (Vandishoeck and Black 1988), it is known that for self-shielding to occur, it is restricted to the absorption region around 105 nm. At this wavelength there is the $^{12,13}C^{16,17,18}O_2$ line spacing available for differential isotopic absorption to occur (Fig. 6) and a hydrogen shielding window. In addition, there is a window in H_2 absorption available for photolysis. Therefore, at 105 nm

and that region, self-shielding is potentially viable. At 107 nm however, the isotopic lines are only separated by 1 cm^{-1} and $^{13}C^{16}O$, $^{12}C^{17}O$, $^{12}C^{18}O$ and overlap (Vandishoeck and Black 1988) and may not self-shield and consequently must be distinct in their isotopic fractionation products compared to 105 nm. Figure 17 is the CO potential energy surface diagram showing various excited states and relevant wavelengths. The CO photodissociation experiments were carried out using synchrotron radiation at the Advanced Light Source at the Lawrence Berkeley National Laboratory. At these wavelengths light is opaque to transmission through widows and a windowless photocell is required. The differentially pumped system designed for this is described in detail by Chakraborty et al. (2008). A flow system is employed to maintain an infinite reservoir of CO and there is also a cryogenic system to trap the products for transport the products is needed. The results across six different wavelengths and three different temperatures in a series of CO photodissociation experiments are summarized in Figure 18 for the product atomic oxygen.

The CO photodissociation experiment results are clear. The 105.17 and 107.61 nm results lie along the same slopes (Figs. 18a,b). At 107.61 nm self-shielding is not possible as the isotope lines $^{12}C^{16}O$, $^{12}C^{17}O$, $^{12}C^{18}O$ overlap. The beam profile determination also allows resolution of the 107.61 vs 105.17 nm dependence. The identical isotopic composition of the products for the two wavelengths rules out self-shielding. A second important aspect is that the slope of the products (Fig. 18) is not the required $\delta^{17}O/\delta^{18}O = 1$ slope for either the meteorites (Figs. 5a and 16) or self-shielding models (Fig. 6) and is very reproducibly so.

The temperature dependence was further probed with a new photolysis system that allows access to lower temperatures (80K) (Chakraborty et al. 2016; Chakraborty et al. 2018). In the experiments, careful measurement of the beam profile was done so that the isotope effect and the states accessed are assigned at high specificity. Figure 18 also shows that there is a massive variation with temperature and varies with electronic state by more than 1000‰ for $\Delta^{17}O$ and as high as nearly 4000‰ for $\delta^{18}O$. The very strong temperature suggests that the involvement of rotational states involved as both the line width and rotational state population are strong functions of temperature.

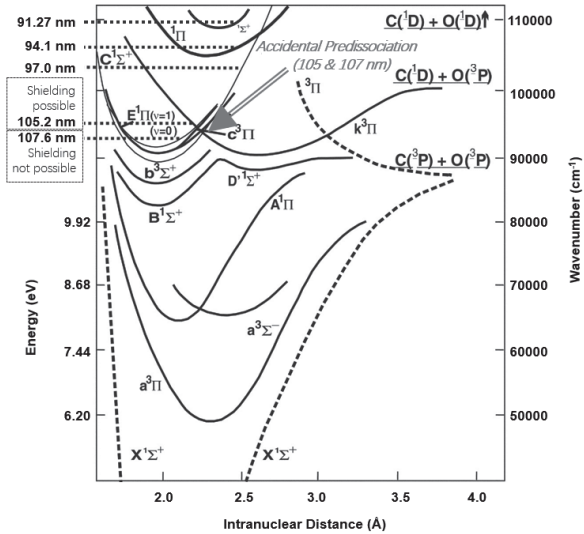

Figure 17. Schematic potential energy surfaces of CO excited states relevant to CO photolysis experiments. Modified from Chakraborty et al. (2008, 2012).

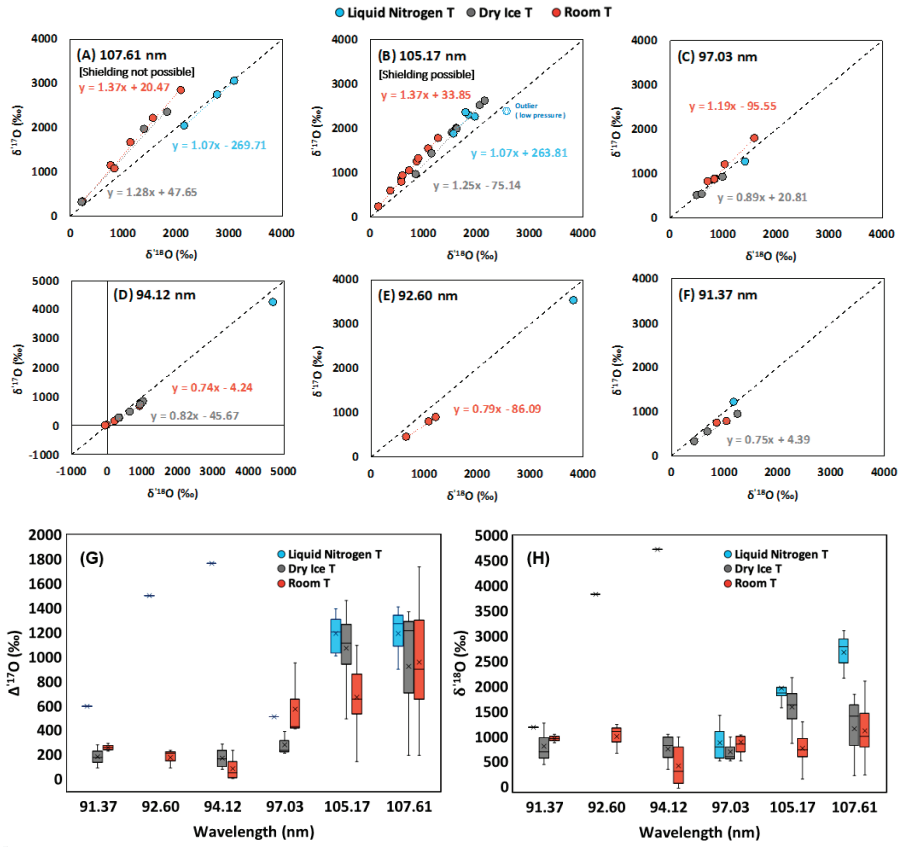

Figure 18. A summary of triple oxygen composition of product atomic O in CO photodissociation experiments. Wavelength and temperature dependencies are shown. Data obtained from Chakraborty et al. (2008, 2012, 2018). Based on the self-shielding theory and isotopologue cross-sections, a shielding effect should be proven in 105.17 nm (**panel A**) but not in the 107.61 experiments (**panel B**). It is however observed that 107.61 nm experiments exhibit the same behavior as in 105.17 nm experiments, inconsistent with an origin in shielding.

The experimental data have further shown the effect of wavelength on $\delta^{17}O/\delta^{18}O$ and $\Delta^{17}O$ (Fig. 18). The wavelength-dependent variation of the photolytic isotopic products is apparent and not explainable by self-shielding. In fact, the data is consistent with the isotope effect in CO dissociation being driven by the process of dissociation post absorption and not light filtration. The comparison of the 105.17 and 107.71 nm experiments outlined above is consistent with this. As will be discussed, the use of cross sections only does not capture the isotope effect as it does not reveal the factors that influence the processes and are dominated by the overall isotopically selective bond breakage features captured by the photolytic bond breakage.

Another evidence that self-shielding does not dominate the mass independent isotope effects in CO photodissociation experiments comes from the pressure dependency. The process of self-shielding is driven by the column density of the gas molecules and for astrophysical applications of self-shielding it is the column density that is most significant (Vandishoeck and Black 1988). The column density (*cl*) in an absorption process is the local number of molecules per cm^3 (molecule number density, *c*) times the light optical path length (*l*; unit: cm). The light absorbance is exponentially dependent of this feature and is expressed as:

$$\frac{I}{I_0} = e^{-\sigma c l} \tag{5}$$

where I_0 is the initial photon flux of the light source, I is the photon flux at a given distance l, and σ is the cross section (cm^2). For the different isotopically substituted molecules the I/I_0 vary differently as they are a function of the isotopic abundances of ^{16}O, ^{17}O and ^{18}O and are incorporated in the c term above and shown in Figure 6. The variation in the isotope with pressure then should capture this effect of shield as a linear change in pressure is expressed in the exponent for the isotopic species. There are disagreeing comments on the first CO photodissociation experiment (Chakraborty et al. 2008), pointing out that the deviation of $\delta^{17}O/\delta^{18}O$ from unity might be an optical depth effect (Federman and Young 2009; Lyons et al. 2009b; Yin et al. 2009) and were answered in Chakraborty et al. (2009). In the follow-up CO experiments, the pressure was varied over two orders of magnitude and as a function of temperature and wavelength and the oxygen and carbon isotopes were measured (Chakraborty et al. 2012, 2018). The experimental pressures are done for those that allow the windowless experiments that are differentially pumped. If self-shielding could have dominated the isotopic fractionation in the experiments, an increasing $\delta^{17}O/\delta^{18}O$ slope along with pressure (i.e., column density) was expected. It is however observed that over a large pressure range the $\delta^{17}O/\delta^{18}O$ values are consistent or varying in a way different the prediction of the self-shielding model (Fig. 19). In addition, they are not a value of 1 required for meteorites. There is no pressure dependency observed over nearly 2 orders of magnitude pressure range as expected from shielding and the exponential dependency upon pressure given in Equation (5) and illustrated in Figure 6. Again, the shielding (105.17 nm) and non-shielding (107.61 nm) wavelength gave the same slope which rules out shielding as it does not occur. The results cannot be explained as an overlap of states within beam as the beam profile is measured, reported and accounted for. Following the Clayton (2001) paper re- suggesting self-shielding of CO, these are the only experiments that directly measure the isotope effect in CO dissociation.

A final problem for self-shielding is also experimentally shown by Chakraborty et al. (2018). For the first time the ^{13}C of the carbon monoxide product of the photolysis was measured. As discussed and shown in model calculations of self-shielding (Chakraborty et al. 2018), experimental results for the experiments are not that expected for self-shielding. The calculations were done at wavelengths where the isotopic cross sections are known. The problem of the overlap of discrete CO absorption bands within the beam (full width at half maximum: ca. 2 nm) raised by previous comments (Chakraborty et al. 2009; Federman and Young 2009; Lyons et al. 2009b; Yin et al. 2009) are carefully considered in the experiment and calculation. For carbon, the difference is as much as 3000‰ in $\delta^{13}C$! For oxygen,

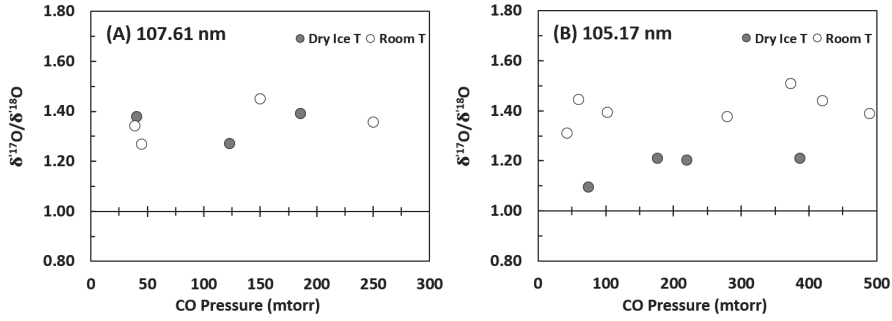

Figure 19. Variation of $\delta^{17}O/\delta^{18}O$ in different pressures (column densities) in CO photodissociation experiments. Data obtained from Chakraborty et al. (2012, 2018). The unshielded wavelength (107.61 nm; **Panel A**) and shielded (105.17nm; **Panel B**) produced similar slopes over a factor of e^{-5} difference in column density.

the difference in $\delta^{18}O$ is more than 1000‰. Their variation patterns (especially for $\delta^{18}O$) along with wavelength also differ. For the self-shielding models for the meteorites, a 10‰ error in isotopic variation will not account for the data and consequently the calculations themselves have an inherent error bar that has never been adequately discussed. It arises in large part from the assumptions that the cross section and light filtration accounts for all of the isotope variation, which is not substantiated. The second major problem which gives rise to more than a 1000‰ variation error is that the cross-section measurements at the isotope level vary the modeling results by this much simply because of the precision and accuracy of the ability to measure them.

For the self-shielding of carbon monoxide all parameters associated with photodissociation have been measured. The pressure, wavelength, temperature effects do not agree with self-shielding models, the only parameters that are variable. In the next section, further experimental and modeling results of relevance will be given that also show that the process cannot be applied to the solar nebula.

High resolution view of isotopic photodissociation

The foregoing section details the process of photodissociation of from experimental CO, O_3, CO_2 results and models for dissociation. The process of dissociation is complex as schematically illustrated in Figure 14. The process of the actual breaking of the bond following the intimal absorption of light involves a series of isotope selective process. The consequence if there is a filtration effect of the light source leading to absorption of light, this leads in most cases an excitation to another electronic state. The selection of the dissociation isotopic products occurs after this process. A consequence is that for models that utilize cross sections to calculate the dissociation do not incorporate these highly selective processes that are the largest measured isotope effects known. To quantum mechanically incorporate all of the processes shown in Figure 14, each step in the nuclear, electronic and time effects must be included and incorporated. The difficulty at the isotope level is that all of the spectroscopic factors and the potential energy surfaces must be known at high precision. For the molecules of interest and that have been measured, these have not been measured and consequently cannot be measured. For CO for example, the cross sections for several isotopic species have not been measured and must be calculated for some. The real problem however is that the cross sections do not incorporate the isotope effect as will be shown. It is possible that a unity $\delta^{17}O/\delta^{18}O$ slope may be obtained in a complex system where all processes are mixed together (in solar nebular or laboratory chamber photochemical studies), either by self-shielding or by a combination of various isotope effects. However, the CO photodissociation experiments imply that this is likely not be the case. We must understand the chemistry at an isotopic level in each step otherwise all modeling efforts embed large uncertainties.

To further our ability to interpret isotope results for photodissociation, the problem of the requirement of a suitable quantum mechanical model must be overcome. In modeling many kinetic atmospheric reactions, the rate constants are needed for more than 400 reactions. It is often the case that these are not all known and one then adopts a rate constant based upon another reaction that is demonstrably sufficiently similar that its rate constant may be used. For the consideration of CO dissociation, N_2 is isoeletronically the same as CO (Fig. 20) and all of its spectroscopic features and isotope lines have been measured. It is an ideal substitute for CO. Figure 20 shows the potential energy surfaces of these two molecules.

The first full treatment of dissociation process at the isotope level was done by Muskatel et al. (2011). The dissociation does not occur from the ground state. The dissociative surface in each case is shown in Figure 20 by the golden line. When an electronic crossing to this state occurs, it dissociates as it is an unbound (repulsive) as compared to all of the other states which are bound (Rydberg and valence). Valence and Rydberg states for a given molecule refer to different bonding characters of the excited state. A Rydberg state, in general, refers to the energy of an excited state for a given atom separation that moves a single electron away from a core

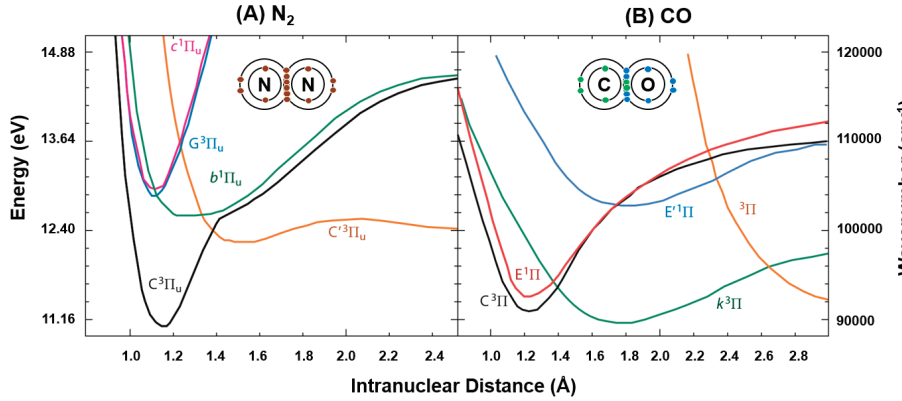

Figure 20. Schematic potential energy surfaces of (**A**) N_2 and (**B**) CO. The two molecules are isoelectronic with one another, as shown by the schematic electronic structures of two molecules embedded in the figure. Modified from Thiemens et al. (2012).

electronic structure. A historically interesting review of Rydberg states is given by Mulliken (1964). The valence state is an excited energy state that may be of the same energy as a Rydberg state, but its chemical bonding character is different that the Rydberg state (Lefebvre-Brion and Field 2004). The bonding is generally weak and the shape of their potential energy curve is shallower and the distance scale of the chemical species is further apart. Given that these electronic states are of the same energy, but different bonding character, the states may cross between each other. The valence state, e.g., in nitrogen is the state that leads to the crossing to the repulsive surface (dissociation) and as Muskatel et al. (2011) discuss the valence state is the gateway state to dissociation. However, it is not connected to the ground state by absorption of energy and it is only by coupling to the excited Rydberg state that initiates the dissociation process. In the first step of the Rydberg states have a force constant and atom-atom separation is highly effective, which is known as a Franck Condon region. Following access to this state, it may cross to the valence state, a highly selective process, and then dissociates. In the first step of the process in both cases it is the same. For nitrogen for example the ground state absorbs a photon and goes to the excited states $G^3\Pi_u$ and $c^1\Pi_u$. There are multiple embedded states that mix. It is in this step that crossing to the gateway valence state and exit to the dissociation state there is a very high selectivity occurring. The probability of crossing from one energy surface to another (diabatic crossing) is a very specific process as the energy (vibration and rotational) levels between the two states must match. As discussed, these also have isotopic lines associated with them. The consequence is that the energy levels are very sensitive to the energy separations and must match and this then selects which isotope lines are most closely aligned.

Muskatel et al. (2011) calculated the selection processes between states by solution of the Schrodinger equation for both the electronic and nuclear motions of the Rydberg and valence states as well as the time dependence and observed strong and selective isotope effects in the N_2 predissociation step. Figure 21 is schematic diagram showing the alignments between states of differing symmetry and isotopic composition. In the Σ symmetry (Fig. 21a), the red (b′) and black (e′) curves overlap at the left side of the surfaces. In the close up, the $^{14}N^{14}N$, $^{14}N^{15}N$, $^{15}N^{15}N$ lines are shown and for the mass range of 28–30 amu. The same is shown in the ∏ symmetry (Fig. 21b) for different parts of the energy surfaces. In the Σ symmetry, the overlap is for e′(0) and b′(18) levels, and in the ∏ symmetry, the overlap is for b(5) and c(o) levels. For $^{14}N^{15}N$, there is an essentially exact resonance between b(5) and c(o) levels in the ∏ symmetry, as highlighted by a yellow shaded area in Figure 21b. These crossings facilitated by the shift of vibrational states resulted from isotope substitution are the ones that access the gateway valence state for

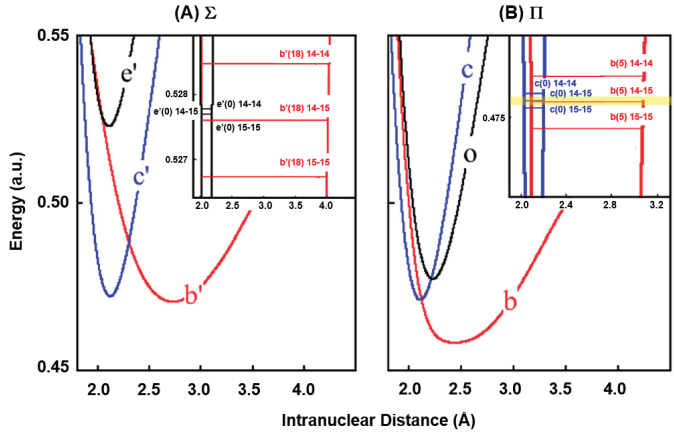

Figure 21. Schematic potential energy surfaces of N_2 excited states of (**A**) Σ and (**B**) ∏ symmetry. The resonance of $^{14}N^{15}N$ at c(o) with b(5) states is highlighted by the **yellow shaded area**. Modified from Muskatel et al. (2011). The overlap between the electronic states and their isotopic lines is required to cross between surfaces. Greater overlap leads to enhanced crossings between states.

an isotopologue to dissociate. It is this feature that gives rise to the isotope effect seen for CO in Figure 18. At 105 and 107 nm the CO excitation states (Fig. 17) are similar to the ones for N_2 shown by Muskatel et al. (2011) (Fig. 21) and follow a similar path to dissociation. At different wavelengths different electronic surfaces are accessed and the fractionation effects differ. The model is applicable to the CO_2 dissociation process shown in Figure 15. The significant changes in oxygen isotope effects for CO_2 molecules substitution of ^{13}C for ^{12}C derives from the shift of vibrational rotational lines as shown in Figure 21. This fits the concept of isotopic selectivity in dissociation, but not self-shielding. We do not attempt to completely preclude the self-shielding isotope effect in an optically deep photochemical column, but we argue that isotopic selectivity during predissociation plays a pivotal role in explaining many features shown in photodissociation experiments and must be included which it presently is not. Figure 19 showed that for over a 2 order of magnitude range in CO pressure the $\delta^{17}O/\delta^{18}O$ remained constant where one expects a change in that ratio for shielding. Existing experimental results unambiguously suggest that the isotope effect is sensitive to wavelength due to perturbation in predissociation rather than pressure due to self-shielding. A larger variation of pressure (column density) may be carried out in future experiments to further verify this interpretation.

The final test of the isotopically selective dissociation effect was N_2 photodissociation experiment carried out by Chakraborty and colleagues (Chakraborty et al. 2014, 2016). Using a modified version of the synchrotron experiment for CO, N_2 was photodissociated. Wavelength and temperature dependency were done and repeated to test models. The results (Fig. 22) show that there is a massive isotope effect at the wavelength expected from the gateway isotope selective process model by Muskatel et al. (2011). The room temperature curve (red) appears to be small, but in fact varies between more than 100‰ to above 2000‰. A very strong temperature effect is observed and at the otherwise same conditions. Lowering the temperature causes the effect to increase from 2000‰ to 12000‰. The only effect for this change is at the rotational level, and is a decrease in the line width of the rotational lines (making them sharper) and a lowering in the population of higher rotational levels. This makes the crossing even more sharp and selective but would not alter self-shielding. The experiments have been duplicated and beam profiles known as are the relevant non-adiabatic processes.

There is another important facet of Figure 22 that is significant and was a specific test of the curve crossing model. At 90 nm (111,111 cm^{-1}) there is an extraordinary enrichment in ^{15}N observed. The choice for this wavelength was specifically focused on a wavelength that would underline the crossing effect on the isotope process. The calculated and experimental comparison of the N_2 dipole moments across wavelengths were determined by Spelsberg and Meyer (2001) and shown in Figure 23. Comparison of the experimental and observed dipole moments in Figure 23 shows that at 111,111 cm^{-1} (90 nm) exhibits disagreement between experimental and calculated dipole moments (shaded area). The dashed lines are cuts through the potential energy surfaces and show that the most diabatic crossings occur here and thus be a perturbation not captured by models must be the source of the disagreement. It also would be the region where the most diabatic crossings would simultaneously occur and differ from other wavelengths. The selective crossings and multiple pathways should produce greater access to exit channels. The largest isotope effect would occur at this specific wavelength, as observed (Fig. 22). The isotope effect observed at 111,111 cm^{-1} by the enormous enrichment and may not be attributable to experimental errors as the value was highly reproduced by replicated experiments.

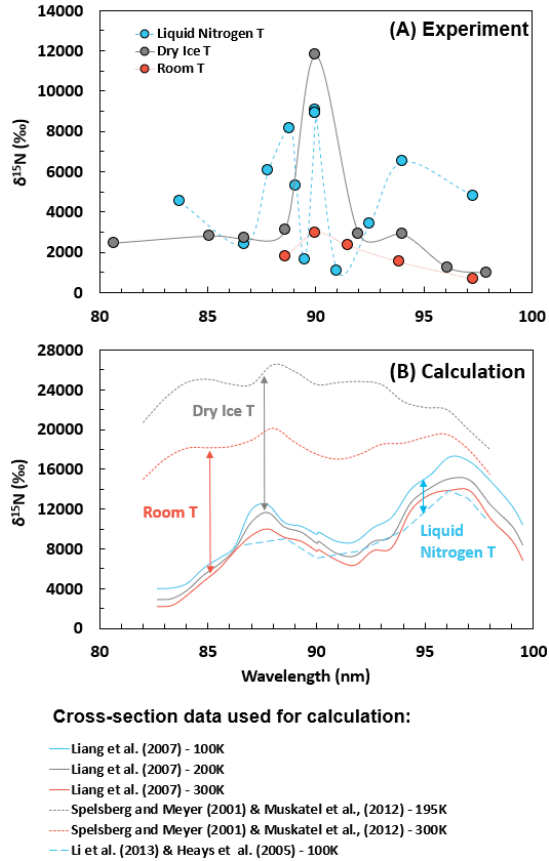

Figure 22. A result summary of N_2 photodissociation experiments. Data from Chakraborty et al. (2014, 2016). **Panel (A)** shows the enormous change in isotope ratio with only a change in temperature. All other parameters are exactly the same. **Panel (B)** shows calculated self-shielding effects expected for the experiments. No assumptions are made. It may be seen that shielding does not account for the data. It also shows that if everything is held constant and the different published cross sections are used there is a variation of nearly 10,000‰. This is in fact the error in the shielding calculation.

Self-shielding final test and errors

There are two final tests of the self-shielding model. First is shown in Figure 22b. A self-shielding model was used with three different sets of N_2 isotopic cross sections (Spelsberg and Meyer 2001; Liang et al. 2007; Muskatel et al. 2011; Li et al. 2013; Heays et al. 2014) to compare both with one another and determine how the best cross sections available differ in self-shielding results and how they compare to one another (Chakraborty et al. 2014, 2016). This is a measure of error of the models. Nothing was changed except the cross sections. It is observed that in this internal test of shielding with everything constant except application of isotopic cross sections from three groups that the difference may be as large as 20,000‰! The best comparison shows that the disagree by 1000‰. This observation is a clear demonstration of the best that a shielding model can do given the error associated with measuring cross sections. To apply a self-shielding model over a range photolysis experiments and ascribe to or not from self-shielding one would need an error of 10‰ or less to test the slope variation. In the case of CO, the cross sections, especially for $C^{17}O$ are not all experimentally determined as for N_2 and the error may exceed 1000‰, even for a simple model. In the CO self-shielding models none of the published plots show error bars.

Finally Figure 22 is a recognition that the large isotope effects are post photon absorbance. The plot shows experimentally determined isotope effects in the dissociation curve crossings and the massive peak at 90 nm (Fig. 22) is where the effect of curve crossings is a maximum (Figs. 21 and 23) that is not captured in any of the self-shielding models. This is further confirmation that the isotope effect of dissociation is post absorption. Any model reliant upon only cross section may not capture the actual dissociation process and isotope effects (Fig. 22b). Theoretical and experimental determination of a highly accurate and precise cross sections at the isotopic level is vital.

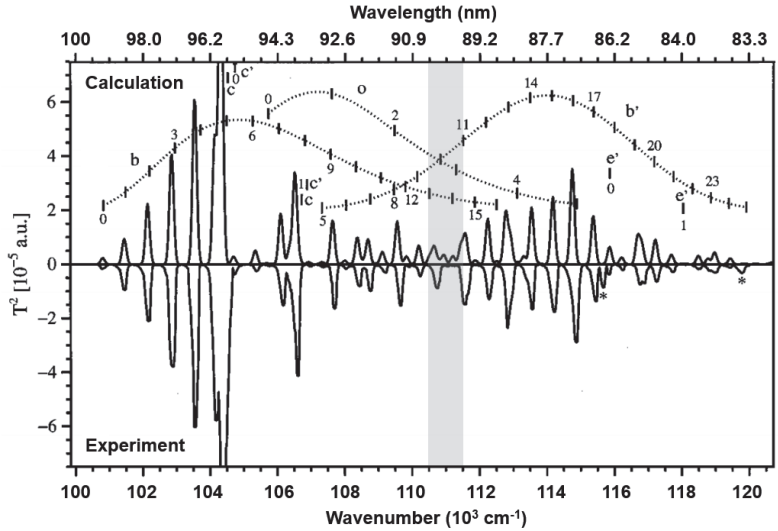

Figure 23. N_2 dipole strength distribution (**solid lines**). **Dotted lines** are slices through electronic surfaces of excited electronic states. The disagreement between experimental and calculated results at 111,111 cm^{-1} (90 nm) is highlighted by a **shaded area**. Modified from Spelsberg and Meyer (2001). This area is where the three different states come closest and perturbation of one state upon the other should be the greatest. The prediction was that this should show the largest isotope effect. This is clearly the case as shown in Figure 22a.

Nebular fate of water and water ice from photodissociation

Most astronomical photochemistry occurs on the edges of proto nebulae or large molecular clouds. In all self-shielding models for oxygen isotopes in meteorites, the product oxygen atom is trapped as water ice and is the molecular species that converts by an undefined chemical mechanism into silicates following the intact transport across the nebulae. Ice occurs in this environment predominantly on grain surfaces. Not considered in the models is the issue of water ice stability during its nebular traverse or immediately following its trapping on a grain surface. As a first consideration is survival of the oxygen isotopes of ice formed in the presence of the stellar UV field that photolyzes the parental CO at 105 nm as H_2O ice also photo decomposes.

In a review paper of photodissociation and photoionization of astronomically important molecules, Heays et al. (2017) have reviewed the fate of water in the background UV field (Fig. 24a). The water absorption spectrum is shown, and it is observed that the cross section for water has a rich and strong absorption spectrum in the region of 105 nm (Fig. 24b). The UV absorption of water is competitive with that of CO (Fig. 24c), and consequently the stability of water ice in a catalytic chemical environment must be considered. Besides being dissociative at the same region where CO occurs, the water spectra and dissociative process has an onset at 190 nm and consequently is dissociative over a larger wavelength range. From the spectra shown in Figure 24a, one expects with increasing UV output towards

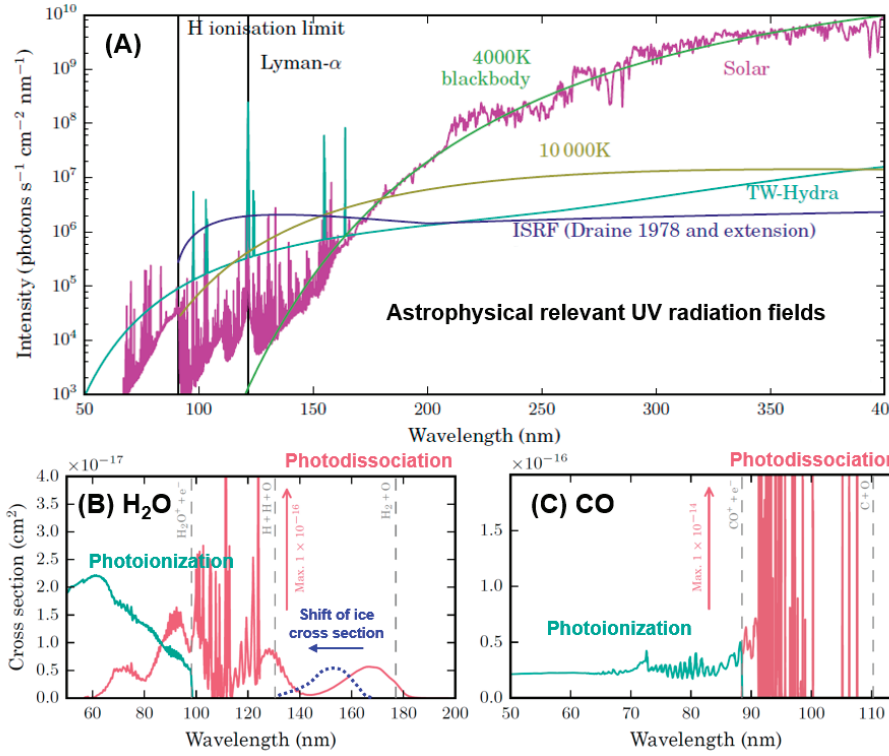

Figure 24. **(a)** Background UV fields relevant to the solar system. **(b)** Cross-section of H_2O vapor. The shift of H_2O ice cross-section is schematically shown in the ca. 140-180 nm region as a **blue dashed curve**. **(c)** Cross-section of CO. The wavelength for CO isotopic self-shielding is at 105 nm and compared to water that is assumed to be the stable host of the oxygen anomalies that will produce CAI. Modified from Heays et al. (2017) and van Dishoeck et al. (2013).

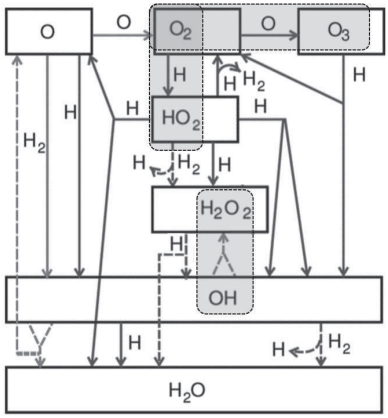

Figure 25. Schematic diagram defining the reaction network leading to the formation of water ice which is in nearly all cases on a silicate surface. The reactions that have been demonstrated to acquire mass independent isotope effects are highlighted by shaded boxes. Modified from van Dishoeck et al. (2013).

longer wavelength increasing the probability of water dissociation at 190 nm. Due to the photodissociation of water, the repository molecule from self-shielding is clearly not stable in regions with strong UV radiation. The storage of the anomalous oxygen isotopes from CO shielding was hypothesized to circumvent the exchange issue raised by Navon and Wasserburg (1985) and Kaye and Strobel (1983). The ice storage is nearly exclusively of grain surfaces initially. If the formation of water ice was in the outer edges of the solar system where CO photodissociation occurred, water ice then has to be considered stable and the oxygen isotopic composition maintained until it transfers from the outer edges of the solar system to the inner solar system where it becomes incorporated into a silicate and unfractionated by the chemical transformation process. The model across this many AU requires zero secondary alteration of the water ice. Figure 24b shows the cross section of H_2O ice compared to H_2O gas. The difference is wavelength shifted only ~20 nm which places it in the region of UV field for CO and H_2O photodissociation and consequently water ice is not stable. Amorphous or crystalline water ice undergoes undefined photodissociation.

To solve these issues, Young (2007) considered the transport and formation rates of water ice in a box model and showed that the conversion of CO to water ice was on a time scale of 10^5 years, and the transport from the disk surface to midplane between 10^5–10^6 years. It was suggested that the buildup of water ice could have been in the midplane where UV radiation was not as strong as the disk surface, and the isotopic composition of water ice in the midplane at ca. 20K could be well preserved. A spatially sophisticated disk model simulating water vapor distribution in protoplanetary disks shows rich water directly beneath the photon dominated region of the disk (Du and Bergin 2014). Recent observations by ALMA (Atacama Large Millimeter/submillimeter Array) on the protoplanetary disk of the young star V883 Ori also reveal that water ice accompanied with complex organic molecules can even exist in the photodissociation region of the protoplanetary disk (Lee et al. 2019). These however are not isotopic measurements and do not include the effects of radial distance reprocessing that occurs in transit the dark cold region.

Although there are observational and computational evidences that water ice is not completely unstable in the protoplanetary disk, water ice dissociation processes in the radiation field that CO dissociates, which occurs on surfaces of many bodies in the outer solar system (Johnson and Quickenden 1997; Watanabe et al. 2000; Yabushita et al. 2008), remain a critical factor to consider, especially at an isotopic level. On icy satellites for example, water ice photolyzes and at temperatures above 20K the recombination to water is slow and the $H+H \rightarrow H_2$ reaction on a surface dominates. The hydrogen is lost from the system by diffusion and Jeans escapes. The sticking coefficient is low and amplifies H_2 loss and oxygen remains as

either an oxidant of reduced species, or formation of O_2 and OH. The OH is spectroscopically observed and it too has a large photo destruction cross section at 105 nm. It has also been observed that the D/H of the residual water is enriched and the oxygen isotope ratios should also be affected. The photolytic of production of H_2 also is consistent with the observation of vibrationally excited H_2 ($\nu = 5$) by sensitive multibeam microwave detection systems (Green et al. 2009). The chemical dynamics of the H and OH on surficial ice has been modeled for amorphous and crystalline ice (Andersson et al. 2006; Al-Halabi and Van Dishoeck 2007). It is also well known that water ice on grains as a consequent of the UV and IR radiative fields desorbs thermally, adding to its instability (Fraser et al. 2001). Another factor not fully considered in models at the triple oxygen isotopic level is the actual process by which the water is actually formed during deposition on the grain surface as ice that may be photodissociated. It is the pseudo steady state of water formation and dissociation processes that leads to the "stability" of water ice in the protoplanetary disk. The process is highly complex and is not a single step, rather many other processes are involved in the steady state radiative environment. Figure 25 illustrates the complexity of the process. It should be noted that the transfer of the atomic oxygen from CO photodissociation to the ice there are many intermediates that includes reactive free radicals (OH, O, HO_2) which may react either with surrounding reduced species in the gas phase or with the surface itself. Note also that there is a buildup on the surface of ozone which results in the mass independent isotope effect and, loses the original isotopic composition as discussed. $O_2 + H$ and $OH + OH$ reactions shown in the Figure 25 also produce mass independent isotope effects in H_2O_2 (Savarino and Thiemens 1999; Velivetskaya et al. 2016, 2018), which is likely driven by symmetry similar to the $O + O_2$ reaction. If there is hydrogen leakage from the system, then the water ice will derive its mass independence from the water by way of ozone and not self-shielding. The mass dependent and independent isotope effects in these processes are not included or not fully considered in many models. Dominguez (2010) modelled some of these reactions and predicted $\Delta^{17}O$ of molecular cloud H_2O to be ca. 20‰ without considering any CO self-shielding effect.

At steady state, besides the formation of ice and the photo destruction of the water vapor and ice, there is also the loss of ice by sublimation (or thermal desorption) that can occur between 10 and 30K when involved in ice complexes with CO ice (van Dishoeck et al. 2013). Temperatures below those considered a safe haven for ice in nebular self-shielding models. Adding to the complexity of the water system is the adsorption of CO onto the ice surfaces to form formaldehyde (H_2CO) which is stable and also desorbs from the system (Noble et al. 2012), likely fractionating the residual water ice from which it was synthesized. Carbon monoxide adsorption on the surface of water ice grains is in steady state equilibrium between adsorption and removal by sublimation and photochemical desorption. The process has been studied in great detail and e.g., using isotopically (^{12}C,^{13}C) labeled CO layer have detailed the process and shown it occurs via an indirect sub-surface process (Fig. 26), which is heavily suppressed in the CO–H_2O ice (Bertin et al. 2012). The water and CO ices are also the progenitor of interstellar methanol (CH_3OH), which may be linked to grain formation and subsequent chemical processing is significant (Fuchs et al. 2009) and will be discussed in the next paragraph. The chemical and physical altering of the water ice and formation of new molecules is known to be an agent of catalytic chemical production in the interstellar environment. Young (2007) carried out a relatively large astrochemical reaction network (>500 species and >7600 reactions) to consider these reactions and showed that these side-reactions would not influence the isotopic composition of the large water reservoir. A limitation is that all reactions are presumed to be mass-dependent by estimating reaction rates of isotopologues using reduced masses for collisions between reactants. As shown in Figure 25, there are several mass independent reactions even in a relatively small reaction network. It is clear that the role of these well-known and other unidentified reactions that may lead to significant mass independent isotope effects in a much more complex reaction network should be carefully evaluated.

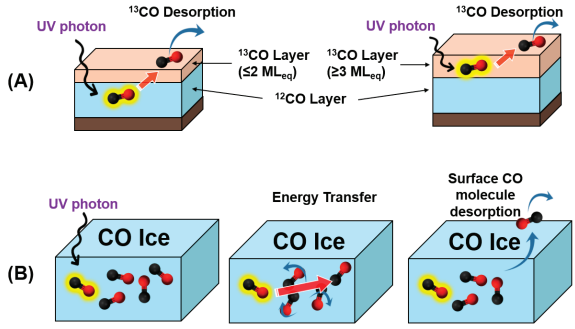

Figure 26. **(a)** Schematic diagram of the CO ice photodesorption experiment (Bertin et al. 2012): By labeling the top layer with ^{13}CO (with varying thickness), the authors found that the desorbed gaseous CO is always from the surface layer of CO ice (< 2 monolayer equivalents for CO, ML_{eq}). A synchrotron monochromatic beam was used in the experiment. **(b)** Proposed scheme of the photodesorption mechanism: CO molecules in the subsurface of CO ice were excited to its $A^1\Pi$ state by UV photons, and the energy is subsequently transfer to the neighboring CO molecules. The CO molecule in CO ice surface is ejected after receiving enough energy. Modified from Bertin et al. (2012).

The fate of water ice in different astronomical environments is highly complex and there is a rich literature on observations in molecular clouds, proto stellar environments, cold and warm. There are relevant laboratory experiments that help define the role of all contributing processes. This includes the chemistry rates for the reactions shown in Figure 25 as well as photo and thermal desorption, ice properties of crystalline and amorphous ice, photo destruction and chemical reactions within the ice (van Dishoeck et al. 2013), especially the interaction between H_2O and CO to form CH_3OH as outlined earlier. Many of these processes have been defined by laboratory measurements and models of satellite interferometric observations of D_2O/HDO in ice in protosolar cores (Furuya et al. 2016). The measurements show that the D_2O/HDO ratios are not that expected by simple ice formation and require secondary chemical evolution to account for the observations. The processing is schematically shown in Figure 27. The models and application of the isotopic fractionation process show the formation of a water ice layer from stage 1 and the layer of pure water ice with a lower D_2O ratio than HDO, to the second stage with a chemical evolution and associated fractionation associated with all of the processes mentioned above and re-partitioning of the deuterium (Furuya et al. 2016). This is further evidence that storage in ice is not stable and the processes of formation/sublimation and chemistry within the ice is substantial and interactive with the surrounding gas during transport. The hydrogen isotope effect also provides observational constraints for testing the validity of current models that have already considered isotope effects. Most of the individual contributing factors have been described in the literature (Johnson and Quickenden 1997; Watanabe et al. 2000; Fraser et al. 2001; Andersson et al. 2006; Al-Halabi and Van Dishoeck 2007; Yabushita et al. 2008; Bertin et al. 2012; Noble et al. 2012; van Dishoeck et al. 2013).

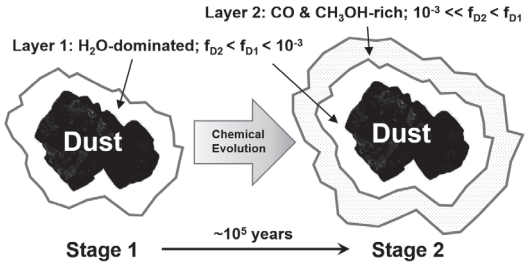

Figure 27. Schematic diagram showing the formation of H_2O-dominated and CO and CH_3OH-rich layers on grains that significantly influence the partitioning of deuterium. Modified from Furuya et al. (2016).

With the ability to use satellite data, our understanding of these processes has advanced greatly. Using the far infrared spectrometer on the Herschel Space Observatory it was possible to use the emission lines from the cold water vapor around the young star TW Hydrae to map out the distribution of ice (Hogerheijde et al. 2011). The authors being mapped the water/ice lines and the observations amplify understanding of the processes associated with ice formation. The emission lines are measured and derived from the cold water vapor associated with the ice coated dust grains at the edge of the disk. In Figure 28a the number density of H_2 is shown in a cut through the protoplanetary disk, and Figure 28b is the associated thermal structure. Note that the blue contours in Figure 28b is the layer of maximum water vapor concentration. Figure 28c is most important as it shows logarithmic variation of the water molecules/water ice. The equilibrium between the photodissociation of water to the photo desorption of water providing an equilibrium water column (Woitke et al. 2009; Hogerheijde et al. 2011) even though it is well below the freezing point of water. It is not until deeper into the disk that the temperature is lower and the amount of photons become too low for photo desorption to occur. Figure 29 shows the effect of photons on water/ice number density distribution in a cut of a solar nebula and a component of the equilibrium (Bethell and Bergin 2009). The self-shielding in this case is not for CO or isotopes but rather the effect of water opacity on its own gas/solid phase processes. The left panel is the complete consideration which includes its self-shielding of photons.

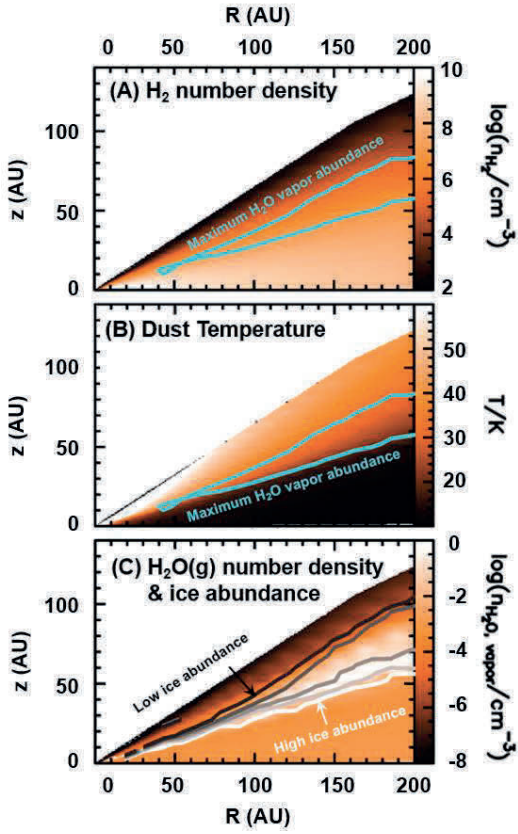

Figure 28. Distribution of **(a)** H_2, **(b)** dust temperature, and **(c)** water vapor and ice in the TW Hydrae protoplanetary disk. Modified from Hogerheijde et al. (2011). It is to be noted that there is a significant amount of water vapor into the nebula before it is effectively made into ice.

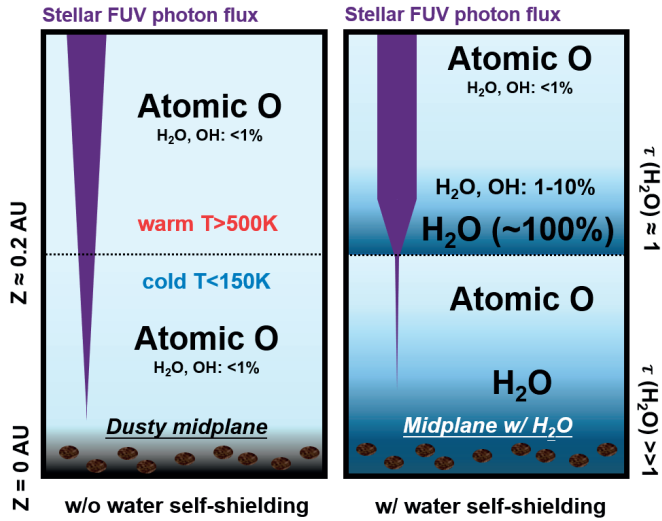

Figure 29. Schematic diagram showing the effect of H_2O self-shielding on distribution of H_2O in solar nebular. Modified from Bethell and Bergin (2009).

In the upper layer there are sufficient photons to photodissociate water and deeper in there remains water but less dissociation due to the decrease of photons. These observations somehow support the theoretical prediction (e.g., Young 2007; Du and Bergin 2014) that water may be "stable" in some region of the protoplanetary disk. However, it does show although the isotopic composition of the ice reflects the CO dissociation process in any way and that requires most importantly, experimental data of ice photochemical processes for all oxygen isotopes and, across all relevant wavelengths.

There are aspects of the grand titration associated with the transport of the $\delta^{17}O = \delta^{18}O$ ice and reacted with nebular CO to form secondary products to consider. This includes, but not limited to (1) the solar nebula is turbulent; and (2) the ice preserved must be formed and transported intact. Ciesla (2014) has provided an analysis of the fate during formation of ice and its cycling in the environment and subsequent transport. The work shows the difficulty from effects of nebular diffusivity, different temperature regimes, gas densities, chemical compositions and photons. Ciesla (2010) discuss the turbulence of the nebula as a significant driving force in condensation. The requirement is that the ice particles before doing the titration to form the many meteorite classes with the preserved is that ice oxygen isotopic composition must survive intact for 10^5–10^6 years and transported through the different regimes totally intact. Indeed, Young (2007) considered both chemistry and vertical/radial mixing and showed that the transport of the $\delta^{17}O = \delta^{18}O$ water ice produced by CO photodissociation and self-shielding from the disk surface to midplane is on a time scale of 10^5 years. Furuya et al. (2016) however showed that the chemical evolution of water on grains that may lead to additional isotope effects could be less than 10^5 years (Fig. 27). These reactions have been considered by Young (2007) as mass dependent reactions. Nevertheless, potential mass independent reactions shown in Figure 25 remains not well considered. Whether such reactions significantly alter water triple oxygen isotopic composition is an open question and needy of relevant experimental work to progress. Dominguez (2010) has suggested that $\delta^{17}O = \delta^{18}O$ water could have been produced without any CO self-shielding effect if some of these mass independent reactions are considered. The sum of the foregoing discussion is that the fate of water formed from self-shielding might not be an isotopically stable reservoir due mostly to ice photolysis and subsequent complicated chemical reactions accompanied with isotopic partitioning. A much more comprehensive

reaction network that consider all possible mass independent isotope effects is needed. As will be discussed, the oxygen isotopic composition of the meteoritic oxygen isotopes places stringent limits on the source of oxygen and how much it may vary from secondary alteration.

Summary

In the foregoing sections the development of the theory and understanding of the triple oxygen isotope chemistry in chemical recombination reactions and photo dissociation have been discussed. Much of the discussion has centered on the oxygen isotopic record stored in the meteorite record and consequences for understanding the earliest formation processes in the solar system. The basic physical chemical principles apply to all processes on earth as well and molecules that have isotopic compositions thought to derive from photochemical shielding. The experimental and theoretical chemical, photo and quantum mechanical basis since the discovery of the mass independent isotope effect (Thiemens and Heidenreich 1983) have advanced considerably and have aided in providing a mechanistically better understanding of these processes in nature. Though not relevant to this special issue, the understanding of the Archean processes using sulfur isotopes have been included in this developmental process. For meteoritic oxygen isotopes the discussion has led to basically two fundamental physical chemical processes: dissociation and bond formation.

The intrinsic effects associated with CO self-shielding and the total steps render it unlikely. First, the isotope effects associated with the bond breakage process do not coincide with observed experiments. Secondly, following photolysis, a dissociation effect is immaterial as the reaction that leads to the formation of the solids containing oxygen will eliminate the isotopic record of the shielding in the short-lived transition state of the combination reaction. The consequence is that the most important step in the formation of the solar system, the gas to particle conversion process creates a new isotopic signature that is based upon this step exclusively. The fractionation produces a $\delta^{17}O = \delta^{18}O$ composition in the condensates (Fig. 5). This is consistent with both contemporary experimental and physical chemical theory.

Another uncertainty arises from the inability to store the isotopic anomaly in a species that is stable such as water ice. The assumption is that this ice species will retain the signal of self-shielding, at thousands of ‰ enrichment with near perfect equal ^{17}O,^{18}O enrichment requires transport from the outer edge of the nebulae to the region where it will melt, evaporate and transfer to the local reservoir where it first produces a CAI condensate. Relevant chemical mechanisms are proposed and incorporated in the models for this process, but are significantly incomplete, especially for a thorough consideration of the associated isotope effects across wavelengths. Experiments are required to support the envisioned scenarios. Large oxygen isotopic anomalies of Fe_3O_4 in new-PCP from one meteorite may originate from other sources and may not be a sufficient evidence to reconstruct the isotopic composition of water in the protoplanetary disk. This issue will be further discussed in the next section.

Most importantly, non-CAI components comprise >99 % of solar system materials: the bulk meteorite compositions (Fig. 30). The basic premise is that there are varying mixes between a presumably single valued ice and an inner nebular component. The isotopic difference of two reservoirs are hundreds of per mil. This model for example requires that one mix a component of heavy isotope water ice that survives the transport and mixes it with a titration precision so tight that one can differentiate between eurcrites and diogenites at −0.24‰ and Angrites at −0.04‰! The same is true for all of the features shown in Figure 30. The titration must capture the difference of a 1 to 2‰ between difference between the ordinary chondrites (H, L, LL) and also the original $\delta^{17}O = \delta^{18}O$ CAI line, all in a turbulent environment and on a short time scale. Alternatively, if the small difference among these materials is interpreted as a “noise” during mixing, the overall small variability of oxygen isotopic composition in all planetary materials that formed over a large distance in the disk implies an extremely thorough mixing on a large spatial scale. Large temporal and spatial variabilities of water isotopic compositions (hundreds of per mil) were however shown in models that carefully considered vertical and radial mixing.

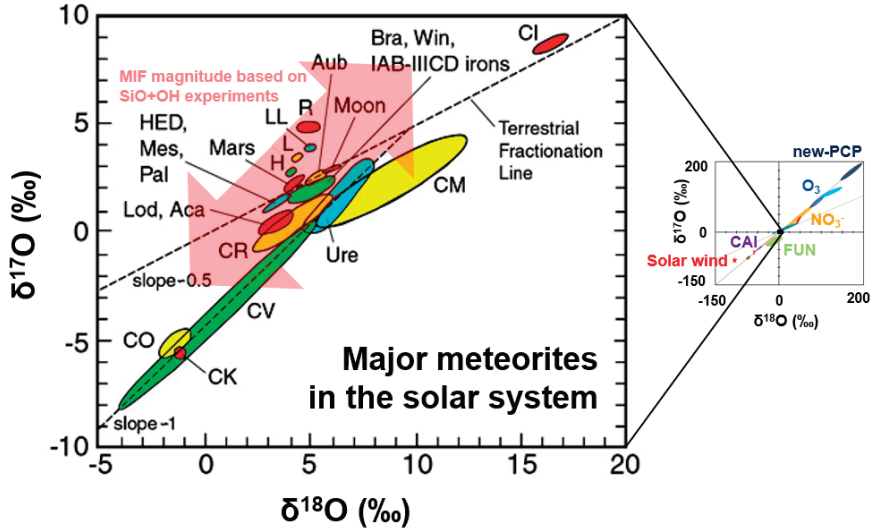

Figure 30. Triple oxygen isotopic composition of the solar system. **Left panel:** The close up of major meteorites in the solar system. Adapted and modified from Northern Arizona Meteorite Laboratory. **Right Panel:** A scaled-down version of Figure 16. Note that with Bulk earth as a starting composition, the formation from the SiO + OH reaction includes nearly all meteorite types and requires no mixing except for the back mixing of CAI which are <1% of the mass and of no influence to the bulk of the solar system (see discussion in Section "*A New Model for Triple Oxygen Isotopes, Meteorites, and the Origin of the Solar System*"). In a self-shielding and mixing model, all of the individual classes require very precise mixing on an ice far outside the figure at very high positive enrichments and of contestant value with a reservoir that is far outside the figure in the third quadrant near $\delta^{17}O = \delta^{18}O = -50‰$ or even farther. The mixing and conversion of the ice to solid must be sufficiently precise to account, e.g., the differences between the H, L, LL, and R chondrites. That process also assumes no isotope effect in the gas to particle conversion.

A requirement in the transport phenomena and concomitant photochemical, nebular dynamical processes is for the $\delta^{17}O = \delta^{18}O$ source to be derived from self-shielding. This fractionation process only occurs in a restricted optical region of the actual shielding zone at a given time, and at greater optical depth ^{18}O becomes opaque and ^{17}O is selectively dissociated (Fig. 6). At low opacity, there is a range in $\delta^{17}O/\delta^{18}O$ between 0.5 and 1.0, with no effect at the shortest depth. In additional, the product must be transported intact to the zone of condensation as discussed earlier. These processes have been modeled and suggested to be plausible, though actual isotope effects in the reaction network are not comprehensively characterized nor include relevant fractionation processes.

Even all problems outlined above can be overcome, there are final photochemical requirements. There are built in assumptions in the basic photochemical spectral requirements not discussed but required is in the CO absorption process. The slope one is only be attained if the **cross section σ and quantum yields for ^{16}O, ^{17}O and ^{18}O are exactly identical and their absorption lines are well separated**. As shown in Figure 22 a difference in experimental measurements of σ magnifies to more than a factor of 1000‰ in the product of photolysis due to the exponential $e^{-\sigma cl}$ absorption relation and, the large differences in the isotopic abundances in ^{16}O and $^{17,18}O$. No error bars including this effect for CO have been reported. The issue is amplified if an isotopic line must be calculated, this folds in another error which must be included. Finally, the likelihood that all cross sections are the same is limited by perturbations of the electronic states. The CO states at the 105 nm region (Fig. 17) are highly congested between excited states and perturbation is most probable at these wavelengths producing

anomalous cross sections. Box 1 is a summary of the outstanding issues concerned with self-shielding in the nebula and other environments. Some issues in Box 1 related to solid formation will be further discussed in the ensuing session.

BOX 1
SELF-SHIELDING PROBLEMS

1. There remain no experiments that provided clear unambiguous support for models of self-shielding, only the contrary.
2. The self-shielding models relies on unavailable high precision cross sections for the important minor species and must be calculated.
3. The error in self-shielding models is driven by the accuracy of the cross sections. For molecules of well-known measured lines, the error has been shown to be hundreds if not thousands of ‰. This is due to the difficulty of obtaining the cross sections for the minor isotopes.
4. The photochemical isotope effects in post absorption that lead to dissociation have been experimentally shown at self-shielding wavelengths to not produce the required isotope fractionation to explain any meteorite observations.
5. It has been experimentally and theoretically shown by different groups that the actual dissociation process is highly mass independent and does not retain the self-shielding record required for explaining the $\delta^{17}O/\delta^{18}O = 1$ line.
6. The storage of the oxygen anomaly irrespective of its isotopic composition in water ice is not retained. The cross section for water and ice water photolysis at CO shielding wavelengths is large and ice dissociates and loses its isotopic signature.
7. The ice must be transported over astronomical unit length scales through the protosolar nebula and be 100% stable.
8. Once the ice has been delivered to the site of creating a stable solid non ice product, there remains no step wise chemical mechanistic models to establish how this record is converted from ice to silicate or a perovskite species without any fractionation.
9. During the overall process, a highly precise titration must be done to add exactly the right proportions of an ice from beyond 20 A.U. to an inner solar system region for solid formation. This must be done in a way that creates the meteoritic class identities, that are statistically isotopically separable at a sub ‰ level. These reservoirs may be differing more than 1000, and the ice value must be assumed to be constant.
10. The ice that is created for the $\delta^{17}O = \delta^{18}O$ slope via shielding only arises from a slice through the optical region between no effect and where ^{18}O becomes opaque. There is no mechanism for how this 3-D slice is extracted from the turbulent nebula and transported intact.
11. The observation of mineral phases that are thought to represent reaction of ice of heavy isotope water composition with troilite to create Fe_3O_4 require the ice to be delivered with complete conservation of its original signature. The anomaly may simply be created in situ by the oxidation of troilite with OH from water that is the same composition of the bulk meteorite. It is the process itself that creates the anomaly and requires no transport or preservation. Relevant reactions are observed in atmospheric gases and solids as well as water.
12. The assumption of the starting point at as a solar value has not been validated by models. Recent models do not match Genesis isotopic or abundance measurements and conclude that the link between protosolar and photosphere has not been established yet. The assumption of the CAI point as being solar remains inferred.

SOLID FORMATION IN THE EARLY SOLAR SYSTEM

Simultaneous formation of the first solids and their isotopic anomalies

The final aspect is perhaps ultimately the most significant. Even if an isotopic anomaly does get captured in ice and heroically survives to arrive at the very highly restricted space and time required, it is a moot point. It is suggested that exchange of oxygen atoms in minerals between water at high temperature in the inner disk accounts for the anomalous oxygen isotopic compositions in planetary materials. If oxygen atoms in original minerals are normal ($\delta^{17}O/\delta^{18}O=0.5$), the final isotopic composition will superimpose a slope ½ species and a slope 1 may not be obtained, depending on the sizes of two reservoirs which restricts the process. Alternatively, the gas-to-particle formation step is the very first chemical reaction that occurred in the solid formation and should be included as it is one of the most significant steps in solid formation. As discussed in the section on ozone formation mechanism the well-known features of a gas phase reaction of any variety is that to proceed to a stable product there is a transient metastable state. During the combined process for collision of reactant molecules or atom–molecule, a transition state is formed that either stabilizes, or, re dissociates. In the reactions to be discussed, the ratio of stabilization to falling apart is approximately a million to one. For the mass independent ozone reactions discussed this time scale to be around 10^{-11} seconds. It is this process where the high selectivity that gives rise to the mass independent isotope effect. Indeed, the actual time scale to populate the states may be even shorter, which is on the order of 10 femtoseconds for N_2 (Ajay et al. 2018). The consequence of this is that irrespective of the anomaly being present in the ice, there must ultimately be a chemical reaction between that (or any) oxygen species that leads to a solid. That process proceeds through a transition state and eliminates the original signal on a 10^{-11} s time scale per reacting molecule. The consequence is that the critical factor for the meteoritic oxygen isotopes, the gas to solid formation process becomes of particularly important and controls the ultimate product. As shown in Figures 5a and 5b, the slope 1 line of CAI is identically produced in the $O+O_2$ reaction. In the ensuing years since that discovery as discussed in this paper and reviews (Thiemens 2006, 2019; Thiemens and Lin 2019), the mass independent isotope effect is now sufficiently documented to detail the process in the early solar system. The generation of the slope 1 is in the transition state and the isotopic symmetry/asymmetry control is the source of mass independent isotope effect. It is terminal position of $^{16}O^{16}O^{16}$ vs $^{16}O^{16}O^{17,18}O$ that ultimately produces the slope 1 effect. It is this factor plus the position of oxygen on the periodic chart that leads to oxygen typically coordinating other elements, e.g., SiO_4, SiO_2, Al_2O_3, Fe_2O_3, Fe_3O_4, SO_4, CO_3, TiO_3, TiO_4, NO_3, ClO_4, and PO_4 which encompasses a predominance of the geochemical minerals. During condensation and nebular conditions, the conditions are ideal for creation of the slope one effect in the earliest minerals as well as the bulk of the minerals. The symmetry effect is general and was noted in sulfur (Bainssahota and Thiemens 1989; Lin and Thiemens 2020) and has a qualitative quantum chemical explanation (Babikov 2017; Babikov et al. 2017). A massive effect has now been extended to the heavier mass range (titanium) and a massive effect has been experimentally proven by Robert et al. (2020) as shown in Figure 10. The mass independent effect of titanium isotopes was interpreted using a theoretical framework developed by Reinhardt and Robert (2018). According to Reinhardt and Robert (2018), the mass independent effect is not caused by isotope exchange reactions or differences in the interaction potentials. Using trajectory calculations and classical mechanics, these authors show that the complex lifetimes are different if the complexes are formed by reactions involving identical (e.g., $^{16}O^{16}O$) or non-identical (e.g., as $^{17}O^{16}O$) isotopes.

An important step is connecting the production of the oxygen anomalies to the gas-to-particle formation process. Though the role of symmetry for importance in the early solar system has been recognized since the first publication on the mass independent oxygen isotopes via chemical processes, a vital key to the next step is experimental observation in

a cosmochemically relevant process. The difficulty is that such experiments must be done in a system that insures gas phase reactions in a controlled manner. A first experimental demonstration of the production of a mass independent isotopic composition arising from such a chemical reaction was shown by Kimura et al. (2007). Using a high temperature (>1000 °C) flow system with precursor iron (from $Fe(CO)_5$) and Silane (SiH_4) in the presence of a third body such as He and with different oxidants, including O_2, H_2O and N_2O in the presence of an electrical discharge to produce reactive oxygen species, a mass independent isotopic composition was observed in the solids produced, with $\Delta^{17}O$ extending to greater than 4‰. This is consistent with prediction of a symmetry-based production mechanism for both Fe and Si. The products collected in this system have unreacted Fe and Si present which makes it impossible to state the magnitude of the effect and theory. Even for the well-studied ozone case state of the art quantum mechanically based models do not allow for determination of a single stage fractionation factor. The $\Delta^{17}O$ value of 4‰ is a lower limit.

In a more recent work, Chakraborty et al. (2013) used a laser-based ablation system to create controlled amounts of gas phase SiO and determine its isotopic fractionation to SiO_2 via O (O_2) and OH. SiO is the dominant nebular gas leading to the formation of the first condensates and subsequent ones leading to silicates. It is a key step in the very first formational processes in the solar system. In the experiments, pure SiO was laser ablated at 248 nm providing a reproducible number density of gas phase SiO molecules. Oxidants were provided as OH as this is a likely oxidant is the solar nebula. The results are shown in Figure 5c. In these experiments a mass independent fractionation is observed. As in previous experiments there are contributions from more than one reaction, however in this case all of the rate constants for relevant reactions are known and the isotopic contribution for a given reaction may be determined. Consequently, the mass independent component in the reaction network can be unambiguously extracted. The Figure 5c shows the contribution for the SiO + OH reaction, arguably one of the most likely early reactions in the solar system. It is seen in the figure that the slope one required for the meteorites is observed. All variables are known and clearly defined and thus the assumption for this as a mechanism for production of the meteoritic anomalies is consistent with the most recent physical chemical models for production of the anomaly and experiments. In the experiment, the H_2/O_2 ratio is significant to acquiring a unity slope as that ratio determines the production of OH radical in the laser system. In the solar nebular, if the SiO + OH reaction dominates the production of SiO_2 solid, a pure unity slope can be directly observed. A detailed chemical model quantitatively accounting for various SiO_2 production pathways is needed in the future. ***The take-away point is that the assumption that a reaction of mass dependent nebular species may produce a $\delta^{17}O = \delta^{18}O$ composition in a solid and is likely a meteoritic mineral precursor has been experimentally observed.***

It has been known since the classic paper of Grossman (1972) that a first condensate should be corundum at around 1758 degrees, followed by perovskite ($CaTiO_3$) and melilite. In each case the oxygen is in a position where a symmetry factor is relevant. The experiments of Chakraborty et al. (2013) show that the slope 1 effect is a feature associated with gas to particle conversion. It also shows that the effect arises and the original oxygen species in ice covered grains of shielding is lost. In the solar nebula this would suggest that the origin is near the bulk earth and Mars. In Figure 16, triple oxygen isotope composition of the putative self-shielding precursor water from self-shielding (Fe_3O_4 in new-PCP) is shown as well as different terrestrial species. In the model, water is brought to the inner solar system and reacts with troilite either in the pre-condensation of on a planetary surface. The probability of the water possessing the anomaly has been discussed in the previous section. It is stated that these are the heaviest isotopic enrichments in the solar system though stratospheric ozone extends to the same enrichment factors is not discussed. Sakamoto et al. (2007) suggested that the anomalous feature arises from the net stoichiometric reactions with either troilite or native nickel:

$$3FeS + 4H_2O \leftrightarrow Fe_3O_4 + 3H_2S + H_2 \quad \text{(R12)}$$

$$3Fe + 4H_2O \leftrightarrow Fe_3O_4 + 4H_2 \quad \text{(R13)}$$

In this reaction the water is presumed to lie along an extension to the end member somewhere in the outer solar nebula (as high as 1000‰ in $\delta^{18}O$) (Lee et al. 2008; Lyons et al. 2009) and reacts passing along the anomaly to the Fe_3O_4, which under the ambient conditions is the thermodynamically stable phase. The water $\delta^{18}O$ is presumably between 150‰ and 200‰. In the model of Lyons et al. (2009), the $\delta^{18}O$ value of water produced by self-shielding that is responsible for creation of the Fe_3O_4 is at approximately 200‰ (Fig. 31a). A difficulty is that the required isotopic composition ($\delta^{17}O = \delta^{18}O$) in water is not widely observed and the two lines (1: CO photodissociation line segments in which $\delta^{17}O/\delta^{18}O$ slope may not be one based on experimental results; 2: the $\delta^{17}O = \delta^{18}O$ line of O_3 formation that likely involved in the processes) converge for only a limited time. Even in a self-shielding model, for much of the time the $\delta^{17}O/\delta^{18}O$ ratio in product water is not exactly 1 (Fig. 31a). Furthermore, the ca. 200‰ for $\delta^{18}O$ of Fe_3O_4 in new-PCP (Acfer 094) is required to produce for a minute period of time in this model. Figure 31b further shows that the variation of ice along a hypothesized slope 1 line varies considerably. The $\delta^{17}O$ and $\delta^{18}O$ values depending on UV light intensity, radial distance and time varies from 0‰ to ca. 1000‰. To achieve the proper value for new-PCP of Acfer 094 at 200‰ it has been suggested there may be mixing of ice at different values must occur. At present measurements are too scarce to evaluate the variability induced by the mixing effect. Photodesorption is included as a factor but it is not stated how. The isotope effect and its wavelength dependence has not been measured for oxygen. Water photolysis is included but only as a rate of oxygen atom formation not isotopes. For the model to explain the Acfer 094 new-PCP measurements there are restrictions in mixing, radial distance, light intensity, time, isotope effects in water dissociation and mixing of ice proportions that may differ by hundreds to thousands of per mil to acquire the right isotopic composition of ice. Also not included directly in the models are the chemical reactions that actually produce the anomalous ice along with their isotopic fractionations or as discussed side reactions with e.g., CO. A significant point is that the chemical production of water is thought to occur on grain surfaces and proceeds by many reactions:

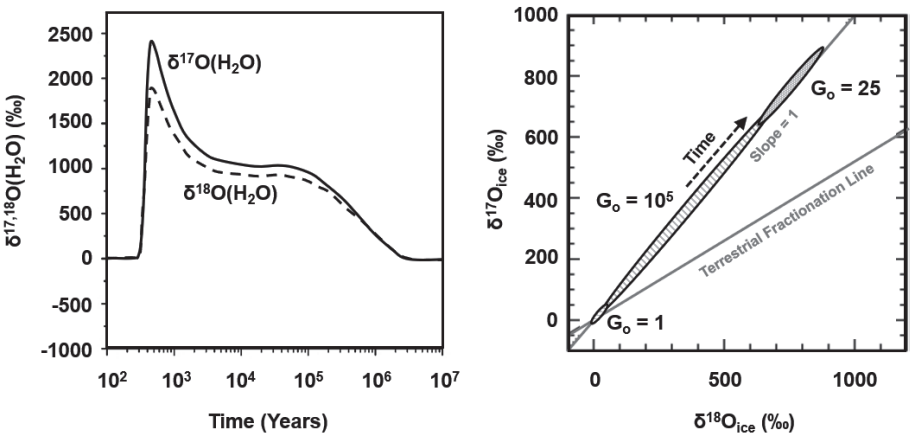

Figure 31. (a) Model results of time-dependent triple oxygen isotopic compositions of H_2O at 30 AU from the protosun at the disk midplane (Lyons et al. 2009). **(b)** Three isotope plot of H_2O ice at 125 AU from the protosun at the disk midplane simulated by Lee et al. (2008) with different G0 value, a parameter scaling the strength of the local FUV radiation field relative to the standard interstellar radiation field. Modified from Lyons et al. (2009) and Lee et al. (2008).

These reactions have been suggested by Tielens and Hagen (1982), Hasegawa et al. (1992), Cuppen and Herbst (2007), Nunn (2015). This reaction network to actually form ice will not necessarily store the shielding record in ice. Young (2007) did consider mass dependent fractionation processes in a relatively large reaction network in the self-shielding model, but the isotope effect was not treated in an isotopically relevant selective chemical reaction mechanism.

For the new-PCP results of Sakamoto et al. (2007) shown in Figure 16, the matrix of the material is shown near the origin in the triple oxygen isotope plot at the terrestrial fractionation line of the host meteorite Acfer 094, an ungrouped primitive carbonaceous chondrite (Fig. 30). To account for the data measured in the Fe_3O_4, the ice composition has numerous restrictions. Apart from the ice compositions, the aqueous alteration reaction is not well known. An analogy is serpentinization in which water reacts with iron-bearing rocks to form oxide, a mass dependent process. In this case, the oxygen isotopic composition of iron oxides is determined by oxygen in the large water reservoir. However, it is noted that the new-PCP are tiny grains. Elemental mapping suggests that most new-PCP grains are less than 7 μm^2, with the largest 160 μm^2 (Sakamoto et al. 2007). This is very similar to the observation of iron sulfate on terrestrial aerosols measured by NanoSIMS (Li et al. 2017), a reaction product of SO_2 and iron oxides formed in the aqueous aerosol surface of some 10s of nanometers. Therefore, water that directly reacted with carbonaceous chondrite to form new-PCP may not be a large reservoir, but potentially a thin surface layer. Therefore, an alternate chemically plausible to interpret the anomalous oxygen in the new PCP comes from heterogeneous reactions on liquid layers of terrestrial aerosols, as thoroughly discussed by Thiemens (2018). It is known that in such reactions, the isotopic anomaly from gaseous ozone is passed along from the 10 nm liquid water layer to the mineral surface. Most carbonate minerals on the Earth are isotopically normal due to their interaction with the large isotopically normal water reservoir. Shaheen et al. (2010) have observed that atmospheric crustal-derived $CaCO_3$ possess a significant mass independent oxygen isotopic composition ranging from 0 to more than 3‰ in $\Delta^{17}O$ (Fig. 7). The aerosols were collected as a function of particle size and observed that the sub-micron particles have the smallest value and the micron sized particle the largest. Laboratory experiments defined that the odd oxygen with isotopic anomaly from ozone or OH is transferred to the surface carbonate in the water-solid thin layer. The same scenario would occur on the troilite surface in the presence of the oxidizing water of isotopic composition of new-PCP in Acfer 094. It is well known that water on a surface such as FeS or FeS_2 undergoes dissociation via electron transfer reaction producing OH. This is the actual radical that oxidizes the reduced species and not direct reaction with water. A recent paper has performed a density functional theory/plane wave calculation for pyrite. The initial step of the surface, which will be the case for troilite is that the two Fe(II) sites on the surface react with water and produce Fe(III)–OH^- (Dos Santos et al. 2016). This species then in reducing environments will successively produce Fe_3O_4, and these reactions are all subject to symmetry isotopic fractionation effects. In this case, the anomalous oxygen did not originate from water per se but reactive oxidizing species with mass independent isotopic signatures.

Indeed, the reaction sequence referenced above by Sakamoto et al. (2007) is not a mechanistic reaction but rather the net stoichiometric reaction of several steps. For the two Reactions (R12) and (R13), it is important to note that water does not react with FeS directly and the initiating step is from an OH reaction, followed by a series of oxidation steps that ultimately produce Fe_3O_4 (Dos Santos et al. 2016). If the water in the troilite had a composition similar to the host meteorite the anomaly in Fe_3O_4 would be produced from the reverse of that from self-shielding produced exotic water. The simplest explanation is that the troilite begins with oxidation from OH derived from the host meteorite near the terrestrial fractionation line. OH is produced on surfaces by water dissociation (Dzade et al. 2016). For the beginning of the oxidation processes leading to the thermodynamically stable Fe_3O_4, the reaction is very much analogous to the SiO + OH reaction and proceeding by successive oxidations such as the intermediate:

$$Fe + OH \leftrightarrow FeOH \leftrightarrow FeO + 1/2\ H_2 \quad \text{(R14)}$$

$$FeO + OH \leftrightarrow OFeO + H \quad \text{(R15)}$$

The Reaction (R14) would produce a mass independent fractionation as observed in the experiment of Chakraborty et al. (2013). As seen in Figure 16, the magnitude of the Fe_3O_4 fractionation is close to that observed in the stratosphere and troposphere in ozone, which derives from $O + O_2$ with an extent as high as 150‰ for $\delta^{18}O$ and >26‰ for $\Delta^{17}O$. It should be noted that for the mass independent fractionation process, there is an inverse temperature effect where a higher temperature enhance the isotope effect (Morton et al. 1990). In that case, for the oxidation of troilite oxidation, if the process were at e.g., 200–400 degrees the magnitude of the effect in oxygen would be more than sufficient to produce a fractionation from above mentioned reactions and seen in Figures 5 and 16. The high temperature effect is also observed in the most recent titanium experiment that was carried out at ~1000K and the mass independent isotopic effect mimics the observation from meteorites (Fig. 10) (Robert et al. 2020). Atmospheric ozone (produced from symmetry-dependent reactions) and nitrate (inheriting the isotopic signature from ozone) are also nearly overlapping with the meteoritic Fe_3O_4 as seen in the figure. *Consequently, this process does not require a photochemical process, preservation of an isotopically labeled ice, and transport trans nebula and quantitative reaction without fractionation. The process is a single step starting with water at the mass fractionation line where the bulk meteorite lies. It had been suggested that the ice to solid occurs at high temperature and no isotope effect occurs.* ***The symmetry reactions have a negative temperature effect, and the isotope effect in forming the solids at high temperatures produce a larger effect rather than no effect.*** In this case it is simply the oxidation process, as in experiments and the atmosphere and no reservoir mixing is required. The reactions are known and the basic physical chemical symmetry relations known at a level to model, and requires no major assumptions.

Therefore the bottom line for the presence of heavy water is that it is not required and the indirect evidence in magnetite is not an anomaly from water. Based upon experiments, atmospheric species isotopic composition and chemical reaction theory is most plausible that this is locally produced and hence not subject to secondary processes. The reaction leading to the stable products would be the relevant host phase.

Oxygen isotopic composition of the Solar System

Ultimately the main objective is that a model for well-known oxygen isotopic composition of meteorites shown in Figure 16. A prediction of mixing models, inculding self sheilding is that a reservoir of oxygen exisits at a $\delta^{17}O = \delta^{18}O$ value of approximately −40‰ or lighter (−50‰ is more likely) (Krot et al. 2019). This CAI reservoir was predicted to be the sun. The Genesis spacecraft mission collected solar wind for two years and returned samples for a high precion measurement of the elemental and isotopic composition of the solar wind for a large portion of solar wind elements. In the return samples, the first after Apollo, the oxygen isotopes of the solar wind were measured by MegaSIMS, an instrument that combines the advantages of secondary ion microscopy with accelerator mass spectrometry (McKeegan et al. 2011). At the low concentrations of the solar wind an electrostatic concentrator was used to concentrate the solar wind for a greater quantity of solar wind material. A series of correction factors for instrumental and Genesis concentrator electrostratic fractionations is applied and the data obtained for the measurements after correction is shown in Figure 16. It may be seen that the actual solar wind does not lie at the point predicted by self shielding models at $\delta^{17}O = \delta^{18}O = -50$‰ and is at $\delta^{18}O = -102$‰ and $\delta^{17}O = -80$‰. In McKeegan et al. (2011), it was speculated that there is a fractionation in the formation of the solar wind from the solar

photosphere and the sun lies along a slope one line, with the 40‰ fractionation factor difference in $\delta^{18}O$ attributed to solar wind formation. Heber et al. (2012) modeled and deterimened the solar wind isotopic fractionation factor for helium (63‰/amu), neon (4.2‰/amu) and argon (2.6‰/amu). For a charge state of +6 for oxygen (which may also possesses a component of +7), a fractionation between sun and solar wind must be known and compared to what is expected to test if the inferred value for the sun is correct (Fig. 16).

In a more recent study (Laming et al. 2017), oxygen isotopes were modeled using a electromagneic model and applying a pondermotive inetractive force in the solar chromosphere, with maintainence of the first adiabtic invariant in the lower corona. Laming et al. (2017) developed a solar wind formation mechanism specifically to understand oxygen concentrations and isotopes. In their calculations they have determined the isotopic fractionation factor between the bulk solar wind and the photosphere for low mass dependent fractionation and high mass depeendent fractionation prcesses that typify solar wind energy regimes. It is found for the low mass regime the $^{16}O/^{18}O$ value ranges between 0.8–0.9 %/amu and for high MDF, 1.57–1.62 %/amu compared to the measured Genesis value at 2.2 %/amu. In their models, the calculated range of $^{25}Mg/^{26}Mg$ and $^{15}N/^{14}N$ values agree with the Genesis measurements. The oxygen isotopes do not however, thus there is some component missing in the model or different values for input parameters are needed. In Laming et al. (2017), the elemental abundances have also been calculated by the ponderomotive model and compared to Genesis measurements (Fig. 32). It is observed that the model results for the element concentrations with respect to solar are close and do the best at low values of the First Ionization Potential, or FIP. A most important point is that the modeled elemental abundance of oxygen does not agree with the model by a significant factor, as highlighted in Figure 32. It is suggested that the photospheric values assumed are too small, and the assumed values do not agree with those of von Steiger and Zurbuchen (2016). Part of the issue is concerned with fractionation factors in slow and fast wind regimes and their relation to the first ionization potential. The polar coronal holes are of particular importance. The bulk oxygen isotopic composition of the sun and solar system remains unknown. Laming et al. (2017) conclude that more data and analysis is needed to solve the existing inability to model both the oxygen isotopic and elemental compositions of Genesis. "*Once this has been achieved then a full assessment of whether the solar photospheric values may be used as a proxy for the pre-solar nebula.*"

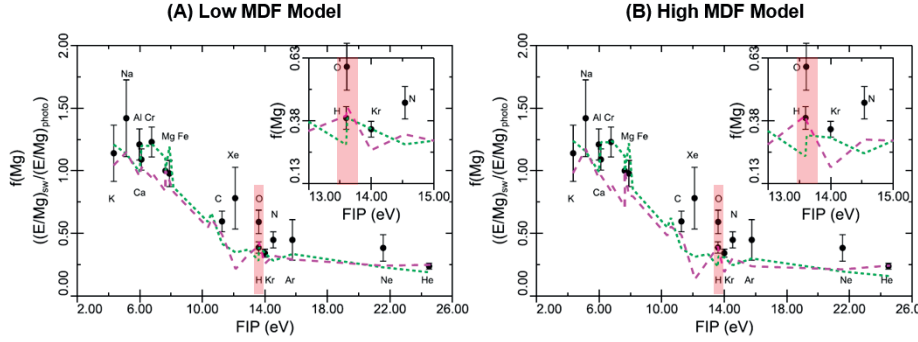

Figure 32. Left panel: The close up of triple oxygen isotopic composition of selected CAIs. The fractionation processes of CAI after formation are schematically shown by **green dotted line**. FUN CAIs distribute in the region with **green dotted lines**. CCAM and PCM stands for "carbonaceous chondrite anhydrous mineral line" and "primitive chondrule mineral line", respectively. Modified from Krot et al. (2019). HAL data from Lee et al. (1980). **Right Panel:** A scaled-down version of Figure 16.

A NEW MODEL FOR TRIPLE OXYGEN ISOTOPES, METEORITES, AND THE ORIGIN OF THE SOLAR SYSTEM

As reviewed, the history of models on the origin of the meteoritic isotopic anomalies has several categories, ranging from the original nucleosynthetic, to self-shielding, to the origin arising during the bond formation that occurs during the actual formation of the first solids in the proto solar environment due to experimentally and theoretically determined symmetry dependent reactions. A nucleosynthetic case for the anomalies has been ruled out. Self-shielding, while still utilized has been discussed in great detail in the forgoing section is unlikely. This then leaves a mass dependent isotopic fractionation process associated with formation of solids as a source of the meteoritic oxygen isotopic class differences. Here we analyze existing measurements and propose a new Chemical Mechanism Model for production of meteorite oxygen isotopic anomalies and the origin of the solar system.

Revisiting triple oxygen isotopes of CAI

Many of the models for solar system formation revolve around CAI and their formation. These objects as well as chondrules are among the most primitive and oldest objects in the solar system and the interest is warranted. This leads to the outstanding issues with the source of meteoritic oxygen isotopic compositions arising from self-shielding/ice transport and addition to an inferred solar system oxygen at $\delta^{17}O = \delta^{18}O = -60‰$. The short comings suggest that an alternative route to synthesis of the observations shown in Figure 16 is warranted. It is suggested that the early nebula was at the point in three isotope space resembling the Calcium Aluminum Inclusions (CAI) that is subsequently titrated with ice created in the nebular fringes. As discussed by Laming et al. (2017), the inability to model the oxygen elemental and isotopic data of Genesis solar wind sufficiently well to conclude with certainty that the solar wind is fractionated and to an exact extent that it intersects with the CAI line. The consequence is that the link between solar nebular processes and the sun is not solidly established. Though CAI studies have been a Rosetta stone for development of nebular formation, chemistry, and alteration understanding, they are 15% of a rare meteorite class (CV) that constitute about 0.84% of meteorite falls (Sears 1998) and in the interest of material balance for nebular oxygen, the other classes of meteorites need to be included and how many reservoirs and processes are needed. If one assumes the $^{18}O/^{17}O$ ratio of the solar system was on the CAI line, it is estimated to be 5.2 ± 0.2, which is quite different from the galactic value of 4.1 (Young et al. 2011). A better evaluation of the triple oxygen isotope composition of our solar system for a deepening understanding of their origins is needed.

In the case of oxygen, it is reasonably well established that based on the original paper by Lee et al. (1980) there is a select group of FUN (Fractionated Unknown Nuclear) CAI that possesses isotopic anomalies in oxygen that differ from other CAI and requires a very different interpretation. The range of FUN triple oxygen isotope composition is schematically shown in Figures 16 and 33. Lee et al. (1980) interpret the data as starting with the original CAI at $\delta^{17}O = \delta^{18}O = -40‰$ and resembling most CAI. The CAI then undergo an extensive heating that results in evaporative material loss and a 25‰ amu^{-1} mass-dependent fractionation. A variable amount of this fractionation moves the individual core along a mass fractionation line, with Allende inclusion HAL undergoing a greater fractionation (red stars in Fig. 33). Subsequent to that heating event the CAI core undergoes an exchange with a gas reservoir that converge upon a reservoir that also intersects with the normal CAI line at a point that is very near $\delta^{17}O = \delta^{18}O = 0‰$ suggesting that this is a major nebular gas phase reservoir. This finding is later supported by further triple oxygen isotope and detailed mineralogy and petrology studies on FUN CAI (Krot et al. 2010, 2014). These processes are schematically shown in Figure 33.

Krot et al. (2019) in a recent review have studied other inclusions ("normal CAI") and carefully documented the complex mineralogy to define the different processes associated with

its formation some $3–5 \times 10^6$ years before the complete melting of some CAI and meteorite formation. Grossite ($CaAl_4O_7$) bearing CAI with the canonical initial $^{26}Al/^{27}Al$ ratio (5×10^{-5}) is a record of the antiquity of these CAI. The $\Delta^{17}O$ composition of these CAI is $-24 \pm 2‰$ (Krot et al. 2019). In the ensuing 3–5 million years the CAI will exchange and the most labile oxygen species will exchange the most. $\Delta^{17}O$ values of many CAI with Wark–Lovering rims vary between −40 and −5‰ (Krot et al. 2019). As exchange proceeds and planetary body become molten and have incomplete aqueous exchange, their $\Delta^{17}O$ values range between 0 and −2‰ as observed in CO and CV meteorites (Krot et al. 2019). The time scale is a few million years post CAI formation. These values (Fig. 33) cover the full range of CAI isotopic composition shown in Figure 16. Figure 33 clearly illustrates the end member, the minerals of exchange, and the final product of exchange being the aqueous exchange near $\delta^{17}O = \delta^{18}O = 0‰$. The data are also clear that there is a reservoir at $\delta^{17}O = \delta^{18}O =$ ca. −50‰ and it is well produced but only resides in a very minor phase with respect to the volume of the other meteorites.

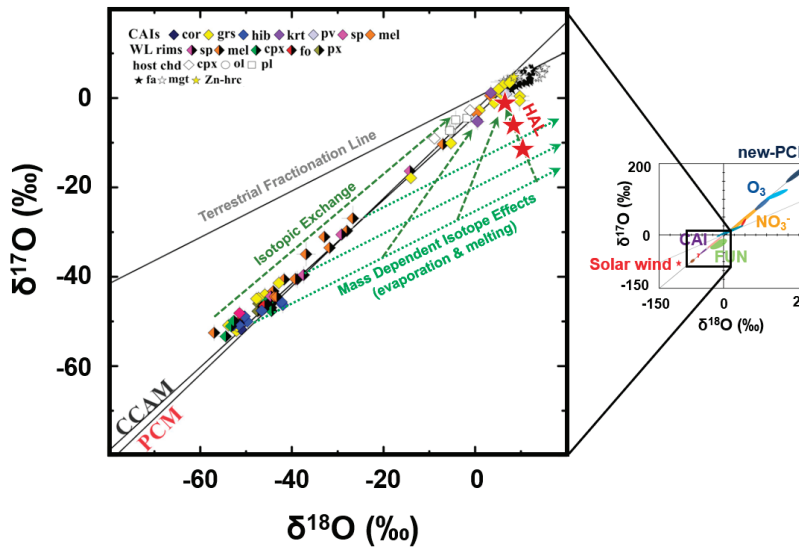

Figure 33. Left panel: The close up of triple oxygen isotopic composition of selected CAIs. The fractionation processes of CAI after formation are schematically shown by green dotted line. FUN CAIs distribute in the region with green dotted lines. CCAM and PCM stands for "carbonaceous chondrite anhydrous mineral line" and "primitive chondrule mineral line", respectively. Modified from Krot et al. (2019). HAL data from Lee et al. (1980). **Right Panel:** A scaled-down version of Figure 16.

Material balance of bulk meteorites oxygen isotopes

It has been suggested in the self-shielding model that the ice produced from CO photolysis may vary depending on time, UV field and vary from 1000‰ downward (Lee et al. 2008) (Fig. 31). The many problems associated with this have been discussed. The heavy isotope effect observed by Sakamoto et al. (2007) does not require a heavy ice production and may be a consequence of the oxidation process itself with the starting species at $\Delta^{17}O = 0‰$. As discussed, it is well known that the $\Delta^{17}O$ in atmospheric nitrate and ozone is near that of the "heavy water" point (new-PCP) and would overlap at slightly higher temperatures. Ozima et al. (2007) noticed that CAI (and some other meteorites with large non-zero $\Delta^{17}O$ values) is a minor component and the mean oxygen isotope composition of the solar system should be characterized by $\Delta^{17}O = 0‰$. As shown in Figure 30, the $\delta^{18}O$ composition of

99% of meteorites lie near the point $\delta^{18}O = 5‰$ and $\delta^{17}O = 2.5‰$. This is not considering the CAI. The entire range of bulk meteorites is only ca. 4‰ near terrestrial fractionation line ($\Delta^{17}O = 0‰$). If one uses NASAs meteorite collection (>20,000 Falls) as a very rough guide as to the amount of material, approximately 92% are H, L, LL and carbonaceous 4%. Most carbonaceous chondrites (expect for CI) possess negative $\Delta^{17}O$ values and the lowest was found in CV (ca. −6‰). Besides carbonaceous chondrites the other meteorites: ureilites, acapulcoites, lodranites, angrites, aubrites, pallasites, howardites, eucrites and diogenites all have slightly negative $\Delta^{17}O$ values and altogether are only 2–3% of falls. Aubrites and eucrites have terrestrial values ($\Delta^{17}O = 0‰$). In addition, Comet 81/P Wild 2 bulk composition (McKeegan et al. 2006) is located near $\delta^{18}O = 5‰$ and $\delta^{17}O = 2.5‰$ and only a small fractionation (polymineralic refractory grain) in the Stardust mission returned sample possess isotopic signature similar to CAI ($\delta^{17}O = \delta^{18}O = -40‰$) (Fig. 16). $\delta^{18}O$ values of 67P/Churyumov-Gerasimenko dust and CO_2 measured by the Rosetta Mission are also near $\delta^{18}O = 5‰$ ($3 \pm 50‰$ and $10 \pm 15‰$, respectively) (Hassig et al. 2017; Paquette et al. 2018), although there are large uncertainties and $\delta^{17}O$ values are unable to measure. We acknowledge that an isotopic balance cannot be quantitatively done since 1) these numbers reflect the survivability of falls and the most fragile ones are least abundant 2) this is a number of falls but one cannot say that this is equivalent to a mass balance 3) in a true mass balance Earth, Mars, Venus (and Vesta) should be included with earth at $\Delta^{17}O = 0‰$, Mars $\Delta^{17}O = 0.3‰$, Vesta $\Delta^{17}O = -0.2‰$ and Venus unknown. The current safest statement with respect to the bulk meteorite, comet and planet compositions is that there are both positive and negative values and the observed range is modest.

The basic considerations for a chemical local production of the meteorite oxygen isotopes we note the following:

1. The presence of what has been observed is considered evidence of a heavy water may be produced locally and isotopically similar to components in the terrestrial atmosphere where the reactions are all known and isotopically characterized. The observed meteoritic composition may be explained by chemical reactions of isotopic compositions of water that is the same as the bulk meteorite, which is near terrestrial.

2. Based upon CAI and anomalous FUN (e.g., HAL) CAI oxygen isotopic measurements and the back exchange captured in minerals of CAI converge on the major solar system reservoir at a value near $\Delta^{17}O = 0‰$, ***this point is the most likely isotopic value to consider as a starting value to explain bulk isotopic values. Given that bulk Earth, moon, Mars and HED meteorites, comets, CAI and "heavy water" lines lie near 5‰, this is reasonable value to assume as a nebular reservoir. Given the data spread in several of the datum, this might vary by 1–2‰.***

3. The solar component at $\delta^{17}O = \delta^{18}O = -50‰$ has yet to have a model that is capable of quantitatively justifying the large correction applied to Genesis measurement and Genesis inferred. Present models may not account for either elemental or isotopic abundances (Laming et al. 2017). The link between solar nebular processes including CAI may not be directly coupled.

If the bulk isotopic values observed in meteorites can be explained by a chemical model, the requirement for multiple isotopic reservoirs that mix vanishes. It is well known from several independent observations that in the symmetry driven reactions, it has been known since the very first experiments that in the reaction both positive and negative reservoirs are created with complete mass balance observed. The positive ozone reservoir is exactly matched by the negative O_2 reservoir (Fig. 5). There is no mixing required as it is simply one chemical reaction with extensive theoretical and experimental measurements by numerous laboratories. Indeed, the mass independent effect can be positive or negative according to the type of chemical reaction

sampling the intermedia complex (Robert et al. 2020). This has been observed for titanium but not for oxygen yet. In a boarder view, a complete mass balance is not a necessary requirement. The positive and negative $\Delta^{17}O$ reservoir observed in the solar system could have been due to different chemical reactions, which are required future identification though.

If the solar nebula is defined as at a value of $\Delta^{17}O = 0‰$ and approximately somewhere with $\delta^{18}O$ between 3‰ and 6‰ and we consider a symmetry dependent reaction that produces positive and negative reservoirs, the possible consequences may be see in Figures 5 and 30. The results show that if we use the measured experiments of Chakraborty et al. (2013) for the reaction SiO+OH, one of the first reactions in gas to particle conversion process, for an equal partitioning between a nebular value centered around $\delta^{18}O = 5$ and $\delta^{17}O = 2.5‰$ (presumed starting nebula), *all meteorite classes, Earth, Mars, Vesta, comets, CAI positive terminus, "water ice", chondrules fall within this range.* The consequence is that there is a requirement of only one reservoir. The entire solid bodies of the inner solar system are created by one process. Transport, storage and mixing are not required. The chemical reaction is required as SiO does not react with CO or H_2O but rather OH is considered the dominant reaction. The fractionation factor has been experimentally measured and the results are interpretable in terms of known theory and a wide range of experimental tests by multiple groups of the symmetry dependent reaction. The use of equal partitioning may be varied and still incorporate all members. In the schematic arrow shown in Figure 30, we have employed a 10‰ fractionation factor, a lower limit. The value may be higher.

Another important point to be made is the Earth's atmosphere. As shown in the Figure 7 there is a $\delta^{17}O = \delta^{18}O$ fractionation factor observed in the Earth's atmosphere as those in the solar system (Fig. 16). It should be noted that atmospheric ozone isotope effect is double the magnitude of CAI (Fig. 16). It has more variation from the pure effect because of its exchange reactions in oxidations and secondary photolysis in the stratosphere. Its origin is molecular oxygen, not bulk earth. With the exception of CAI, most meteorites are not plotted in Figure 16 but in an enlarged version in Figure 30 as their range is too small to be seen on Figure 16. An important point to be made with respect to Figures 16 and 30 is the mass balance. In Figure 16, there is a >100‰ enrichment factor in ozone (up to 150‰). As shown in Figure 7 this very large positive effect has a slightly negative counterpart in a large reservoir (O_2). The >100‰ enrichment effect arises in the stratosphere in ozone formation, which has a concentration of on average about 3 ppm. Tropospheric ozone has the same large enrichment, and a concentration on average of 40 ppb. The troposphere is ca. 80% and stratosphere ca. 10% of the Earth's atmosphere by mass. The balance is between the ozone and in part, molecular oxygen. As discussed by Miller and Pack (2021, this volume), there is a mass independent $\Delta^{17}O$ of –0.467‰ in O_2 that is the counter balance. It is not exact because the ozone enrichment is passed to CO_2 in the stratosphere as need first in return balloon and rocket samples by the Thiemens group (Thiemens et al. 1991, 1995) and is maintained in the troposphere (Thiemens et al. 2014) (Fig. 7). This has been modeled by Hoag et al. (2005) and is used to determine global primary productivity. The CO_2 loses its signal in steady state by exchange with water in the stomata of green plants as first detected by Luz et al (1999). In a recent model, Young et al (2014) quantified the mass independent component of the negative $\Delta^{17}O$ value to be ca. 1/3 while the remaining signature is a result of mass-dependent fractionation due to respiration. Mass-dependent fractionation processes can lead to small $\Delta^{17}O$ values but cannot account for all non-zero $\Delta^{17}O$ components. Overall, the Earth's atmosphere is in a steady state with simultaneous positive and negative $\Delta^{17}O$ reservoirs. This is a natural proof that in a single interactive environment positive and negative $\Delta^{17}O$ reservoirs may be produced and does not require mixing of preserved reservoirs from different places and production times. In Box 2, we summary several critical points of our Chemical Mechanism Model for production of meteorite oxygen isotopic anomalies.

BOX 2
SUMMARY OF CHEMICAL MECHANISM MODEL FOR PRODUCTION OF METEORITE OXYGEN ISOTOPIC ANOMALIES

1. There is only one reservoir required and no mixing. The basis for the production is the slope one effect discovered for ozone and experimentally observed in SiO + OH reaction, a likely first gas-to-solid formation reaction in the nebula. The process requires no photons. The reaction is the step that determines isotopic composition of the solids independent of the source of the oxygen, consistent with gas phase isotopic models and experiments
2. The fractionation factor associated with the fractionation factor assumes the nebula has isotopic composition on the earths bulk solid fractionation line at about $\delta^{18}O = 5‰$ and $\delta^{17}O = 2.5‰$. The value is at the Nexus of bulk earth, enstatite chondrites, aubrites, CAI and FUN CAI back reaction intersections
3. If the nebula starts a value at $\delta^{18}O = 5‰$ and $\delta^{17}O = 2.5‰$ and assumes the fractionation factor measured for the SiO + OH of 10‰ ($\Delta\Delta^{17}O$, $\theta = \ln\alpha^{17}/\ln\alpha^{18} = 1$) from that point, one produces two reservoirs with the values dependent upon reservoir sizes. If both are e.g., equal in equal amounts all reservoirs are overlapped: Earth, Mars, Vesta, all meteorite classes, comets, CAI, chondrules. Other proportions will do the same.
4. At higher temperature, the isotope effect increases as it is known to be an inverse isotope effect. The effect is still $\delta^{18}O = \delta^{17}O$. The high temperature condition is relevant to the environment where the first solids were formed in the solar system.
5. The earth's atmosphere shows the same simultaneous partitioning into positive and negative $\Delta^{17}O$ reservoirs without mixing and $\delta^{18}O$ extends past 100‰; twice that of CAI
6. The nebular reservoir is at a point in part set by the oxygen isotopes in individual minerals in CAI and FUN inclusions. The starting composition of the CAI has no influence on the bulk nebula and the isotope composition. At high temperatures however, the first condensates to form CAI lie along the slope one line and might be a minor but interesting process that chemically produces CAI as proposed by Nobel Laureate Marcus (2004). In this model CAI are produced from the nebula as proposed and not by the sun's inferred composition.
7. The solar wind measured value at $\delta^{18}O = -102.3‰$ and $\delta^{17}O = -80.5‰$ or the inferred value at $\delta^{18}O = \delta^{17}O = -60‰$ does not play a role. As concluded by Laming et al. (2017) the link between the solar wind and solar value and the protosolar nebula has not been proven. The present model depends on the value of the nebula at the time of back reaction of CAI at $\delta^{18}O = 5‰$, $\delta^{17}O = 2.5‰$.

Overall, the present model has avoided the need to create reservoirs and transport ice on grains and mix at ultra-high $\delta^{18}O$ precision by undefined processes. The major components of the model have been experimentally measured and are consistent with the underlying quantum chemical models by different groups. The measurements and models of the present and past atmosphere on Earth and Mars is a testing ground for how reactions in nature occur, transfer chemically and are preserved. The mass independent isotopic anomaly of water in sulfate on Mars has been preserved for billions of years' time scale for example (Thiemens 2006).

For the future, experiments that lead to a deeper understanding of the gas-to-particle conversion process would be of high value. Isotopic measurements of the oxidation process for different elements and oxidants will be of importance, especially for the magnitude of effects as observed in present-day's terrestrial atmosphere. Theory cannot predict the models

due to lack of precise details of the relevant potential energy surfaces. This will lead to better understanding of the first condensates and CAI. The catalytic oxidation on surfaces is fundamental to grain and larger and is not understood at the quantum level. There is a need for studies of the temperature effect of the mass independent fractionation processes at high temperature, especially near condensation temperatures. It is expected to be larger and the reverse of classical mass dependent isotope effects. The CAI do not play a role in influencing the isotopic composition of the meteorites, but they play a highly valuable role in defining the nebular composition and the timing of the major events. Future studies that examine the role of chemical processes in this process might be illuminative.

The new model simplifies the larger details in the meteoritic oxygen isotopic formational process. The case for photochemical shielding has been discussed and the details of the obstacles for the models listed, but not all included. The present model based on experiments, theory and atmospheric and meteoritic observations reduces many long-standing barriers and at the same time presents a range of new experiments that would deepen understanding and are needed in the future.

ACKNOWLEDGEMENTS

We thank François Robert and Edward Young for their critical reviews and Andreas Pack and Ilya Bindeman for their editorial handling and suggestions. All greatly improved this paper. M.H.T. is supported by the Chancellors Associates fund. M.L. is supported by Key Research Program of Frontier Sciences from Chinese Academy of Sciences (GML2019ZD0308).

REFERENCES

Airieau SA, Farquhar J, Thiemens MH, Leshin LA, Bao H, Young ED (2005) Planetesimal sulfate and aqueous alteration in CM and CI carbonaceous chondrite. Geochim Cosmochim Acta 69:4167–4172

Ajay JS, Komarova KG, Remacle F, Levine RD (2018) Time-dependent view of an isotope effect in electron-nuclear nonequilibrium dynamics with applications to N_2. PNAS 115:5890–5895

Al-Halabi A, Van Dishoeck EF (2007) Hydrogen adsorption and diffusion on amorphous solid water ice. Mon Not R Astron Soc 382:1648–1656

Andersson S, Al-Halabi A, Kroes GJ, van Dishoeck EF (2006) Molecular-dynamics study of photodissociation of water in crystalline and amorphous ices. J Chem Phys 124:064715

Aston FW (1919) A positive ray spectrograph. Philos Mag 38:707–714

Babikov D (2017) Recombination reactions as a possible mechanism of mass-independent fractionation of sulfur isotopes in the Archean atmosphere of Earth. PNAS 114:3062–3067

Babikov D, Semenov A, Teplukhin A (2017) One possible source of mass-independent fractionation of sulfur isotopes in the Archean atmosphere of Earth. Geochim Cosmochim Acta 204:388–406

Babikov D, Kendrick BK, Walker RB, Schinke R, Pack RT (2003a) Quantum origin of an anomalous isotope effect in ozone formation. Chem Phys Lett 372:686–691

Babikov D, Kendrick BK, Walker RB, Pack RT, Fleurat-Lesard P, Schinke R (2003b) Formation of ozone: Metastable states and anomalous isotope effect. J Chem Phys 119:2577–2589

Bahou M, SchriverMazzuoli L, CamyPeyret C, Schriver A (1997) Photolysis of ozone at 693 nm in solid oxygen. Isotopic effects in ozone reformation. Chem Phys Lett 273:31–36

Bainssahota SK, Thiemens MH (1989) A mass-independent sulfur isotope effect in the nonthermal formation of S_2F_{10}. J Chem Phys 90:6099–6109

Bao H (2015) Sulfate: A time capsule for Earth's O_2, O_3, and H_2O. Chem Geol 395:108–118

Becquerel H (1896a) Sur les radiations émises par phosphorescence. CR Hebd Seances Acad Sci 122:420–421

Becquerel H (1896b) Sur les radiations invisibles émises par les corps phosphorescents. CR Hebd Seances Acad Sci 122:501

Becquerel H (1896c) Sur quelques propriétés nouvelles des radiations invisibles émises par divers corps phosphorescents. CR Hebd Seances Acad Sci 122:559

Becquerel H (1896d) Sur les radiations invisibles émises par les sels d'uranium. CR Hebd Seances Acad Sci 122:689–694

Becquerel H (1896e) Sur les propriétés différentes des radiations invisibles émises par les sels d'uranium, et du rayonnement de la paroi anticathodique d'un tube de Crookes. CR Hebd Seances Acad Sci 122:762

Becquerel H (1896f) Émission de radiations nouvelles par l'uranium métallique. CR Hebd Seances Acad Sci 122:1086

Becquerel H (1896g) Sur diverses propriétés des rayons uraniques. CR Hebd Seances Acad Sci 123:1086–1088
Benedix GK, Leshin LA, Farquhar J, Jackson T, Thiemens MH (2003) Carbonates in CM2 Chondrites: Constraints on alteration conditions from oxygen isotopic compositions and petrographic observations. Geochim Cosmochim Acta 67:1577–1588
Bertin M, Fayolle EC, Romanzin C, Oberg KI, Michaut X, Moudens A, Philippe L, Jeseck P, Linnartz H, Fillion JH (2012) UV photodesorption of interstellar CO ice analogues: from subsurface excitation to surface desorption. Phys Chem Chem Phys 14:9929–9935
Bethell T, Bergin E (2009) Formation and survival of water vapor in the terrestrial planet-forming region. Science 326:1675–1677
Bhattacharya SK, Thiemens MH (1988) Isotopic fractionation in ozone decomposition. Geophys Res Lett 15:9–12
Bhattacharya SK, Savarino J, Thiemens MH (2000) A new class of oxygen isotopic fractionation in photodissociation of carbon dioxide: Potential implications for atmospheres of Mars and Earth. Geophys Res Lett 27:1459–1462
Bigeleisen J, Mayer MG (1947) Calculation of equilibrium constants for isotopic exchange reactions. J Chem Phys 15:261–267
Blake AJ, Gibson ST, Mccoy DG (1984) Photodissociation of $^{16}O^{18}O$ in the atmosphere. J Geophys Res-Atmos 89:7277–7284
Bradley CA, Urey HC (1932) The relative abundance of hydrogen isotopes in natural hydrogen. Phys Rev 40:0889–0890
Brickwedde FG (1982) Urey, Harold and the discovery of deuterium. Phys Today 35:34–39
Buchachenko (2001) Magnetic isotope effect: Nuclear spin control of chemical reactions. J Phys Chem A 105:9995–10011
Buchachenko (2013) Mass independent isotope effect. J Phys Chem B 117:2231–2238
Buchachenko (2018) Magnetic isotopes as a means to elucidate Earth and environmental chemistry. Russ Chem Rev 87:727–740
Caballero-Gill RP, Herbert TD, Dowsett HJ (2019) 100-kyr paced climate change in the Pliocene warm period, Southwest Pacific. Paleoceanogr Paleocl 34:524–545
Cano EJ, Sharp ZD, Shearer CK (2020) Distinct oxygen isotope compositions of the Earth and Moon. Nat Geosci 13:270–274
Chakraborty S, Bhattacharya SK (2003) Oxygen isotopic fractionation during UV and visible light photodissociation of ozone. J Chem Phys 118:2164–2172
Chakraborty S, Ahmed M, Jackson TL, Thiemens MH (2008) Experimental test of self-shielding in vacuum ultraviolet photodissociation of CO. Science 321:1328–1331
Chakraborty S, Ahmed M, Jackson TL, Thiemens MH (2009) Response to Comments on "Experimental test of self-shielding in vacuum ultraviolet photodissociation of CO". Science 324:1516
Chakraborty S, Davis RD, Ahmed M, Jackson TL, Thiemens MH (2012) Oxygen isotope fractionation in the vacuum ultraviolet photodissociation of carbon monoxide: Wavelength, pressure, and temperature dependency. J Chem Phys 137:024309
Chakraborty S, Yanchulova P, Thiemens MH (2013) Mass-independent oxygen isotopic partitioning during gas-phase SiO_2 formation. Science 342:463–466
Chakraborty S, Muskatel BH, Jackson TL, Ahmed M, Levine RD, Thiemens MH (2014) Massive isotopic effect in vacuum UV photodissociation of N_2 and implications for meteorite data. PNAS 111:14704–14709
Chakraborty S, Jackson TL, Rude B, Ahmed M, Thiemens MH (2016) Nitrogen isotopic fractionations in the low temperature (80 K) vacuum ultraviolet photodissociation of N_2. J Chem Phys 145:114302
Chakraborty S, Rude B, Ahmed M, Thiemens MH (2018) Carbon and oxygen isotopic fractionation in the products of low-temperature VUV photodissociation of carbon monoxide. Chem Phys 514:78–86
Cicerone RJ, Mccrumb JL (1980) Photo-dissociation of isotopically heavy O_2 as a source of atmosphere. Geophys Res Lett 7:251–254
Ciesla FJ (2010) Residence times of particles in diffusive protoplanetary disk environments. I. Vertical Motions. Astrophys J 723:514–529
Ciesla FJ (2014) The phases of water ice in the solar nebula. Astrophys J Lett 784:L1
Clayton RN (2002) Solar System—Self-shielding in the solar nebula. Nature 415:860–861
Clayton RN, Mayeda TK (1984) The oxygen isotope record in Murchison and other carbonaceous chondrites. Earth Planet Sci Lett 67:151–161
Clayton RN, Grossman L, Mayeda TK (1973) Component of primitive nuclear composition in carbonaceous meteorites. Science 182:485–488
Cole AS, Boering KA (2006) Mass-dependent and non-mass-dependent isotope effects in ozone photolysis: Resolving theory and experiments. J Chem Phys 125:184301
Craig H (1953) The geochemistry of the stable carbon isotopes. Geochim Cosmochim Acta 3:53–92
Crockford PW, Kunzmann M, Bekker A, Hayles J, Bao H, Halverson GP, Peng Y, Bui TH, Cox GM, Gibson TM, Wörndle S (2019) Claypool continued: Extending the isotopic record of sedimentary sulfate. Chem Geol 513:200–225
Cuppen HM, Herbst E (2007) Simulation of the formation and morphology of ice mantles on interstellar grains. Astrophys J 668:294–309
Du F, Bergin EA (2014) Water vapor distribution in protoplanetary disks. Astrophys J 792:2
Dos Santos EC, Silva JCD, Duarte HA (2016) Pyrite oxidation mechanism by oxygen in aqueous medium. J Phys Chem C 120:2760–2768

Dominguez G (2010) A heterogeneous chemical origin for the ^{16}O-enriched and ^{16}O-depleted reservoirs of the early solar system. Astrophys J Lett 713:L59–L63
Dzade NY, Roldan A, de Leeuw NH (2016) DFT-D2 simulations of water adsorption and dissociation on the low-index surfaces of mackinawite (FeS). J Chem Phys 144:174704
Emiliani C (1955) Pleistocene temperatures. J Geol 63:538–578
Farquhar J, Thiemens MH (2000) Oxygen cycle of the Martian atmosphere-regolith system: δ^{17}O of secondary phases in Nakhla and Lafayette. J Geophys Res-Planet 105:11991–11997
Farquhar J, Thiemens MH, Jackson T (1998) Atmosphere-surface interactions on Mars: δ^{17}O measurements of carbonate from ALH 84001. Science 280:1580–1582
Farquhar J, Bao HM, Thiemens M (2000) Atmospheric influence of Earth's earliest sulfur cycle. Science 289:756–758
Federman SR, Young ED (2009) Comments on "Experimental test of self-shielding in vacuum ultraviolet photodissociation of CO". Science 324:1516
Franz HB, Danielache SO, Farquhar J, Wing BA (2013) Mass-independent fractionation of sulfur isotopes during broadband SO2 photolysis: Comparison between ^{16}O- and ^{18}O-rich SO_2. Chem Geol 362:56–65
Fraser HJ, Collings MP, McCoustra MRS, Williams DA (2001) Thermal desorption of water ice in the interstellar medium. Mon Not R Astron Soc 327:1165–1172
Fuchs GW, Cuppen HM, Ioppolo S, Romanzin C, Bisschop SE, Andersson S, van Dishoeck EF, Linnartz H (2009) Hydrogenation reactions in interstellar CO ice analogues A combined experimental/theoretical approach. Astron Astrophys 505:629–639
Furuya K, van Dishoeck EF, Aikawa Y (2016) Reconstructing the history of water ice formation from HDO/H_2O and D_2O/HDO ratios in protostellar cores. Astron Astrophys 586:A127
Gao YQ, Marcus RA (2001) Strange and unconventional isotope effects in ozone formation. Science 293:259–263
Gao X, Thiemens MH (1989) Multi-isotopic sulfur isotope ratios (δ^{33}S, δ^{34}S, δ^{36}S) in meteorites. Meteoritics 24:269–269
Gao X, Thiemens MH (1993a) Isotopic composition and concentration of sulfur in carbonaceous chondrites. Geochim Cosmochim Acta 57:3159–3169
Gao X, Thiemens MH (1993b) Variations of the isotopic composition of sulfur in enstatite and ordinary chondrites. Geochim Cosmochim Acta 57:3171–3176
Giauque WF, Johnston HL (1929a) An isotope of oxygen, mass 18. Nature 123:318–318
Giauque WF, Johnston HL (1929b) An isotope of oxygen of mass 17 in the earth's atmosphere. Nature 123:831–831
Green JA, Caswell JL, Fuller GA, Avison A, Breen SL, Brooks K, Burton MG, Chrysostomou A, Cox J, Diamond PJ, Ellingsen SP (2009) The 6-GHz multibeam maser survey-I. Techniques. Mon Not R Astron Soc 392:783–794
Grossman L (1972) Condensation in primitive solar nebula. Geochim Cosmochim Acta 36:597–619
Harman CE, Pavlov AA, Babikov D, Kasting JF (2018) Chain formation as a mechanism for mass-independent fractionation of sulfur isotopes in the Archean atmosphere. Earth Planet Sci Lett 496:238–247
Hasegawa TI, Herbst E, Leung CM (1992) Models of gas–grain chemistry in dense interstellar clouds with complex organic-molecules. Astrophys J Suppl S 82:167–195
Hässig M, Altwegg K, Balsiger H, Berthelier JJ, Bieler A, Calmonte U, Dhooghe F, Fiethe B, Fuselier SA, Gasc S, Gombosi TI (2017) Isotopic composition of CO_2 in the coma of 67P/Churyumov–Gerasimenko measured with ROSINA/DFMS. Astron Astrophys 605:A50
Hathorn BC, Marcus RA (1999) An intramolecular theory of the mass-independent isotope effect for ozone. I. J Chem Phys 111:4087–4100
Hathorn BC, Marcus RA (2000) An intramolecular theory of the mass-independent isotope effect for ozone. II. Numerical implementation at low pressures using a loose transition state. J Chem Phys 113:9497–9509
Heays AN, Ajello JM, Aguilar A, Lewis BR, Gibson ST (2014) The high-resolution extreme-ultraviolet spectrum of N_2 by electron impact. Astrophys J Suppl S 211:28
Heays AN, Bosman AD, van Dishoeck EF (2017) Photodissociation and photoionisation of atoms and molecules of astrophysical interest. Astron Astrophys 602:A105
Heber VS, Baur H, Bochsler P, McKeegan KD, Neugebauer M, Reisenfeld DB, Wieler R, Wiens RC (2012) Isotopic mass fractionation of solar wind: evidence from fast and slow solar wind collected by the Genesis Mission. Astrophys J 759:121
Heidenreich JE, Thiemens MH (1983) A non-mass-dependent isotope effect in the production of ozone from molecular-oxygen. J Chem Phys 78:892–895
Heidenreich JE, Thiemens MH (1986) A non-mass-dependent oxygen isotope effect in the production of ozone from molecular-oxygen - the role of molecular symmetry in isotope chemistry. J Chem Phys 84:2129–2136
Hoag KJ, Still CJ, Fung IY, Boering KA (2005) Triple oxygen isotope composition of tropospheric carbon dioxide as a tracer of terrestrial gross carbon fluxes. Geophys Res Lett 32:L02802
Hogerheijde MR, Bergin EA, Brinch C, Cleeves LI, Fogel JK, Blake GA, Dominik C, Lis DC, Melnick G, Neufeld D, Panić O(2011) Detection of the water reservoir in a forming planetary system. Science 334:338–340
Huang CH, Bhattacharya SK, Hsieh ZM, Chen YJ, Yih TS, Liang MC (2019) Isotopic fractionation in photolysis of ozone in the Hartley and Chappuis Bands. Earth Space Sci 6:752–773
Hulston JR, Thode HG (1965a) Cosmic-ray-produced ^{36}S and ^{33}S in metallic phase of iron meteorites. J Geophys Res 70:4435–4442

Hulston JR, Thode HG (1965b) Variations in ^{33}S, ^{34}S and ^{36}S contents of meteorites and their relation to chemical and nuclear effects. J Geophys Res 70:3475–3484
Janssen C, Guenther J, Mauersberger K, Krankowsky D (2001) Kinetic origin of the ozone isotope effect: a critical analysis of enrichments and rate coefficients. Phys Chem Chem Phys 3:4718–4721
Jeans J (1904) The Dynamical Theory of Gases. Cambridge University Press, Cambridge
Johnson RE, Quickenden TI (1997) Photolysis and radiolysis of water ice on outer solar system bodies. J Geophys Res-Planet 102:10985–10996
Kaye JA (1986) Theoretical-analysis of isotope effects on ozone formation in oxygen photochemistry. J Geophys Res-Atmos 91:7865–7874
Kaye JA, Strobel DF (1983) Enhancement of heavy ozone in the Earth's atmosphere. J Geophys Res-Oceans 88:8447–8452
Kimura Y, Nuth JA, Chakpaborty S, Thiemens MH (2007) Non-mass-dependent oxygen isotopic fractionation in smokes produced in an electrical discharge. Meteorit Planet Sci 42:1429–1439
Krot AN, Nagashima K, Ciesla FJ, Meyer BS, Hutcheon ID, Davis AM, Huss GR, Scott ERD (2010) Oxygen isotopic composition of the sun and mean oxygen isotopic composition of the protosolar silicate dust: Evidence from refractory inclusions. Astrophys J 713:1159–1166
Krot AN, Nagashima K, Wasserburg GJ, Huss GR, Papanastassiou D, Davis AM, Hutcheon ID, Bizzarro M (2014) Calcium-aluminum-rich inclusions with fractionation and unknown nuclear effects (FUN CAIs): I. Mineralogy, petrology, and oxygen isotopic compositions. Geochim Cosmochim Acta 145:206–247
Krot AN, Nagashima K, Simon SB, Ma C, Connolly HC, Huss GR, Davis AM, Bizzarro M (2019) Mineralogy, petrography, and oxygen and aluminum–magnesium isotope systematics of grossite-bearing refractory inclusions. Geochemistry-Germany 79:125529
Laming JM, Heber VS, Burnett DS, Guan Y, Hervig R, Huss GR, Jurewicz AJ, Koeman-Shields EC, McKeegan KD, Nittler LR, Reisenfeld DB (2017) Determining the elemental and isotopic composition of the pre-solar nebula from Genesis Data analysis: The case of oxygen. Astrophys J Lett 851:L12
Lee T, Mayeda TK, Clayton RN (1980) Oxygen isotopic anomalies in Allende inclusion Hal. Geophys Res Lett 7:493–496
Lee JE, Bergin EA, Lyons JR (2008) Oxygen isotope anomalies of the Sun and the original environment of the solar system. Meteorit Planet Sci 43:1351–1362
Lee JE, Lee S, Baek G, Aikawa Y, Cieza L, Yoon SY, Herczeg G, Johnstone D, Casassus S (2019) The ice composition in the disk around V883 Ori revealed by its stellar outbust. Nat Astron, 3:314–319
Lefebvre-Brion H, Field R (2004) The spectra and dynamics of diatomic molecules. Academic Press. Paperback ISBN 9780124414563
Li X, Heays AN, Visser R, Ubachs W, Lewis BR, Gibson ST, van Dishoeck EF (2013) Photodissociation of interstellar N_2. Astron Astrophys 555:A14
Liang MC, Blake GA, Yung YL (2004) A semianalytic model for photo-induced isotopic fractionation in simple molecules. J Geophys Res-Atmos 109:D10308
Liang MC, Irion FW, Weibel JD, Miller CE, Blake GA, Yung YL (2006) Isotopic composition of stratospheric ozone. J Geophys Res-Atmos 111:D02302
Liang MC, Heays AN, Lewis BR, Gibson ST, Yung YL (2007) Source of nitrogen isotope anomaly in HCN in the atmosphere of Titan. Astrophys J 664:L115–L118
Lin M, Zhang XL, Li MH, Xu YL, Zhang ZS, Tao J, Su BB, Liu LZ, Shen YA, Thiemens MH (2018) Five-S-isotope evidence of two distinct mass-independent sulfur isotope effects and implications for the modern and Archean atmospheres. PNAS 115:8541–8546
Lin M, Thiemens MH (2020) A simple elemental sulfur reduction method for isotopic analysis and pilot experimental test of symmetry-dependent sulfur isotope effects in planetary processes. Geochem Geophys Geosyst 21: e2020GC009051
Lindemann FA (1919) Note on the vapour pressure and affinity of isotopes. Philos Mag 38:173–181
Lindemann FA, Aston FW (1919) The possibility of separating isotopes. Philos Mag 37:523–534
Li WJ, Xu L, Liu X, Zhang J, Lin YT, Yao X, Gao HW, Zhang DZ, Chen JM, Wang WX, Harrison RM, Zhang XY, Shao LY, Fu PQ, Nenes A, Shi ZB (2017) Air pollution–aerosol interactions produce more bioavailable iron for ocean ecosystems. Sci Adv 3, e1601749
Liu P, Harman CE, Kasting JF, Hu YY, Wang JX (2019) Can organic haze and O_2 plumes explain patterns of sulfur mass-independent fractionation during the Archean? Earth Planet Sci Lett 526:115767
Luz B, Barkan E, Bender ML, Thiemens MH, Boering KA (1999) Triple-isotope composition of atmospheric oxygen as a tracer of biosphere productivity. Nature 400:547–550
Lyons JR (2014) Photodissociation of CO isotopologues: Models of laboratory experiments and implications for the solar nebula. Meteorit Planet Sci 49:373–393
Lyons JR (2020) An analytical formulation of isotope fractionation due to self-shielding. Geochim Cosmochim Acta 282:177–200
Lyons JR (2001) Transfer of mass-independent fractionation in ozone to other oxygen-containing radicals in the atmosphere. Geophys Res Lett 28:3231–3234
Lyons JR, Young ED (2005) CO self-shielding as the origin of oxygen isotope anomalies in the early solar nebula. Nature 435:317–320

Lyons JR, Bergin EA, Ciesla FJ, Davis AM, Desch SJ, Hashizume K, Lee JE (2009a) Timescales for the evolution of oxygen isotope compositions in the solar nebula. Geochim Cosmochim Acta 73:4998–5017

Lyons JR, Lewis RS, Clayton RN (2009b). Comments on "Experimental test of self-shielding in vacuum ultraviolet photodissociation of CO". Science 324:1516

Mahata S, Bhattacharya SK (2009a) Anomalous enrichment of ^{17}O and ^{13}C in photodissociation products of CO_2: Possible role of nuclear spin. J Chem Phys 130:234312

Mahata S, Bhattacharya SK (2009b) Temperature dependence of isotopic fractionation in CO_2 photolysis. Chem Phys Lett 477:52–56

Manian SH, Urey HC, Bleakney W (1934) An investigation of the relative abundance of the oxygen isotopes ^{16}O:^{18}O in stone meteorites. J Am Chem Soc 56:2601–2609

Marcus RA (2004) Mass-independent isotope effect in the earliest processed solids in the solar system: A possible chemical mechanism. J Chem Phys 121:8201–8211

Mauersberger K (1981) Measurement of heavy ozone in the stratosphere. Geophys Res Lett 8:935–937

Mauersberger K, Morton J, Schueler B, Stehr J, Anderson SM (1993) Multi-isotope study of ozone - implications for the heavy ozone anomaly. Geophys Res Lett 20:1031–1034

Mauersberger K, Erbacher B, Krankowsky D, Gunther J, Nickel R (1999) Ozone isotope enrichment: Isotopomer-specific rate coefficients. Science 283:370–372

Mauersberger K, Lammerzahl P, Krankowsky D (2001) Stratospheric ozone isotope enrichments-revisited. Geophys Res Lett 28:3155–3158

McCabe JR, Boxe CS, Colussi AJ, Hoffmann MR, Thiemens MH (2005) Oxygen isotopic fractionation in the photochemistry of nitrate in water and ice. J Geophys Res-Atmos 110: D15310

McCabe JR, Thiemens MH, Savarino J (2007) A record of ozone variability in South Pole Antarctic snow: Role of nitrate oxygen isotopes. J Geophys Res-Atmos 112:D12303

Mcelroy MB, Yung YL, Nier AO (1976) Isotopic composition of nitrogen—implications for past history of Mars atmosphere. Science 194:70–72

McKeegan KD, Aléon J, Bradley J, Brownlee D, Busemann H, Butterworth A, Chaussidon M, Fallon S, Floss C, Gilmour J, Gounelle M (2006) Isotopic compositions of cometary matter returned by Stardust. Science 314:1724–1728

McKeegan KD, Kallio AP, Heber VS, Jarzebinski G, Mao PH, Coath CD, Kunihiro T, Wiens RC, Nordholt JE, Moses RW, Reisenfeld DB (2011) The oxygen isotopic composition of the Sun inferred from captured solar wind. Science 332:1528–1532

Miller MF, Pack A (2021) Why measure ^{17}O? Historical perspective, triple-isotope systematics and selected applications. Rev Mineral Geochem 86:1–34

Miller CE, Onorato RM, Liang MC, Yung YL (2005) Extraordinary isotopic fractionation in ozone photolysis. Geophys Res Lett 32:L14814

Morton J, Schueler B, Mauersberger K (1989) Oxygen fractionation of ozone isotopes $^{48}O_3$ through $^{54}O_3$. Chem Phys Lett 154:143–145

Morton J, Barnes J, Schueler B, Mauersberger K (1990) Laboratory studies of heavy ozone. J Geophys Res-Atmos 95:901–907

Mulliken RS (1964) The Rydberg states of molecules. Parts I–V. J Am Chem Soc 86:3183–3197

Muskatel BH, Remacle F, Thiemens MH, Levine RD (2011) On the strong and selective isotope effect in the UV excitation of N_2 with implications toward the nebula and Martian atmosphere. PNAS 108:6020–6025

Navon O, Wasserburg GJ (1985) Self-shielding in O_2—a possible explanation for oxygen isotopic anomalies in meteorites. Earth Planet Sci Lett 73:1–16

Ndengue SA, Schinke R, Gatti F, Meyer HD, Jost R (2012) Ozone photodissociation: isotopic and electronic branching ratios for symmetric and asymmetric isotopologues. J Phys Chem A 116:12271–12279

Ndengue S, Madronich S, Gatti F, Meyer HD, Motapon O, Jost R (2014) Ozone photolysis: Strong isotopologue/isotopomer selectivity in the stratosphere. J Geophys Res-Atmos 119:4286–4302

Nier AO (1947) A mass spectrometer for isotope and gas analysis. Rev Sci Instrum 18:398–411

Noble JA, Theule P, Mispelaer F, Duvernay F, Danger G, Congiu E, Dulieu F, Chiavassa T (2012) The desorption of H_2CO from interstellar grains analogues. Astron Astrophys 543:A5

Nunn M (2015) The Oxygen Isotopic Composition of Water in the Inner Solar System. PhD University of California, San Diego

Omidvar K, Frederick JE (1987) Atmospheric odd oxygen production due to the photodissociation of ordinary and isotopic molecular-oxygen. Planet Space Sci 35:769–784

Ozima M, Podosek FA, Higuchi T, Yin QZ, Yamada A (2007) On the mean oxygen isotope composition of the Solar System. Icarus 186:562–570

Paquette JA, Engrand C, Hilchenbach M, Fray N, Stenzel OJ, Silen J, Ryno J, Kissel J, Team C (2018) The oxygen isotopic composition ($^{18}O/^{16}O$) in the dust of comet 67P/Churyumov-Gerasimenko measured by COSIMA on-board Rosetta. Mon Not R Astron Soc 477:3836–3844

Reinhardt P, Robert F (2018) On the mass independent isotopic fractionation in ozone. Chem Phys 513:287–294

Robert F, Tartese R, Lombardi G, Reinhardt P, Roskosz M, Doisneau B, Deng ZB, Chaussidon M (2020) Mass-independent fractionation of titanium isotopes and its cosmochemical implications. Nat Astron 4:762–768

Rutherford E, Soddy F (1903) Radioactive change. Philos Mag 5:576–591
Sakamoto N, Seto Y, Itoh S, Kuramoto K, Fujino K, Nagashima K, Krot AN, Yurimoto H (2007) Remnants of the early solar system water enriched in heavy oxygen isotopes. Science 317:231–233
Savarino J, Thiemens MH (1999) Mass-independent oxygen isotope (^{16}O, ^{17}O, ^{18}O) fractionation found in H_x, O_x reactions. J Phys Chem A 103:9221–9229
Schmidt JA, Johnson MS, Schinke R (2013) Carbon dioxide photolysis from 150 to 210 nm: Singlet and triplet channel dynamics, UV-spectrum, and isotope effects. PNAS 110:17691–17696
Sears DWG (1998) The case for rarity of chondrules and calcium-aluminum-rich inclusions in the early solar system and some implications for astrophysical models. Astrophys J 498:773–778
Shaheen R, Abramian A, Horn J, Dominguez G, Sullivan R, Thiemens MH (2010) Detection of oxygen isotopic anomaly in terrestrial atmospheric carbonates and its implications to Mars. PNAS 107:20213–20218
Shaheen R, Abaunza MM, Jackson TL, McCabe J, Savarino J, Thiemens MH (2014) Large sulfur-isotope anomaly in nonvolcanic sulfate aerosol and its implications for the Archean atmosphere. PNAS 111:11979–11983
Shaheen R, Niles PB, Chong K, Corrigan CM, Thiemens MH (2015) Carbonate formation events in ALH 84001 trace the evolution of the Martian atmosphere. PNAS 112:336–341
Soddy F (1913) Intra-atomic charge. Nature 92:399–400
Spelsberg D, Meyer W (2001) Dipole-allowed excited states of N_2: Potential energy curves, vibrational analysis, and absorption intensities. J Chem Phys 115:6438–6449
Teplukhin A, Babikov D (2018a) Several levels of theory for description of isotope effects in ozone: Symmetry effect and mass effect. J Phys Chem A 122:9177–9190
Teplukhin A, Babikov D (2018b) Properties of Feshbach and "shape"-resonances in ozone and their role in recombination reactions and anomalous isotope effects. Faraday Discuss 212:259–280
Teplukhin A, Gayday I, Babikov D (2018) Several levels of theory for description of isotope effects in ozone: Effect of resonance lifetimes and channel couplings. J Chem Phys 149:164302
Thiemens MH (1999) Atmosphere science—Mass-independent isotope effects in planetary atmospheres and the early solar system. Science 283:341–345
Thiemens MH (2006) History and applications of mass-independent isotope effects. Annu Rev Earth Planet Sci 34:217–262
Thiemens MH (2018) The discovery of chemically produced mass independent isotope effects: The physical chemistry basis and applications to the early solar system, planetary atmospheres, and the origin of life. Acceptance Speech of the Leonard Medal July 2017. Meteorit Planet Sci 54:231–248
Thiemens MH, Heidenreich JE (1983) The mass-independent fractionation of oxygen—a novel isotope effect and its possible cosmochemical implications. Science 219:1073–1075
Thiemens MH, Jackson T (1990) Pressure dependency for heavy isotope enhancement in ozone formation. Geophys Res Lett 17:717–719
Thiemens MH, Lin M (2019) Use of isotope effects to understand the present and past of the atmosphere and climate and track the origin of life. Angew Chem Int Edit 58:6826–6844
Thiemens MH, Jackson T, Mauersberger K, Schueler B, Morton J (1991) Oxygen isotope fractionation in stratospheric CO_2. Geophys Res Lett 18:669–672
Thiemens MH, Jackson T, Zipf EC, Erdman PW, Vanegmond C (1995) Carbon-dioxide and oxygen-isotope anomalies in the mesosphere and stratosphere. Science 270:969–972
Thiemens MH, Chakraborty S, Dominguez G (2012) The physical chemistry of mass-independent isotope effects and their observation in nature. Annu Rev Phys Chem 63:155–177
Thiemens MH, Chakraborty S, Jackson TL (2014) Decadal $\Delta^{17}O$ record of tropospheric CO_2: Verification of a stratospheric component in the troposphere. J Geophys Res-Atmos 119:6221–6229
Tian F, Kasting JF, Solomon SC (2009) Thermal escape of carbon from the early Martian atmosphere. Geophys Res Lett 36:L02205
Tielens AGGM, Hagen W (1982) Model-calculations of the molecular composition of inter-stellar grain mantles. Astron Astrophys 114:245–260
Troe J (1977) Theory of thermal unimolecular reactions at low-pressures 2. Strong collision rate constants—Applications. J Chem Phys 66:4758–4775
Tyra MA, Farquhar J, Wing BA, Benedix GK, Jull AJT, Jackson T, Thiemens, MH (2007). Terrestrial alteration of Antarctic CM chondrite meteorites in a suite of Antarctic CM chondrites: evidence from oxygen and carbon isotopes. Geochim Cosmochim Acta 71:782–795
Uemura R, Masson-Delmotte V, Jouzel J, Landais A, Motoyama H, Stenni B (2012) Ranges of moisture-source temperature estimated from Antarctic ice cores stable isotope records over glacial-interglacial cycles. Clim Past 8:1109–1125
Urey HC (1947) The thermodynamic properties of isotopic substances. J Chem Soc:562–581
Urey HC, Brickwedde FG, Murphy GM (1932a) A hydrogen isotope of mass 2 and its concentration. Phys Rev 40:1–15
Urey HC, Brickwedde FG, Murphy GM (1932b) A hydrogen isotope of mass 2. Phys Rev 39:164–165
van Dishoeck EF, Herbst E, Neufeld DA (2013) Interstellar water chemistry: from laboratory to observations. Chem Rev 113:9043–9085
Vandishoeck EF, Black JH (1988) The photodissociation and chemistry of interstellar CO. Astrophys J 334:771–802

Velivetskaya TA, Ignatiev AV, Yakovenko VV, Vysotskiy SV (2018) Experimental studies of the oxygen isotope anomalies ($\Delta^{17}O$) of H_2O_2 and their relation to radical recombination reactions. Chem Phys Lett 693:107–113

Velivetskaya TA, Ignatiev AV, Budnitskiy SY, Yakovenko VV, Vysotskiy SV (2016) Mass-independent fractionation of oxygen isotopes during H_2O_2 formation by gas-phase discharge from water vapour. Geochim Cosmochim Acta 193:54–65

von Steiger R, Zurbuchen TH (2016) Solar metallicity derived from in situ solar wind composition. Astrophys J 816:13

Watanabe N, Horii T, Kouchi A (2000) Measurements of D_2 yields from amorphous D_2O ice by ultraviolet irradiation at 12 K. Astrophys J 541:772–778

Wen J, Thiemens MH (1990) An apparent new isotope effect in a molecular decomposition and implications for nature. Chem Phys Lett 172:416–420

Wen J, Thiemens MH (1991) Experimental and theoretical-study of isotope effects on ozone decomposition. J Geophys Res-Atmos 96:10911–10921

Woitke P, Thi WF, Kamp I, Hogerheijde MR (2009) Hot and cool water in Herbig Ae protoplanetary disks A challenge for Herschel. Astron Astrophys 501:L5–L8

Wolf S, Bitter M, Krankowsky D, Mauersberger K (2000) Multi-isotope study of fractionation effects in the ozone formation process. J Chem Phys 113:2684–2686

Yabushita A, Hama T, Iida D, Kawanaka N, Kawasaki M, Watanabe N, Ashfold MNR, Loock HP (2008) Release of hydrogen molecules from the photodissociation of amorphous solid water and polycrystalline ice at 157 and 193 nm. J Chem Phys 129:044501

Yang JM, Epstein S (1987a) The effect of the isotopic composition of oxygen on the non-mass-dependent isotopic fractionation in the formation of ozone by discharge of O_2. Geochim Cosmochim Acta 51:2011–2017

Yang JM, Epstein S (1987b) The effect of pressure and excitation-energy on the isotopic fractionation in the formation of ozone by discharge of O_2. Geochim Cosmochim Acta 51:2019–2024

Yin QZ, Shi X, Chang C, Ng CY (2009) Comments on "Experimental test of self-shielding in vacuum ultraviolet photodissociation of CO". Science 324:1516

Young ED (2001) The hydrology of carbonaceous chondrite parent bodies and the evolution of planet progenitors. Philos Trans R Soc Lond A 359:2095–2110

Young ED (2007a) Time-dependent oxygen isotopic effects of CO self shielding across the solar protoplanetary disk. Earth Planet Sci Lett 262:468–483

Young ED (2007b) Geochemistry - Strange water in the solar system. Science 317:211–212

Young ED, Gounelle M, Smith RL, Morris MR, Pontoppidan (2011) Astronomical oxygen isotopic evidence for supernova enrichment of the solar system birth environment by propagating star formation. Astrophys J 729:43–55

Young ED, Yeung LY, Kohl IE (2014) On the $\Delta^{17}O$ budget of atmospheric O_2. Geochim Cosmochim Acta 135:102–125

Yung YL, Demore WB, Pinto JP (1991) Isotopic exchange between carbon-dioxide and ozone via O(1d) in the stratosphere. Geophys Res Lett 18:13–16

Yurimoto H, Kuramoto K (2004) Molecular cloud origin for the oxygen isotope heterogeneity in the solar system. Science 305:1763–1766

Zmolek P, Xu XP, Jackson T, Thiemens MH, Trogler WC (1999) Large mass independent sulfur isotope fractionations during the photopolymerization of $^{12}CS_2$ and $^{13}CS_2$. J Phys Chem A 103:2477–2480